NAVAL POSTGRADUATE SCHOOL

MONTEREY, CALIFORNIA

THESIS

MECHANICAL AND ELECTRICAL CHARACTERIZATION OF NOVEL CARBON NANO FIBER ULTRALOW DENSITY FOAM

by

D. Chris Daskam

December 2013

Thesis Co-Advisor: Claudia Luhrs
Jonathan Philips

Approved for public release; distribution is unlimited

THIS PAGE INTENTIONALLY LEFT BLANK

REPORT DOCUMENTATION PAGE			Form Approved OMB No. 0704-0188
Public reporting burden for this collection of information is estimated to average 1 hour per response, including the time for reviewing instruction, searching existing data sources, gathering and maintaining the data needed, and completing and reviewing the collection of information. Send comments regarding this burden estimate or any other aspect of this collection of information, including suggestions for reducing this burden, to Washington headquarters Services, Directorate for Information Operations and Reports, 1215 Jefferson Davis Highway, Suite 1204, Arlington, VA 22202-4302, and to the Office of Management and Budget, Paperwork Reduction Project (0704-0188) Washington DC 20503.			
1. AGENCY USE ONLY ***(Leave blank)***	**2. REPORT DATE** December 2013	**3. REPORT TYPE AND DATES COVERED** Master's Thesis	
4. TITLE AND SUBTITLE MECHANICAL AND ELECTRICAL CHARACTERIZATION OF NOVEL CARBON NANO FIBER ULTRALOW DENSITY FOAM		**5. FUNDING NUMBERS**	
6. AUTHOR(S) D. Chris Daskam			
7. PERFORMING ORGANIZATION NAME(S) AND ADDRESS(ES) Naval Postgraduate School Monterey, CA 93943-5000		**8. PERFORMING ORGANIZATION REPORT NUMBER**	
9. SPONSORING /MONITORING AGENCY NAME(S) AND ADDRESS(ES) N/A		**10. SPONSORING/MONITORING AGENCY REPORT NUMBER**	
11. SUPPLEMENTARY NOTES The views expressed in this thesis are those of the author and do not reflect the official policy or position of the Department of Defense or the U.S. Government. IRB protocol number ____N/A____.			
12a. DISTRIBUTION / AVAILABILITY STATEMENT Approved for public release; distribution is unlimited		**12b. DISTRIBUTION CODE** A	

13. ABSTRACT (maximum 200words)

Concomitant mechanical and electrical testing of carbon nanofiber foam samples, generated using the constrained formation of fibrous nanostructures process reveal the material to be a unique ultra-low-density foam with electrical properties appropriate for application as strain gauge. Samples of CFF, essentially a solid mat of intertwined nanofibers of pure carbon, were grown in a steel mold at ~550 ºCelsius (C) from a variety of catalysts exposed to fuel rich mixtures of ethylene and oxygen. Only those created from palladium (Pd) particle catalysts were found to produce macroscopic objects sufficiently robust for static and dynamic stress/strain tests. Transient and dynamic tests were used to fully characterize the mechanical properties of the novel foam. These tests clearly demonstrated that the material generated from Pd particles has viscoelastic behavior. The foam was subjected to compression cycles over diverse periods of time employing a die to maintain a fixed cross sectional area. The ultralow density material has a modulus of ~3.5 MPa, close to the one encountered in rubber-like substances. Given its carbonaceous nature, the new foam maintains its thermal stability up to 550 ºC in air. Simultaneous resistance/stress/strain measurements showed that there is a linear relationship between electrical resistance and strain that is remarkably consistent over many cycles. The novel ultralow density foam has many potential applications including sensing element of a strain gauge or energy absorber.

14. SUBJECT TERMS Carbon, fiber, carbon nanofiber, viscoelastic, strain gauge, gauge factor, ultra-low-density foam, relaxation modulus, and creep compliance.			**15. NUMBER OF PAGES** 125
			16. PRICE CODE
17. SECURITY CLASSIFICATION OF REPORT Unclassified	**18. SECURITY CLASSIFICATION OF THIS PAGE** Unclassified	**19. SECURITY CLASSIFICATION OF ABSTRACT** Unclassified	**20. LIMITATION OF ABSTRACT** UU

NSN 7540-01-280-5500 Standard Form 298 (Rev. 2-89)
Prescribed by ANSI Std. 239-18

THIS PAGE INTENTIONALLY LEFT BLANK

Approved for public release; distribution is unlimited

MECHANICAL AND ELECTRICAL CHARACTERIZATION OF NOVEL CARBON NANO FIBER ULTRALOW DENSITY FOAM

D. Chris Daskam
Lieutenant Commander, United States Navy
B.S., Florida State University, 2000

Submitted in partial fulfillment of the
requirements for the degree of

MECHANICAL ENGINEER
AND
MASTER OF SCIENCE IN MECHANICAL ENGINEERING

from the

NAVAL POSTGRADUATE SCHOOL
December 2013

Author: D. Chris Daskam

Approved by: Claudia Luhrs
Thesis Co-Advisor

Jonathan Philips
Thesis Co-Advisor

Knox Millsaps
Chair, Department of Mechanical and Aerospace Engineering

THIS PAGE INTENTIONALLY LEFT BLANK

ABSTRACT

Concomitant mechanical and electrical testing of carbon nanofiber foam samples, generated using the constrained formation of fibrous nanostructures process reveal the material to be a unique ultra-low-density foam with electrical properties appropriate for application as strain gauge. Samples of CFF, essentially a solid mat of intertwined nanofibers of pure carbon, were grown in a steel mold at ~550 ºCelsius (C) from a variety of catalysts exposed to fuel rich mixtures of ethylene and oxygen. Only those created from palladium (Pd) particle catalysts were found to produce macroscopic objects sufficiently robust for static and dynamic stress/strain tests. Transient and dynamic tests were used to fully characterize the mechanical properties of the novel foam. These tests clearly demonstrated that the material generated from Pd particles has viscoelastic behavior. The foam was subjected to compression cycles over diverse periods of time employing a die to maintain a fixed cross sectional area. The ultralow density material has a modulus of ~3.5 MPa, close to the one encountered in rubber-like substances. Given its carbonaceous nature, the new foam maintains its thermal stability up to 550 ºC in air. Simultaneous resistance/stress/strain measurements showed that there is a linear relationship between electrical resistance and strain that is remarkably consistent over many cycles. The novel ultralow density foam has many potential applications including sensing element of a strain gauge or energy absorber.

THIS PAGE INTENTIONALLY LEFT BLANK

TABLE OF CONTENTS

LIST OF FIGURES

LIST OF TABLES

THIS PAGE INTENTIONALLY LEFT BLANK

LIST OF ACRONYMS AND ABBREVIATIONS

Ar	Argon
BSE	Back scatter electron
C_2H_4	Ethylene
CFF	Carbon fiber foam
CMC	Carbon micro coils
CNT	Carbon nano tube
CoFFiN	Constrained formation of fibrous nanostructures
ºC	Degrees Celsius
ΔL	Change in length/thickness [mm]
DoD	Department of Defense
EDX	Energy dispersive x-ray spectroscopy
ε	Strain
FLIR	Forward looking infra-red
GF	Gauge factor
GSD	Graphitic structures by design
kPa	Kilo Pascal
L_o	Initial length/thickness [mm]
log	Logarithm
m	Meter
µm	Micrometer
MKS	Meters, Kilograms, Seconds (name of company)
ml	Milli-liter
mm	Millimeter
MPa	Mega Pascal
N	Newtons
N_2	Nitrogen
Ni	Nickel
nm	Nanometer
O_2	Oxygen
Pa	Pascal = [N/m^2]

Pd	Palladium
PDMS	Polydimethylsiloxane
PS	Polystyrene
psi	Pounds per square inch
PTFE	Polytetrafluoroethylene
SEM	Scanning electron microscope
SCCM	Standard cubic centimeter per minute
TGA	Thermo gravimetric analysis
TPO	Temperature programmed oxidation

ACKNOWLEDGMENTS

In the development of this thesis the direction and guidance was provided by Dr. Claudia Luhrs and Dr. Jonathan Phillips. Without their help and instruction through the entire process I would not have been able to complete the amount of work that I had set out to accomplish, nor would I have recognized what all the data I had collected meant.

A grateful acknowledgment to Edwin Gonzalez, an intern from Hartnell College, who was an immense help through several quarters of research. His work ethics and interest in the field were unparalleled.

Learning how to use SEM and achieve pictures that were in focus was a huge undertaking, without the assistance and guidance of Dr. Sarath Menon to help take and focus the SEM photos I used in this thesis.

The visiting professor from University of Colombia, Dr. Hugo Zea, provided research assistance and advice during his visit to Naval Postgraduate School.

To the invaluable team in my office, LCDR Jamie Cook, LT Russel Canty and LT Jason Downs, who kept me sane during the two and a half years I spent studying and researching.

Finally, to my family Yuka and Linn Daskam who supported me through the entire process. Without them, my attention to my work would have been hindered.

THIS PAGE INTENTIONALLY LEFT BLANK

I. INTRODUCTION

A. MOTIVATION

The goal of the research that originated this thesis topic was to develop a material that could be used as sensing element to determine the correct pressure to apply on a wound when using a tourniquet in the absence of a certified nurse or physician.

When open injuries occur during expeditionary operations and immediate care of the wound is required, applying a tourniquet is the most common treatment. However, away from medical personnel, applying a tourniquet with the adequate amount of pressure can be challenging: wound bleeding cannot be stopped if there isn't enough pressure in the bandage and too much pressure could result in lost limbs. Using the right amount of pressure is then paramount for the well-being of the injured person.

Having identified the need for a material that could detect diverse levels of both, static and dynamic loads, with enough sensitivity but meant for low levels of pressure (less than 100 N), our research group proposed to develop a carbon nanofiber porous structure that could be used as the sensing element of a disposable, thin and flexible pressure sensor. With such overarching goal, the central topic of this manuscript is the generation of a carbon fiber tridimensional structure, an ultra-low density foam-like material, herein called carbon fiber foam (CFF), consisting solely of nano-scale carbon fibers and the catalyst particulates used for their growth, along the mechanical and electrical characterization needed to determine its viability for the application proposed.

B. LITERATURE REVIEW OF THE USE OF CARBONACEOUS STRUCTURES FOR USE AS PRESSURE/STRAIN SENSORS

Carbon nanotubes, in particular as single wall tubes (SWCNT), have been demonstrated to present remarkable response as piezoresistive elements [1-4]. Individual tube gauge factors, which can be described as the sensitivity of the sensor, have been reported to reach values up to 1,000 [5]. However, the generation of defect free and homogenous large samples of single wall carbon nanotubes still remains as a problem to be overcomed. Moreover, having nanometer scales, the orientation and position of the

tubes is extremely difficult to control. So far, efforts in this direction have opted for using random assemblies of individual tubes, both as single and multiwall tubes. Examples of such work have found application on finger sensing electronics, flexible touch sensors, micro-switches and micro-electromechanical systems [6-9]. Yet, the sensors based on CNT assemblies have much lower sensitivities than those of the individual tubes mentioned above, typical ensemble piezoresistive sensor have gauge factors up to 22.4 [10]. Thus, new materials that can attain the expected electrical and mechanical characteristics or novel approaches to develop such materials with high yields and repeatable results will be most welcomed.

Other strategies of using carbon fibers and carbon nanotubes to develop sensor devices have been attempted, however the methods used to build the pressure/strain sensors are still quite complex, difficult to reproduce and expensive. All the examples found in recent publications involve the association of carbon structures with polymeric matrices, thus combining the properties of both materials. Some of the individual instances of such composites are: A study that implanted carbon black, graphite powder and carbon fibers into an insulating polymer matrix and then determined the effects of applying tensile and compressive stresses found that the resistance changed when stretching the polymer by 40 percent or compressing with 0.30 MPa and that it returned to its original value when relaxed [11]. Karimov et al. fabricated a pressure sensor based on CNT encapsulated in a plastic casing, finding that the resistance of the sensors did decreased with increasing pressure, [12]. Carbon microcoils (CMCs) have been generated using chemical vapor deposition and sandwiched between layers of polydimethylsiloxane (PDMS) with the objective of creating a sensing element, results revealed that with very small loads, between 0 and 14 kPa, resistance decreased when increasing pressure from 0 to 3 kPa, but increased when increasing from 3 to 14 kPa [13]. Luo et al. created an aligned array of SWCNT using multiple stages of sonication and a spray coating technique, finding that with large tensile strain, ranging from 20–30 percent the CNTs had a compounding effect on the sensor piezoresisitve behavior [14]. Very few efforts in

the field have used carbon fibers instead of tubes to fabricate the sensors and to the best of our knowledge; no research group has used porous fiber structures to attain this objective.

C. PREVIOUS EFFORTS TO PREPARE POROUS CARBON STRUCTURES

As mentioned above, for the application of carbon nanotubes and nanofibers as pressure and strain gauges (or other uses such as chemical sensors, energy absorption structures and electrodes for energy storage devices) the carbon building blocks (fibers/tubes) need to be arranged in particular patterns or intertwined to form macroscopic assemblies. How to attain a high level of control over their geometry, density and how to create an interface with other components has presented a major challenge. A literature review regarding the efforts conducted by diverse research groups to generate three-dimensional carbon fiber based architectures include both, strategies to assemble them during synthesis and attempts to create the connections post-synthesis. From the former category, CVD generation of CNT has proven an effective way to fabricate dense arrangements of disordered, patterned and aligned tubes into substrates [15–17]. However, despite the products presenting the desired electrical properties, none of those approaches generated highly porous mechanically robust tridimensional architectures. The post-synthetic routes to generate low density structures are dominated by techniques that use of solvents to align nanotube forests, foams or cellular structures aided by the capillary forces that are present as the solvent evaporates [18, 19]. CNTs arrays have also been transferred and aligned into a substrate using low temperature soldering [20]. Efforts to produce low density 3D foam structures have been accomplished as well by the use of monolayer and multilayered silica templates [21], high frequency pulses of electrical discharge to machine targeted shapes [22, 23], radical initiated thermal crosslinking of CNT [22, 23], focused laser beam used to locally burn regions of a dense forest [24] and chemical processes to stitch CNTs together [18].

D. THESIS OUTLINE

This manuscript includes an Experimental Methods chapter that describes all the precursors, protocols and conditions employed for the materials preparation and their

characterization, including a section that refers to the particular instruments used and the testing conditions. The Results chapter presents all the data gathered, from images of the materials as produced, characterization by electron microscopy and thermal analysis, to the mechanical and electrical results conducted in transient and dynamic conditions. A Discussion chapter addresses the evaluation of the data, mechanisms observed and in general, analysis of results. The last chapter, Conclusions, summarizes the milestones achieved and suggests next steps to further the research. The detailed materials fabrication protocols are included as appendix.

1. Thesis Objectives

a. Develop the a viable protocol for growing carbon nanofibers into a foam-like structure capable of withstanding electrical and mechanical testing using a variety of catalysts, gas combinations and temperatures for growth.

b. Perform an analysis of the fiber foam microstructure, as prepared, using electron microscopy techniques and determine its stability over a range of temperatures.

c. Conduct simultaneous electrical and mechanical characterization of properties for CFF, using transient and dynamic loading conditions with both small and large loads ranging between 10 and 90 N.

2. Hypotheses

a. A highly porous carbon substance, having intertwined carbon nanofibers as main structural component, could be grown from Ni or Pd powder catalyst to form a single macroscopic body, foam-like tridimensional structure.

b. The fiber foam will respond to changes in applied load or strain by changing its electrical resistance. The individual nanofibers response will have an effect on resistance that could be measured in the macroscopic object.

c. The effect of applying a load or modifying the strain will present a linear change in the resistance values.

3. Tasks to be Conducted

Employ Ni or Pd as catalyst for carbon growth, either as nanoparticles or deposited as a salt that will, through thermal treatments in diverse atmospheres,

decompose into elemental Ni or Pd. Use ethylene as hydrocarbon for carbon nanofiber structures generation along moderate temperatures.

Generate carbon nanofibers, using diverse conditions of synthesis, to produce a mat of carbon, a carbon foam or any other tridimensional structure of carbon with empty spaces or high level of porosity.

Determine which catalyst produces the optimal microstructure in the generated carbon product. Criteria to select catalyst will include final fiber dimensions, their degree of crystalinity, yield, number of interconnects among fibers and ability to withstand electrical and mechanical testing. Scanning electron microscopy characterization techniques will be used in this step.

Use a matrix of carbon micron sized fibers or silica cloth as support for nanofibers in order to generate a material that preserves its shape rather than a powder aggregate. Employ a high temperature resistant steel container as a volume to fill.

Integrate a mechanical testing system, equipped with low load cells (5N to 100N), with a multimeter in a fashion that will allow the samples of carbon tridimensional structures to be attached to electrical connectors and measure resistivity while they are subject to compression tests.

Measure changes in the sample conductivity as pressure is applied or as space between fibers is reduced and more physical contacts among nanomaterials are created for each of the samples described above. Use transient and dynamic conditions for testing.

Determine reproducibility of results and explore the possibility to use the material in a number of cycles of compression.

Include fibers in a small prototype that includes a layer to isolate the fibers, electrical connections and a display to show diverse levels of pressure as sample is compressed.

4. Contributions of This Work

A carbon foam was fabricated using the constrained formation of fibrous nanostructures process (CoFFiN), which creates a solid mat of carbon fibers that are intertwined at the nanoscale level. The most remarkable characteristic of the material is that at macroscopic level it has the appearance and mechanical characteristics of a viscoelastic foam. Moreover, being carbon the main building block, the resulting product is an electrical conductor and is thermally stable at much higher temperatures that its polymeric counterparts. It is worth noting that, in contrast with the work summarized above, no binders, polymeric matrices or linking additives were needed to produce the CFF or to keep the fibers attached to each other.

The constrained formation of fibrous nanostructures process was developed as a variation on graphitic structures by design (GSD) technology [25, 26]. The primary distinction between those two routes is that the former, used in this thesis, confines the fiber growth to a mold, allowing in theory, the growth of CFF of virtually any shape. The starting catalyst selection and conditions employed to generate the foam, particularly temperature, gas flow rates and reaction times, enabled a high level of control over fiber diameter and solid density. Indeed, the optimal conditions for the carbon fiber growth are based on a substantial body of earlier work conducted by members of our team on the mentioned graphitic structures by design methodology [25, 26]. In such earlier publication it was demonstrated, for CoFFiN materials, that there is a relationship between applied stress and electrical resistance, but the data was insufficient to fully characterize all features, or even to clearly identify the macroscopic class of materials to which these foams belong. Moreover, the mechanical properties were only partially characterized. In this work, a range of transient and dynamic conditions were employed to determine relaxation modulus, stability over time, Poisson ratio, stress and strain versus resistance, gauge factor, etc. The data from the present work permits the following points to be clearly elucidated: i) CFF on the macroscopic scale behaves precisely as a viscoelastic, and is not simply elastic, ii) Only after repeated cyclic compression, that is ‘mechanical aging’, do mechanical and electrical properties stabilize, iii) the material is

not, despite earlier suggestion, particularly suited for use in a pressure gauge, but iv) the material is suitable for use as the sensing element in a strain gauge.

THIS PAGE INTENTIONALLY LEFT BLANK

II. EXPERIMENTAL METHODS

A. OVERVIEW

Experimental methods will cover the preparation and fiber growth methods, based on the constrained formation of fibrous nanostructures (CoFFiN) process used to create a carbon fiber foam, also known as a non-woven carbon fiber fabric, of size and shape appropriate for mechanical testing. The characterization methods used to determine its mechanical properties and to correlate applied pressure and strain with electrical resistance are also included.

One of the key objectives of this study was to optimize a protocol for carbon fiber foam synthesis that could be used as a durable sensing element in a pressure or strain gauge. It was determined that, at a minimum, these properties would be needed: i) the macroscopic object should not break by the cyclic application of small loads (100N) ii) the material could be synthesized in any shape, iii) could be cut without losing integrity, iv) could return to its original shape after repeated compressions, v) had a nearly linear relation between strain and/or stress and resistance over a wide range of strain and /or stress (ca. >50 percent) and vi) retained a consistent relationship between strain and/or stress and resistance over many compression cycles. The first step was to fully characterize the mechanical properties, then explore the relationship between physical and electrical properties and the synthetic approach.

B. GROWTH OF CARBON FIBER SAMPLES

1. Furnace Setup

In all cases studied herein, the growth process employed was a variation on the graphitic structures by design protocol described in detail elsewhere [25, 26]. The key to this process, as shown in earlier work, is the catalyzed growth of solid carbon structures from radical species formed homogenously during a fuel rich combustion process. Using the earlier work as a guide, the following growth conditions were selected: a fuel rich mixture of ethylene and oxygen was flowed over metal particles, or metal salts, spread at the bottom of a steel mold. The mold was placed near the center of an 18” long tube

furnace that was held at 550 C. Moreover, the flow rates of the three gases, nitrogen (diluent), oxygen and ethylene were carefully selected such that the residence time, at the mold entry, of the combustion mixture was at an optimum for fiber foam growth. It should also be noted, that the choice of palladium Aldrich submicron >99.9 percent or nickel Aldrich, 3µm 99.7 percent and Aldrich, <100 nanoparticles 99.9 percent) catalysts, and the furnace temperature were also selected on the basis of earlier growth studies. These studies clearly show that Ni and Pd based catalysts are probably the best, and that in general the growth rate is highest at ~ 550 ºC. As outlined below, one major finding of the current study is only palladium catalyzed fiber foams have the desired physical properties. Appendices A, B and C described the step process to generate CFF from nickel nanoparticles, palladium salt ($Pd(NO_3)*H_2O$) and palladium respectively.

For the growth of the carbon nanofiber foam a catalyst was placed into a boat, made of 304 stainless steel, which constrained the volume for the fibers to grow and promoted their interweaving, shown in Figure 1.

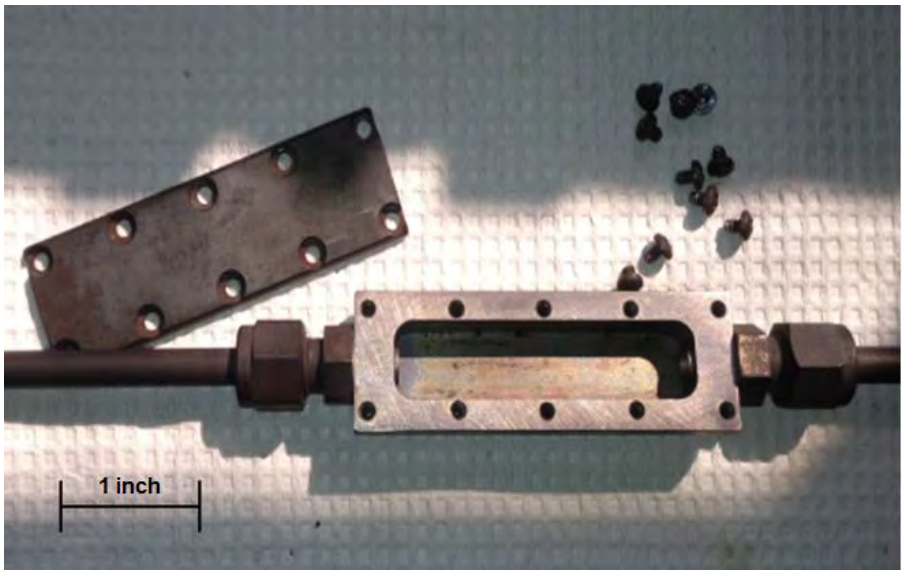

Figure 1. *Mold for CFF Growth*. The cavity (~0.35" x 1" x 2.25") in the stainless steel mold was filled with catalyst, the top fastened, and then placed, near the center of an 18" long tube furnace. The catalysts employed, and protocol for growing foams is provided in the text. Successful growth resulted in the production of foams that completely filled the cavity.

This boat was connected to a mass flow controller in order to precisely regulate the amount of each gas being passed through the boat and across the catalyst. The mass flow controller can be seen in Figure 2. The operation control manual developed for the laboratory can be seen in Appendix D.

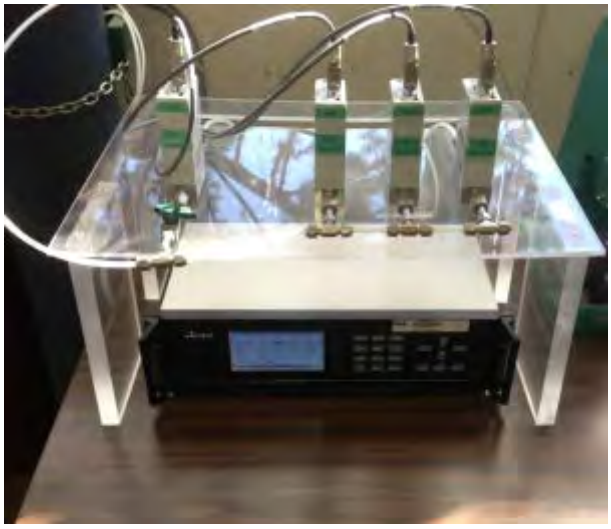

Figure 2. *Gas Flow Control*. An MKS mass flow controller model MKS 647a (shown), was used to control the flow of gasses into the furnace.

The boat was then placed into a quartz tube in order to prevent the boat from touching the thermocouple or heating elements inside the furnace. The quartz tube was then placed into the Lindberg/Blue Mini-Mite furnace shown in Figure 3.

Figure 3. *Furnace*. For all CFF growth, the mold pictured in Figure 1 was filled with catalyst then set horizontally in an 18" x 2" diameter Lindberg/Blue Mini-Mite furnace (shown).

Once the tube has been placed into the furnace such that the heating element was under the boat, then the procedures laid out in the appendices were used in order to promote growth.

2. Catalyst and Growth Processes

a. Overview

Carbon Nanfibers Grown from nickel and palladium went through many different iterations before the final growth on pure palladium provided a viable foam that could be used for compression testing.

b. Carbon Nanofibers Grown with a NickelCatalyst

For the initial carbon fiber foam growth we used the nickel power. One hundred milligrams of the nickel powder was measured and placed evenly around the bottom of the boat. The boat was then sealed and leak tested. Then it was attached to the MKS mass flow controller and placed inside the furnace. Three hundred SCCM of nitrogen gas was then used to flush oxygen (air) from the system. This nitrogen flush was conducted for 20 minutes after which the furnace was set to 350ºC. Once at the desired temperature the nitrogen was then turned off and an argon hydrogen mixture was turned onto provide 20 SCCM for 30 minutes. The argon hydrogen mixture was used to assure that the metal catalyst was fully reduced. The growth step involved the use of 30 SCCM of nitrogen, 42 SCCM of ethylene (source of carbon) and 3 SCCM of oxygen. The oxygen flow was increased from 3 to 15 SCCM over a period of 10 minutes. The temperature was then raised to 550ºC in order to start the growth. After one hour of growth the furnace was turned off and a flow of 30 SCCM's of nitrogen was maintained until cooled to room temperature. Fans were used at this point to expedite the cooling process [26].

c. Carbon Nanofibers Grown Over Carbon Fabric Mat with Nickel Catalyst

In some cases both, catalyst particles and a carbon mat were placed in the mold. The mat employed was a plain weave ultra-light carbon fiber fabric, model number

2363-A from FibreGlast Developments Corporation. This fabric was cut to the shape that would fit inside the boat, as shown in Figure 4. The mat was used "neat," in which case the individual fibers in the mat were covered with a sizing material, and the mat was used after being treated to remove the sizing. The term sizing refers to an organic mixture that commonly covers the surface of commercial fibers prepared by extrusion or injection processes. The step to remove the sizing consisted of heating the carbon to 525 ºC in 100 SCCM's of oxygen for one hour to turn the organic material into pure carbon. After the system cooled to room temperature, the mat was rinsed with ethanol and then heated to just over 100 ºC in order to remove any residue alcohol. A heating plate and the ceramic dish shown in Figure 4 were used, while the temperature was monitored using a thermal imaging camera FLIR xi series.

The temperature used to remove the sizing was chosen after a TGA test was performed on the carbon mat to determine at what temperature breakdown of the sizing in the carbon mat occurs. From the data in the TGA it was determined that the decomposition of the carbon mat by reaction with air or oxygen containing atmospheres starts at 600ºC. Therefore the temperature of 525 ºC was chosen to maintain a defined margin in order to prevent the mat from breaking down and loosing mass and removing only the organic component.

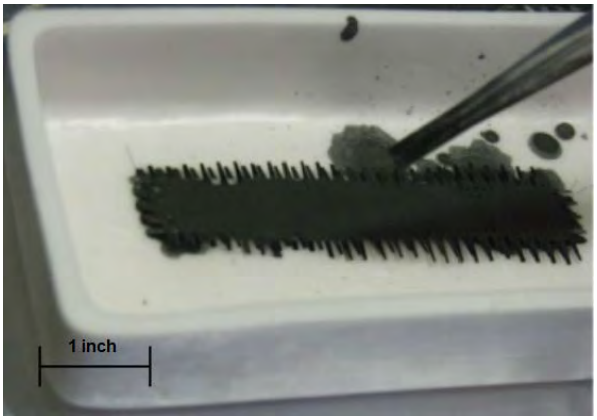

Figure 4. *Carbon Mat*. The process of adding nickel catalyst solution by pipette to carbon mat (~ 2¼ x ½ inch) is shown.

After the carbon mat's sizing was removed, nickel catalyst was well mixed in 10 ml of deionized water. After mixed it was slowly added using a pipet to the mat as shown in Figure 4. The drops were added over a 10-minute period allowing time for the liquid to evaporate. This process, known as wet impregnation, was used in order to achieve a homogenous deposition of nickel particles across the carbon mat. During the process, the mat was maintained between 100–110ºC, on a hot plate while the temperature was monitored using the FLIR camera. The growth process used with the carbon mat was the same one used in the process without the mat. The nickel growth procedure used is described in Appendix A.

d. Carbon Fibers Grown From Palladium Salt

In all earlier studies by Phillips et al. [25, 26], carbon fiber foams were grown from palladium powder. Given the characteristics of the nickel grown fibers, which as will be shown below formed agglomerates that tend to crumble, it was decided to test the use of palladium particles. In this study, two different palladium catalysts precursors were employed: palladium nitrate-hydrate and palladium particles.

We used the stoichiometric amount of palladium nitrate hydrate to produce 50 mg of palladium as product; therefore 160 mg of the palladium nitrate were mixed with 10 ml of deionized water and sonicated until the salt had completely dissolved. The 2510 Branson sonicator used is shown in Figure 5.

Figure 5. *Catalyst Mixing*. Branson 2510 sonicator utilized to mix nickel catalyst in water.

The aqueous solution containing the dissolved palladium nitrate was applied in the same manner to the carbon mat as the nickel was as shown in Figure 4, by wet impregnation. The mat was then placed into the boat. The boat was connected to the same manner as in the nickel process. The palladium salt procedure shown in Appendix B was used to grow the carbon fiber foam.

e. Carbon Fiber Growth from Pure Palladium Particles

Pure palladium catalyst was employed to grow carbon fibers. No woven mat was used in the process. For the pure palladium only 20 mg of powder was used, such was arranged inside of the boat as shown in Figure 6.

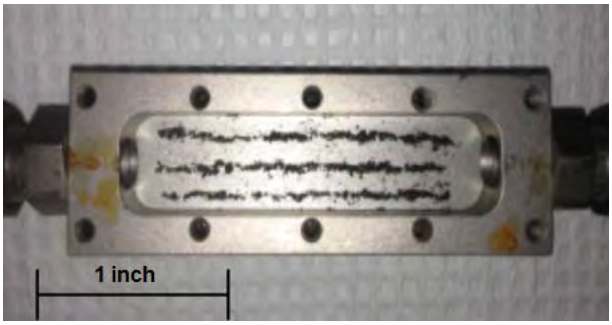

Figure 6. *Catalyst Geometry*. Arranging Pd catalyst particles in the mold (Figure 1) as shown, was found to be a necessary part of the protocol required to create, based on visual inspection, homogenous CFF.

In order to remove the environmental air in the chamber, we used a flow of 100 SCCM of nitrogen gas. This flush was performed while with furnace warmed up to 550°C. After the temperature had reached 550°C the ethylene was turned on to 15 SCCM and the oxygen was turned on at 5 SCCM. After five minutes the oxygen flow was increased to 10 SCCM. After an additional five minutes the oxygen was again increased to 15 SCCM. During the run the nitrogen flow was not changed. After two hours and 45 minutes ethylene, oxygen and the furnace were turned off. Small fans were used at the ends of the tube to help expedite the cooling process. While cooling the nitrogen gas was maintained at 30 SCCM.

From the five procedures described above to grow carbon fibers, only the one using pure palladium particles produced a sample with the desired characteristics. The characterization methods to determine mechanical properties and their relationship with electrical properties described below only refers to samples made by such precursor.

C. CHARACTERIZATION OF CARBON NANO-FIBER FOAM AS PRODUCED

1. Scanning Electron Microscope

In order to characterize the topography of the samples a Zeiss Neon 40 High Resolution Scanning Electron Microscope (SEM) was used to conduct electron microscopy. Images of all the different samples were taken at diverse magnifications and are discussed in the results chapter. Carbon fiber foam samples were attached to an aluminum sample holder after which the samples were placed under vacuum to allow all gases to be removed from the sample. A field emission gun was used to generate an electronic beam with a potential of 10 kV and 20 kV for most samples tested. The images were examined for fiber size and density of fibers within the foam.

2. Thermogravimetric Analysis

Thermogravimetric analysis (TGA) is a method used to determine the temperature effect on the mass of a product. It was used on the carbon fiber mat in order to determine at what temperature the sizing was removed and to perform a temperature programmed oxidation (TPO), to study the stability of the products under oxygen containing atmospheres. The TGA utilized for testing was the Netzsch STA 449 FE Jupiter. The samples analyzed for sizing removal were tested with a flow of 50 ml/minute O_2 and 50 ml/minute Ar purge and a 20 ml/minute Ar protective and a temperature of 0 to 800 ºC with steps of 10 ºC/minute. The TPO study was conducted under an Ar/O_2 80 percent/20 percent atmosphere over similar temperature and heating rates.

D. MECHANICAL PROPERTIES

In order to mechanically characterize the carbon fiber foam, several different test methods were employed: dynamic; with variable loads changing at different rates over

time, and transient; with static loads maintained as a function of time. The tests were also conducted under two different sample cross sectional conditions: unconstrained; where samples dimensions were allowed to vary as response of compression loads, and constrained, using a mold described in the sections below.

1. Equipment Set Up

Both the dynamic and transient tests were studied using the INSTRON 5942 shown in Figure 7. This was used with the 100 N cell and anvils and was configured in order to apply a compressive force onto the carbon fiber foam sample.

Figure 7. *Mechanical Testing Apparatus*: An INSTRON 5942 Compression/Tension tester (shown) was used in all transient and dynamic stress/strain tests of CFF samples.

2. Loading

A transient test was performed on the fiber foam in order to determine resistance under static loads, and was held for approximately two hours. Samples of carbon nanofiber foam were cut into a small rectangular pieces that would fit into the INSTRON. The dimensions of the pieces ranged between 4 and 10 mm in width, while the other two dimensions were set by the shape of the boat at 13mm wide and 9mm deep. The compressive force was selected to remain between 10 and 90 Newtons. The lower limit was selected in order to prevent the carbon nanofiber foam from losing contact with the anvil and copper tape while the upper limit was chosen to prevent reaching the 100 N automatic cutout limit on the instrument used in the test. (Note: One pound force is approximately 4.45 Newtons)

Transient tests were performed on several samples. The INSTRON was programed in order to provide and maintain a constant load. This load was preprogrammed at a designated speed to both reach and maintain the programmed load for a predetermined length of time.

Extended transient tests were performed in order to get an understanding on how the carbon fiber foam would react under a long term pressure. These holds were set at 90 Newtons and held for over 72 hours. The characteristics and results of the transient tests are discussed in the results chapter.

Cyclic tests, generally known as dynamic tests, were performed via programming the INSTRON to raise the pressure to a pre designated value and then to cycle between that pressure and a second designated pressure. The cycle frequency was controlled by setting the linear strain speed to the desired millimeter per second rate, typical values used were 0.01 and 0.05 mm/second. Pressures were cycled between 10 to 40, 40 to 90 and 10 to 90 Newtons, in order to characterize the material at both higher and lower cycling pressures. The cycling was conducted both with the unconstrained samples and with those constrained with the plexiglass device discussed in the next paragraph.

The stress-strain results from the dynamic tests clearly show i) the material is a viscoelastic and ii) the mechanical properties of the viscoelastic do not stabilize until the

material has been cycled at least 10 times. That is, there are clear hysteresis loops in the stress stain curves. As discussed in more detail in the Results section, the electrical studies showed no hysteresis. There is a single value, linear relationship between strain and electrical resistance. However, this is not true of the relationship between the resistance and stress. In this case, a single value of resistance can be found to correspond to two different stress levels, one for the 'load' portion of the cycle and one for the unload part of the compression cycle.

Tests were also conducted on samples that were confined. That is, orthogonal extension during compression was eliminated by placing the sample in a plexiglass ring, Figure 8. The use of the Plexiglas created a need to change both the shape of the sample being compressed and the method at which we measured the resistance. Up until this point we had been using rectangular samples, however in order to find a uniform shape that would be more usable and easier to develop a method of holding the sample the circular shape was adopted. This circular shape was made to match the size and shape of the two anvils shown in Figure 8. These anvils were then used to maintain the pressure on the carbon fiber foam while it is compressed inside the plexiglass. The anvil then became the point of contact with the copper wire used to measure the resistance of the carbon nanofiber foam and therefore the resistance of the anvil needed to be measured in order to determine its effect on the results of the electrical testing. The resistance across the anvils was found to be approximately zero ohms using a FLUKE, a handheld resistance tester, and therefore is ignored in the results discussion. These anvils were needed in order to compress the carbon fiber foam inside the plexiglass, since the foam does compress into a very thin foam when under a load of 90 Newtons.

Figure 8. *Mechanical Constraint*: In order to prevent lateral strain CFF buttons (four shown) were place in a plexiglass anvil (shown) before testing in the INSTRON (Figure 7).

In order to prevent the Plexiglas from resting on the lower anvil of the INSTRON 5942 it is raised using a rubber gasket and its set up can be seen in Figure11. The two smaller anvils that fit into the Plexiglas, also shown in Figure 8 where placed in contact with the upper and lower copper tapes in order to complete the circuit through the carbon fiber foam.

The confined compression results were not fundamentally different from the unconfined results. In particular, in all cases a hysteresis loop characteristic of viscoelastic material was observed, only the parameters, particularly the elastic modulus were found to increase for the confined material. In order to determine if the electrical signal was in any fashion a function of contact resistance, a variation on electrical connection was employed. Specifically, silver paint was employed around the edges of the sample, rather than a copper wire, to make electrical contact with the CFF samples. A couple of different paints were used but only No. 1481 Silver Paint, one half Troy ounces (oz) (Ernest F. Fullam, Inc.) was found to be sufficiently robust to tolerate repeated cycles. No significant impact of the electrical contact method was discovered.

In order to provide a comparison to a different type of carbon compound, Grafoil was used. Several cuts of Grafoil can be seen in Figure8, and are approximately 0.33 mm

think. Tests of its resistance were measured from 10 to 40 Newtons on one, through four of these pieces placed on top of each other. Resistance graphs can be seen in the results chapter.

3. SEM Tension/Compression

The SEM compression/tension tester shown in Figure 9 was used inside and outside of the SEM to conduct compression tests of the carbon fiber foam.

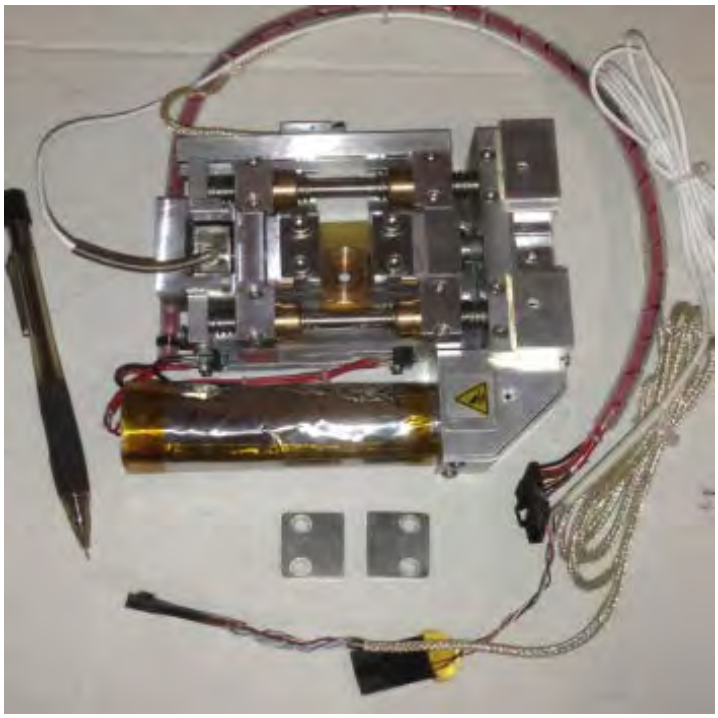

Figure 9. *Microscope Mechanical Tester*: SEM compression/tension tester (shown) permitted SEM images to be acquired of CFF samples under specified specific levels of stress.

This tester was used with the compression grips installed also shown in Figure 9. The device was able to be used inside the SEM and able to provide much higher pressures than the INSTRON 5942. We were able to achieve up to 300 pounds on our sample (the equipment limit of 1,000 pounds). This pressure reached the cutoff point due to the sample becoming too thin to provide any higher resistance to the pressure and reached the minimum allowed distance between the compression anvils. The device

shown was connected to the MTII/Fullan SEM tester DAQ data acquisition system that works with the Mtest Quatro software, all of which were acquired from MTI instruments. Due to interference from the frequency of the motor used to maintain position and move the compression anvils, this device did not work to our required specifications. This interference caused images on the SEM to flicker and move around and caused the photos to be unusable. In order to create a work around the motor was sent back to the manufacturer who grounded the motor to the main box. This helped to improve the images but the images were still unusable and flickered at any magnification. The next step was to create a metal shield around the motor. The motor is the tube shape at the lower side of the tester as shown in Figure 9, and the shield used is installed on the motor as shown. The shield is a thin piece of foil wrapped loosely around the motor. This shield provided enough protection that some useful photos were able to be taken and are shown in the results chapter.

E. ELECTRICAL PROPERTIES

In order to electrically characterize the carbon fiber foam the changes in the resistivity of the carbon nanofiber foam was measured during the mechanical testing described above.

1. Equipment set up

In order to measure the resistance characteristics of the carbon fiber foam an Agilent 34410A 6 ½ Digit Multimeter shown in Figure 10 was used. This was connected to a computer with the Agilent software package that came with the multimeter that uploaded all the data into Excel. All resistance data was then recorded in Excel, which allowed the data to be graphed.

Figure 10. *Resistance Measurement*. An Agilent 34410A 6 ½ Digital Multimeter (shown), was used to measure the resistance across the carbon fiber foam samples as a function of time in both transient and cyclic tests.

In order to connect to the multimeter while at the same time electrically isolate leads from each other and from the metal anvils, a barrier between the wire connecter and the anvil needed to be installed. Clear tape was wrapped around the metal ends of the anvil thereby electrically isolating them from the electrical connections to the carbon fiber foam.

In order to connect the ends of each of the sides of the carbon fiber foam they were clipped onto copper wires, which were then draped through the connector, using alligator clips, as shown in Figure 11. This reduced the weight on the wire connections to avoid pulling, and it assisted in keeping the ends from touching each other and remain isolated. In order to prevent the wire from causing an uneven force on the carbon fiber foam copper tape was used as the connection to the carbon fiber foam. This copper tape was applied to the two anvils and then wrapped around the ends of the electric wires that were connected to the multimeter. This provided a flat surface for the carbon fiber foam to be compressed with, while maintaining electrical contact with the sample.

Figure 11. *CFF Resistance*. CFF samples were placed in the Instron such that each side of the sample was firmly in contact with copper tape attached to the Instron anvils. Measurement showed the only significant resistance was in the CFF.

2. Resistance Measurements

Both the transient and dynamic tests were performed while measuring the changes in resistance of each sample tested. Transient tests were performed in order to determine how the carbon nanofiber foam would change under a steady value of stress and a constant strain. Dynamic tests were performed in order to measure the changes in resistivity during a continuous cycling load. Both of these tests were performed both constrained and unconstrained.

During the tests the small carbon nanofiber foam samples were placed on the anvil where they would be in full contact with the copper tape on both the top and the

bottom in order to maintain a complete circuit with the multimeter. This provided the contacts in order to measure the resistance during the tests.

F. ENVIRONMENTAL TESTING

For the applications envisioned (wound dressing pressure measurement), the fibers will need to be encapsulated and will never become in contact with environmental components. However, in order to determine how the fiber foam properties will change if in contact with sweat, water or oil, that would be potential environments for an operating device if encasing broke, tests were performed to observe the affinity of the foam to those substances. A small sample was cut and tested by putting drops of water onto the sample, after which saline was used as a salt water substitute for sweat. Finally to determine the effect of oil, a vacuum oil, PFEIFRER D-35614 Asslar Oil P3, was used. Results of these tests are discussed in the results chapter.

THIS PAGE INTENTIONALLY LEFT BLANK

III. RESULTS

As described in detail in the Experimental Section, on the basis of earlier studies of the graphitic structures by design [25, 26] process, near optimal conditions of temperature and gas flow were employed for the rapid growth of carbon fiber foams in a rectangular steel mold. The studies carried out in the present work were intended to further delineate optimal growth conditions for a specific outcome: production of carbon fiber foams that are mechanically robust and produce a consistent signature for electrical resistance as a function of stress and/or strain over many compression cycles. Among the parameters studied were metal catalyst identity, particularly Ni versus Pd, form of the metal, specifically metal salt versus metal particles, and the inclusion of a preformed mat in the mold during the growth process.

The primary results are briefly summarized as follows. First, only material made using specific catalysts were mechanically stable (Section A). Second, mechanically stable samples of CFF clearly behave as viscoelastic material as shown by the fact that after appropriate aging, a repeatable hysteresis loop is observed in the stress-strain relationship (Sections B). Third, there is a linear relationship between electrical resistance and strain that becomes remarkably stable after only a few cycles (Section C). The stability and resistance behavior of fiber foams produced under the best conditions studied were also found to be a function of other factors such as the use of a Plexiglas ring to prevent orthogonal strain and the method used to attach the fiber to the compression fitting. However, these changes in protocol did not change the basic phenomenology, only the value of certain parameters such as the material modulus.

A. GROWTH RESULTS

1. Nickel

As demonstrated by repeated trials, the product produced using Ni particle catalyst crumbled when removed from the mold. The product was very brittle and did

not maintain its shape when removed. Thus Ni catalysts do not produce a foam-like substance suitable for electrical resistance testing due to its inability to maintain a shape. The resulting samples can be seen in Figure 12.

Figure 12. *Ni Catalyzed CFF*. CFF grown using Ni particle catalysts (shown) were extremely brittle and shattered during removal from the mold.

The results of all growth using nickel as the catalyst turned out similar to the shown in Figure 12, therefore nickel was ruled out as a good catalyst for growth of carbon fiber foams.

The growth of the nickel catalyst was inspected using the SEM. Inspecting the size of the fibers and particles, and the density of the fibers within the foam.

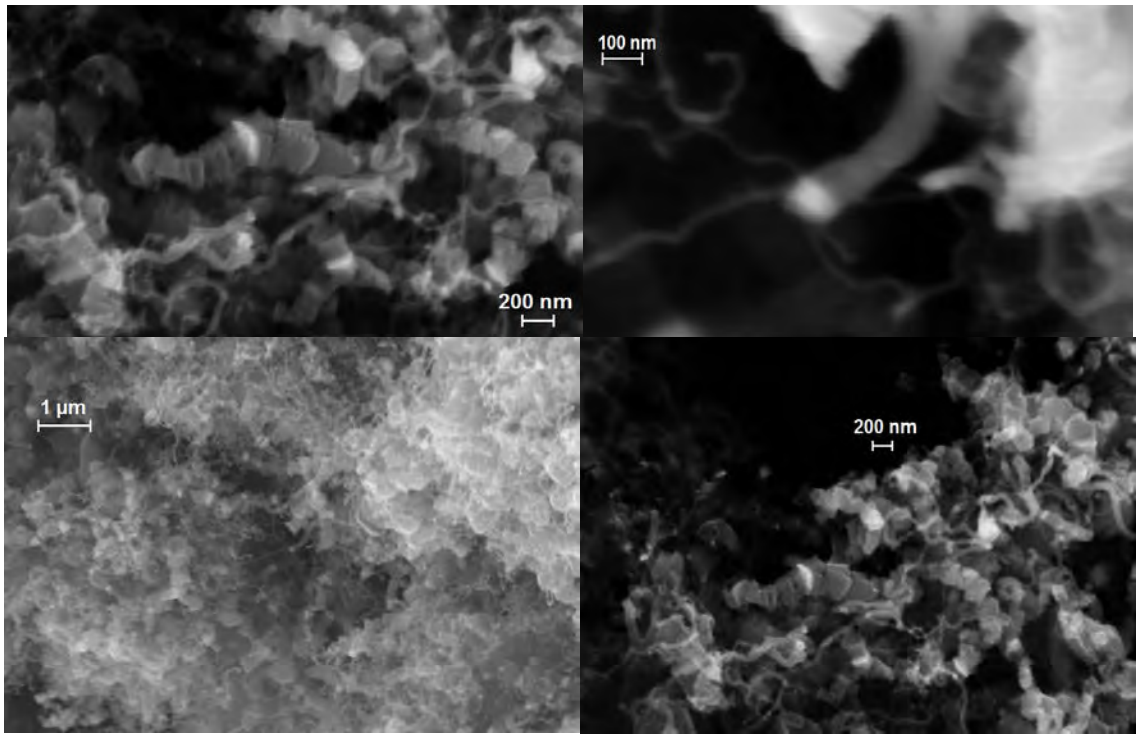

Figure 13. *SEM of CFF from Ni Catalyst*. Fibers in 'CFF' grown from Ni catalysts were found to be very short (ca. <500 nm), many with very small diameters (ca. <20 nm), and more than half of the carbon was not in the form of fibers at all, but rather irregular 'masses'. Top left, taken at 30,000 x magnification; top right 80,000 x bottom left 10,000 x bottom right, 20,000 x. All photos taken at 10 kV.

In the top right photo of Figure 13 it can be seen that the fibers vary in size in the sample. The largest shown is approximately 100 nm in width, while the smallest are approximately one tenth that size. The bright tip of the fiber in the picture located in the top right corresponds to the nickel particle that gave origin to the fiber.

2. Palladium Salt

Palladium salt catalysts where reduced to palladium metal during the preparation process, thus they also produced material that crumbled when removed from the boat. The general morphology seen in Figure 14 was somewhat less fragile than that produced using direct commercial nickel particle catalysts.

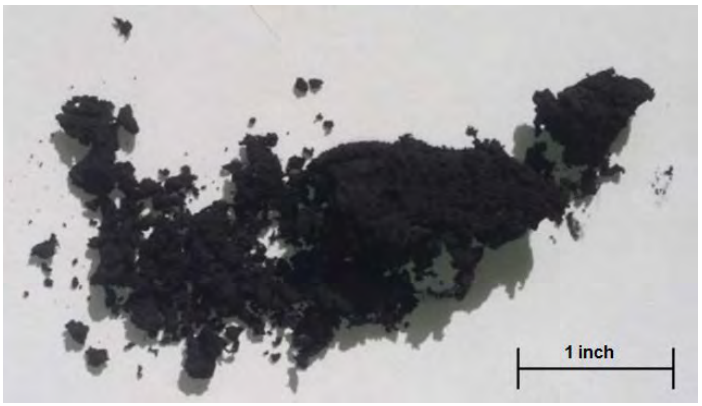

Figure 14. *Pd Nitrate Catalyzed Foam*. CFF grown from Pd nitrate (shown) did not form a large cohesive body. The material appeared to have compression characteristics similar to those observed for CFF formed from Pd particles, but never formed a single body of mold size, but rather only small pieces.

Still, after repeated trials it was clear fiber foams created using palladium generated from salt precursors were not sufficiently robust for mechanical testing.

In order to understand the differences between fiber foams grown using different catalysts, fiber foams grown using palladium salt precursors, which turn into metallic palladium as part of the growth protocol, were inspected using the SEM. Looking for the size of the fibers and particles, as well as the dispersion of the fibers throughout the sample. In the top right photo of Figure 15 that the fibers vary in size from 10 nm and approximately 100 nm, the same range found in fiber foams created with Ni catalyst.

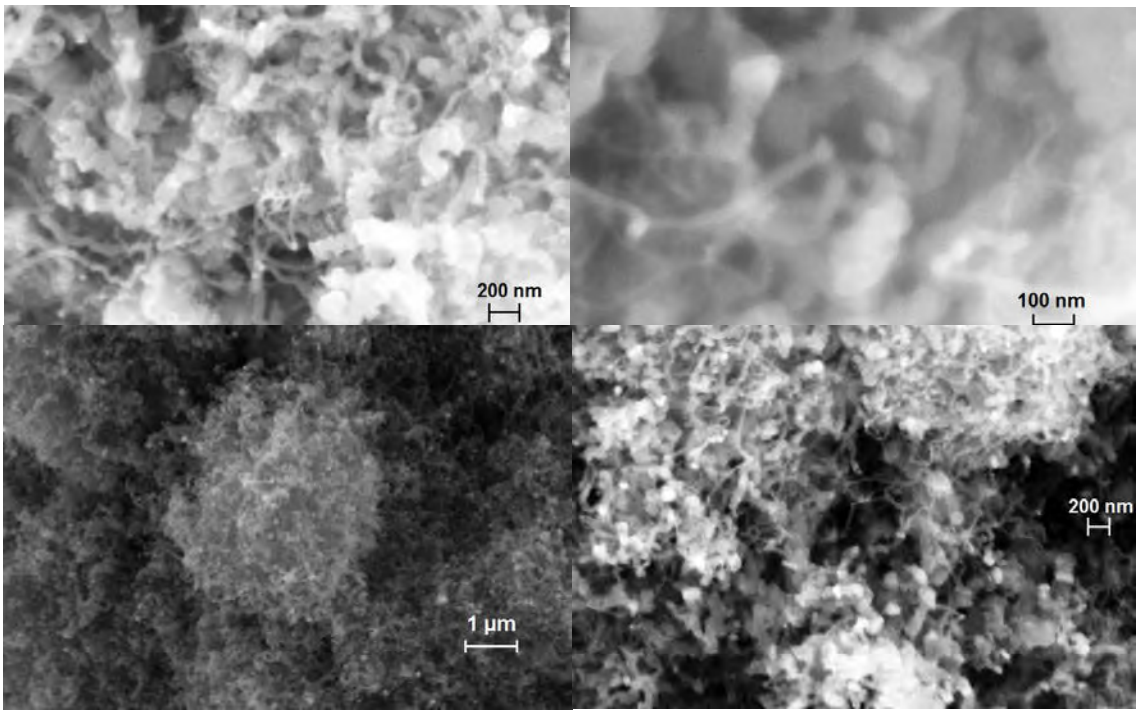

Figure 15. *SEM of CFF from Pd nitrate Catalyst*. Fibers in "CFF" grown from Pd nitrate (shown) were found to be very short (ca. <200 nm), and to be of very small diameter (ca. <20 nm), but in contrast to growth from Ni particles (Figure 13) most of the material was in fiber form. Top left, taken at 30,000 x magnification; top right, 80,000 x; bottom left 10,000 x; bottom right, 20,000 x. All photos taken at 10 kV.

3. Carbon Mat

Both the bare nickel and palladium salt were tested dispersed in a carbon mat. The addition of the carbon mat provided an improvement in maintaining a solid carbon fiber porous object once the sizing of the mat was removed. An image of the results of adding a carbon mat can be seen in Figure 16.

The use of the mat as a filler during the growth process resulted in macroscopic objects that maintained their shape much better than the ones without the mat, however the sample was still quite brittle, and many pieces broke off the mat during removal from the mold.

Figure 16. Carbon fiber foam grown on a carbon mat shows the brittleness of the sample.

However this product still was too brittle to be used in pressure testing, hence the use of a mat to improve durability was judged to be unsuccessful.

4. Pure Palladium Particles

The pure palladium catalyst provided the most solid form without the need of a carbon mat substrate. The carbon fiber foam grown using the pure palladium catalyst can be seen in Figure 17.

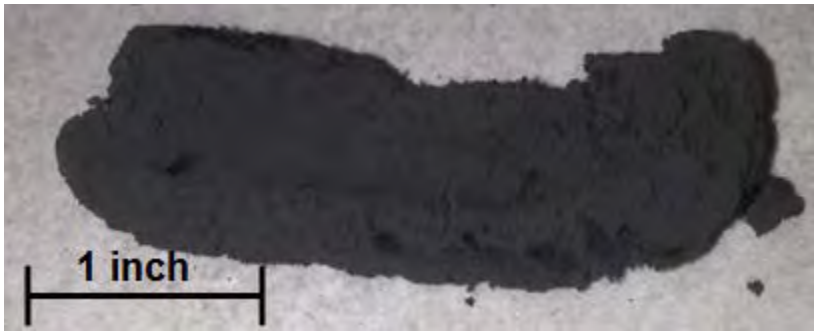

Figure 17. Carbon fiber foam grown on pure palladium. Successful shape with very little crumbling as shown.

The foam generated with pure palladium particles was easily cut into smaller shapes. The behavior while cutting with a razor blade was comparable to cutting into Styrofoam. The product maintained its shape during cutting, and apparently no 'flakes' were produced by the cutting process. Many different shapes were cut from the product. Hence, growth from pure palladium particle catalysts was determined to be the only

viable process, of those tested, for creating a low density, highly porous tridimensional structure (foam) suitably robust for possible use in a sensor or strain gauge.

The fiber foam grown from pure palladium particle catalyst was inspected using the SEM. As shown in Figure 18 the fiber size ranged from approximately 100 nm to 400 nm in width, much larger than those grown from nickel particle and palladium salt catalysts. Moreover, there are very few fibers with a diameter of less than 100 nm. Clearly, the majority of the fibers are around 100 to 150 nm in width. This image demonstrates how the gaps and spaces between the fibers decrease while under pressure. This causes a decrease in the resistance of the material as the load in increased.

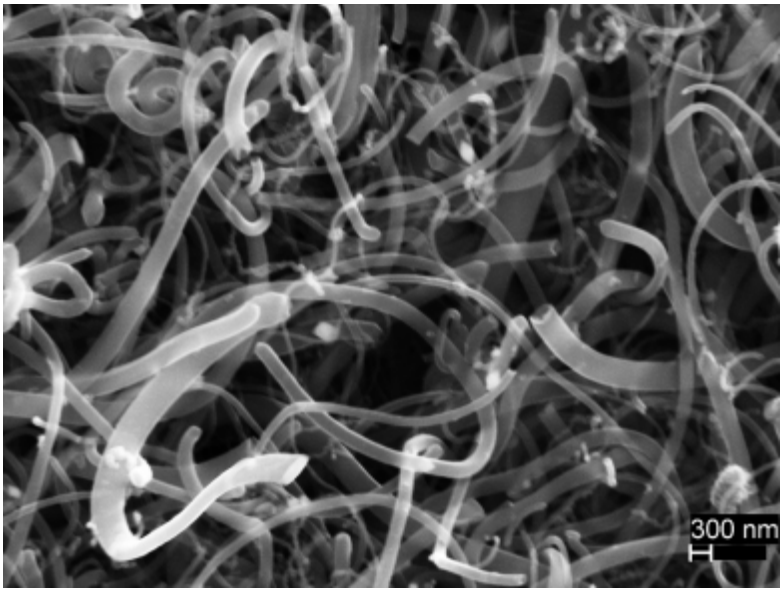

Figure 18. Uncompressed carbon fiber foam grown on pure palladium catalyst. Photo take n at 10,000 times manification and 10 kV. Shows while not under pressure that there are plenty of voids between the fibers.

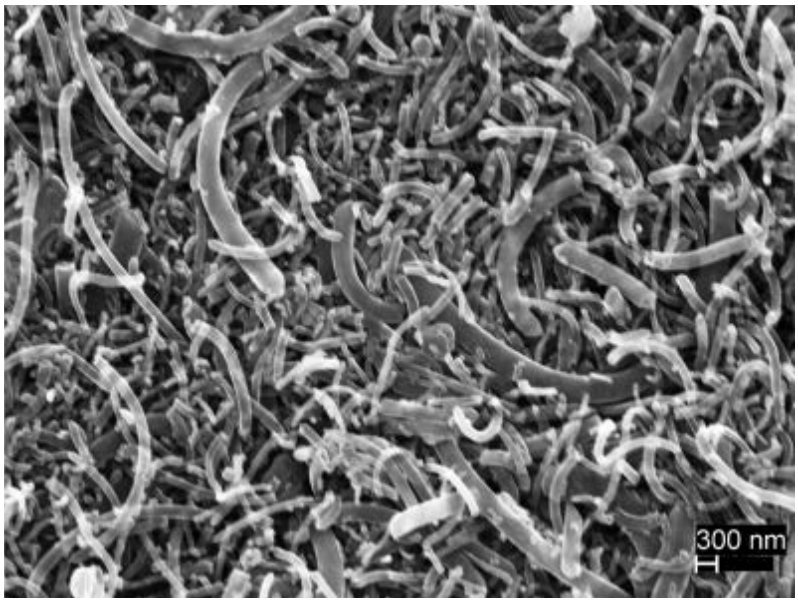

Figure 19. Compressed carbon fiber foam grown on pure palladium catalyst, same sample as in Figure 18. Photo taken at 10,000 times magnification and at 10 kV. Shows that when under pressure the voids between the fibers disappear, this photo is of the interior of the sample.

B. MECHANICAL TESTING RESULTS

Mechanical testing was performed as described in the experimental section.

1. SEM Compression test

The SEM tester discussed in the experimental section was used in the SEM and carbon nanofiber foam was compressed and photos were taken while under pressure. When compressed the voids between the fibers reduce tremendously. However, no fiber delamination or fracture was observed. Videos were attempted however as the sample is compressed the two anvils do not move at the same rate therefore the picture moves around and they were found unusable. Also this caused the photos shown in Figures 18 and 19 to show different sections of the sample.

Figure 19 is an image acquired from a section of the carbon fiber foam that is under pressure near the center of the sample. When the pressure was held the top portion of the sample that was overextending from the anvils was cut off to allow a photo taken of the interior of the sample while under pressure. It is clear that the voids disappear as it

is compressed. This mechanism, that allows individual fibers to touch, generating more contacts, is what it is believed lead to the change in resistance discussed in the Resistance Testing Results section below.

The SEM tester will apply up to 4000 N of pressure; however, when 280 N was reached the cutout switch prevented any further compression. This was caused by the sample becoming too thin under the pressure and the cutout was a self-protection mechanism that prevents the anvils from touching. In the compressed photo Figure 19 shows there appears to be no damage to any of the fibers while compressed with 280 N of force. The sample was unconstrained, however, initial surface area of sample was 9.33 mm x 8.52 mm, which is a surface area of 7.95×10^{-5} m^2. This provides a stress of approximately 3.52 MPa or 511 psi.

2. Unconstrained Mechanical Testing

Both transient and dynamic tests were performed on an unconstrained carbon nanofiber foam sample.

a. Transient Test

A long term 72-hour transient test was performed on the sample to determine how it would react over a long period of time with a constant strain. Hence, the experiment consisted of measuring changes in stress and electrical resistance as a function of time. Initial and final measurements were taken with calipers and a micro scale.

Small "permanent" changes in the foam were created by this process. Although there were no visible changes, simple measurements (Table 1) indicate that permanent deformations on the order of less than 5 percent occurred. These permanent changes are consistent with dynamic tests (below) that show the material needs to be "aged" before it becomes mechanically stable. One example of gradual stabilization that can be extracted from the transient test is the pressure changes. The test was performed by setting the initial pressure to 90 N and then the anvil was positioned and maintained a

constant strain that allowed the carbon fiber foam to relax a little. After the first three hours the pressure reduced to 85 N, after 48 hours the pressure was at 83 N and at 72 hours the pressure was still 83 N and holding.

	Before	After	Change
Mass	143.1 mg	142.2 mg	0.9 mg
Height	4.29 mm	4.11 mm	0.18 mm
Width	10.4 mm	10.06	0.34 mm
Length	14.03 mm	14.03 mm	NC

Table 1. Data recorded from the long term transient test while maintaining a constant strain.

Although there was a relaxation in the stress, there was no measurable change in the electrical resistance. This is the first of several tests that suggested that the carbon fiber foam will make an excellent stress gauge. Several short term (two hour) transient tests were conducted in order to provide electrical information that will be discussed in the discussion of electrical properties later.

Other transient tests, using the same protocol described above, were performed to study material anisotropy. The anisotropic test was performed in order to determine how the carbon fiber foam would react under pressure from different directions. Indeed, some anisotropy is to be expected from the nature of the growth process. Overall the fiber foam grows "up" from the bottom of a mold containing catalyst in the bottom. A cube was cut from the Palladium particle catalyzed foam in order to test having approximately the same dimensions in all three directions. Each of the sides was marked in order to make sure that the directions were not lost during and between the tests. Measurements were taken between each test to verify what changes in each direction occurred during testing, and then the carbon fiber foam was allowed to relax for two hours to determine if the foam attempted to regain its original shape. Data accumulated during the anisotropic test is shown in Table 2.

	Side 1	Side 2	Side 3
Before test	8.25 mm	6.57 mm	7.37 mm
After Side 1 Test	6.41 mm	8.65 mm	8.55 mm
Rest 2 hours	6.30 mm	8.05 mm	9.19 mm
After Side 2 Test	9.08 mm	5.36 mm	10.46 mm
Rest 2 hours	8.76 mm	5.92 mm	10.54 mm
After side 3 Test	7.64 mm	10.28 mm	5.57 mm
Rest 8 hours	8 mm	8.7 mm	6.5 mm

Table 2. Data recorded during the anisotropic test.

b. Dynamic

Two different cyclic frequencies were tested at cycling for 20 cycles between 10 and 90 N. The two frequencies were controlled by controlling the speed at which the INSTRON increased and decreased the pressure. The two speeds chosen for comparison are 0.01 mm/second and 0.05 mm/second. The graph of their stress versus strain can be seen in Figures 20 and 21. Note when calculating the stress the force is applied to the initial measured surface area since the dynamic changing surface area was not measured. The surface area does vary slightly while being compressed and uncompressed. The x and y axis are maintained the same in both figures for ease of comparison.

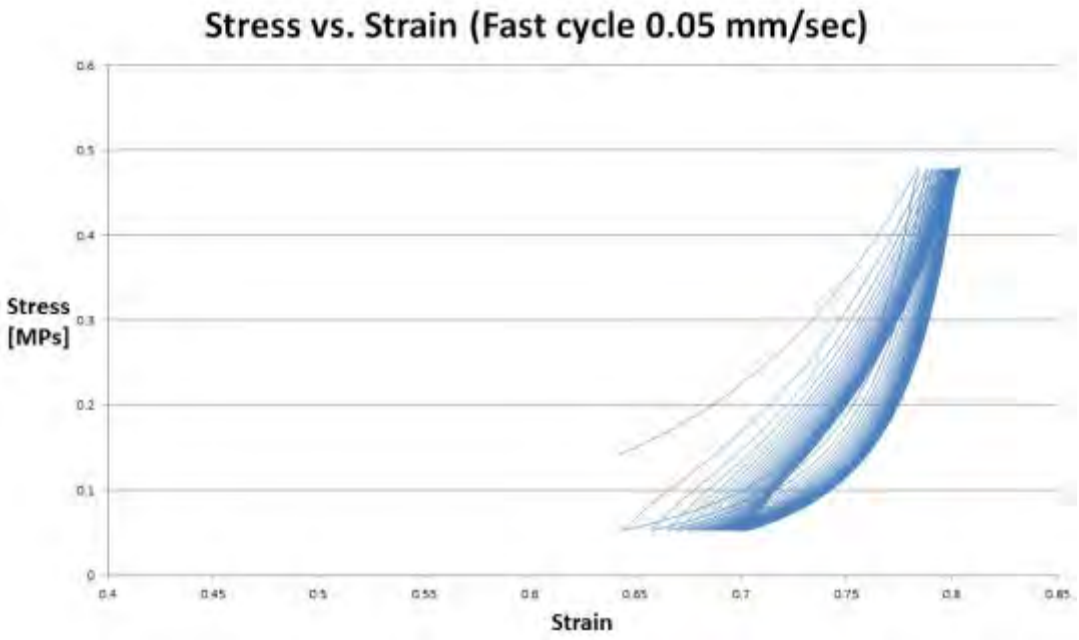

Figure 20. The stress versus strain curve for all 20 cycles for the unconstrained sample ranging between 10 and 90 N at the faster rate of 0.05 mm/second.

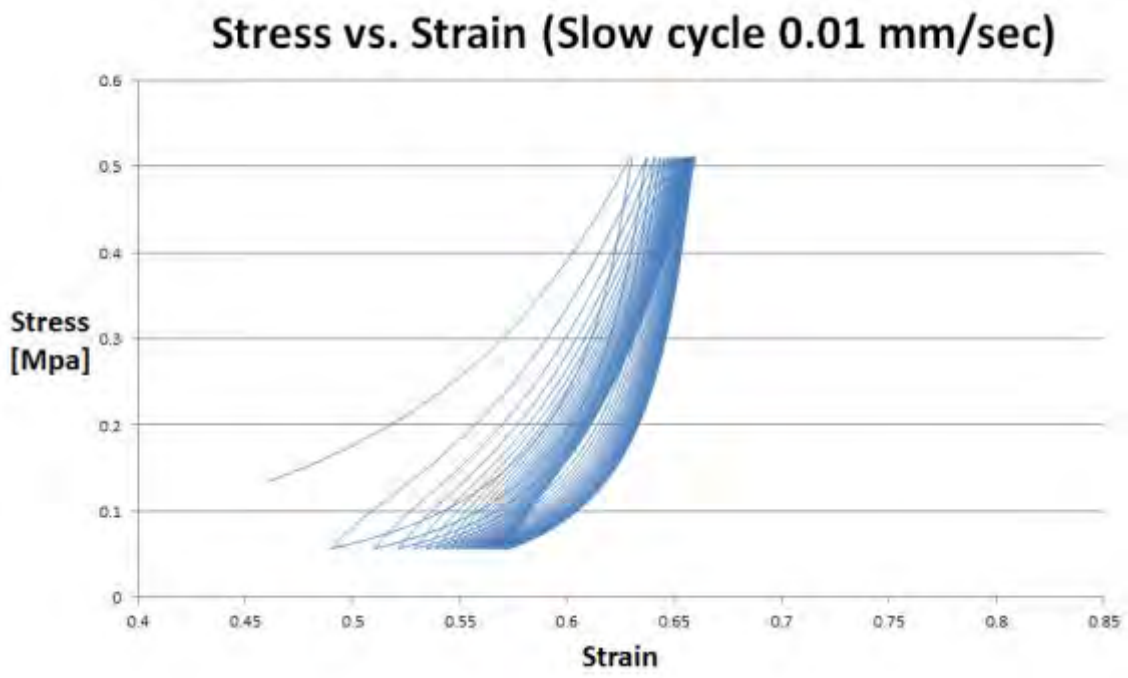

Figure 21. The stress versus strain curve for all 20 cycles for the unconstrained sample ranging between 10 and 90 N at the slower rate of 0.01 mm/second.

The slower dynamic test does have a slightly steeper slope for both the increasing stress cycle and does seem to vary in strain over the cycle more than that of the faster speed.

A modulus was calculated for the linear portion of a stress strain curve cycling between 10 and 90 N, for both the fast and slow cycles. Figure 22 shows the values of the modulus, both of which start to stabilized between 3 and 4 MPa. This calculation is conducted the same as it would be for the Young's modulus however Young's modulus is only valid for strains less than 0.01 where the strains we used were much higher than this value [27] so this sample parameter will just be called modulus without making reference to the "elastic" modulus.

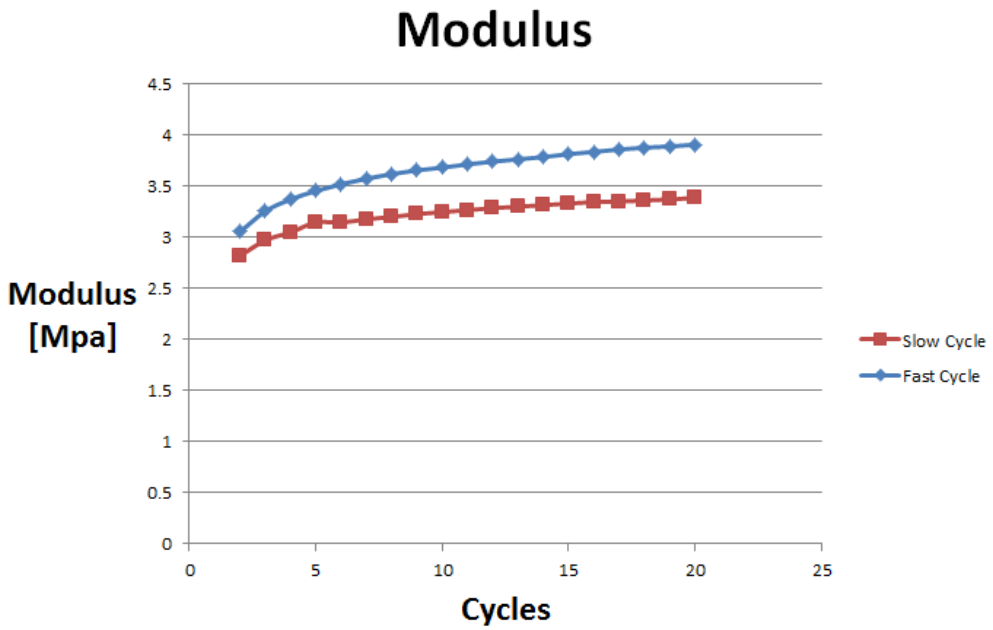

Figure 22. Modulus calculated from the fast and slow constrained dynamic test described above. The modulus for the two cycles is between 3 and 4 MPa.

As seen in Figure 22 the value of the modulus approaches between 3 and 4 MPa, and is equivalent to a Young's modulus calculation. A table of Young's modulus values for various materials is shown in Figure 23, and an arrow has been added to show where the CFF falls in that table.

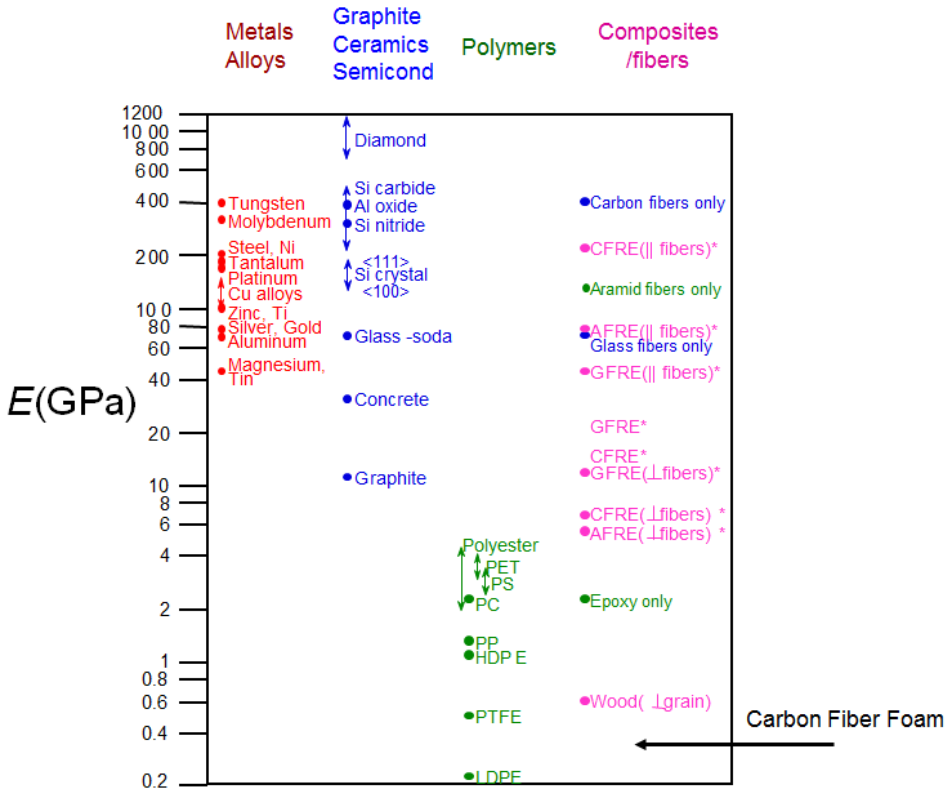

Figure 23. Other materials Young's Modulus for material comparison. Based on data in Table B.2 Callister & Rethwisch 8e Composite data based on reinforced epoxy with 60 vol percent of aligned carbon (CFRE), aramid (AFRE), or glass (GFRE) fibers. [28-32]

3. Constrained Mechanical Testing

Constrained mechanical testing was performed using both a transient and dynamic methods.

a. Transient

A transient test was performed while compressing the sample by 2.5 mm in order to provide an initial force of 50 N on the sample. The sample was allowed to relax while the position was maintained thereby maintaining a constant strain of 0.63 on the sample. The stress on the sample was calculated from the constant surface area of 1.67×10^{-4} m^2. The strain was maintained for a two hour period and is shown in Figure 24 as stress versus time.

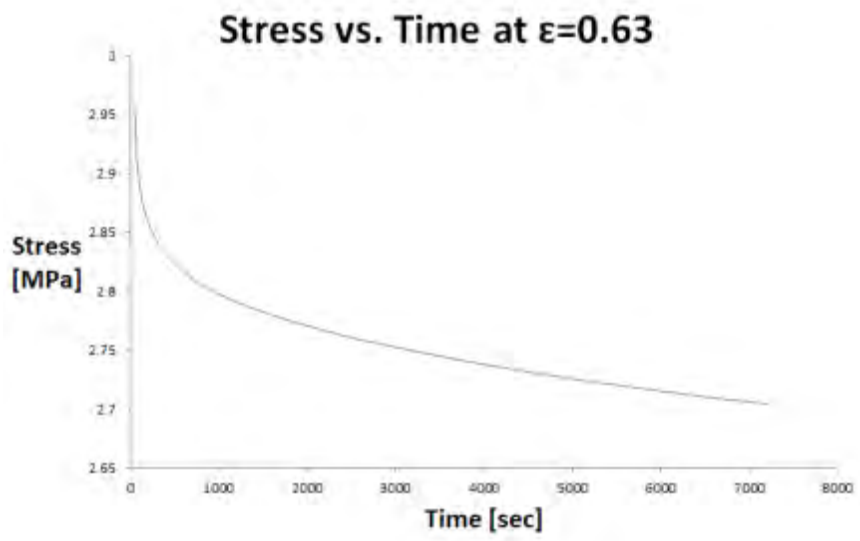

Figure 24. Shows how the stress relaxes over time during the two hour constrained constant strain test.

The relaxation modulus was also calculated using the same data where the relaxation modulus is the stress/strain versus log of time, as shown in Figure 25. This shows the amount of stress required to maintain a constant strain relaxes over time.

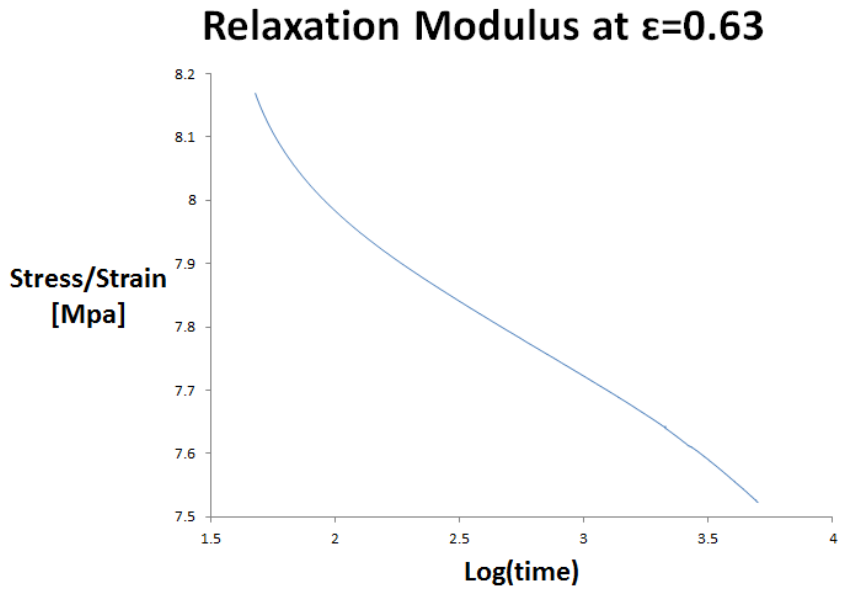

Figure 25. Relaxation modulus of a constrained sample under an initial load of 50 N, maintaining a constant strain of 0.63.

The material shown definitely follows the characteristics of a visco-elastic material; however it does not contain the characteristics that other materials have, such as a glassy section at the beginning of the test or a rubbery for extended periods of time. This result does not mean that the material can't experience a glass transition, it only reflects that such is not observed under the experimental conditions used.

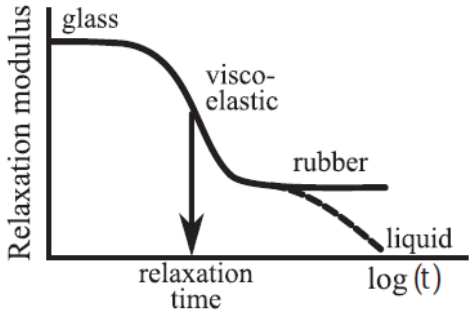

Figure 26. Relaxation modulus curve [27].

The relaxation modulus is the slope of the line during its linear region. Therefore a line has been drawn on the plot in order to determine the relaxation modulus. In order to determine this value on the constant strain test the initial values up to log(time)=2 and all information after log(time)=3.5 was removed to find the linear slope shown in Figure 27.

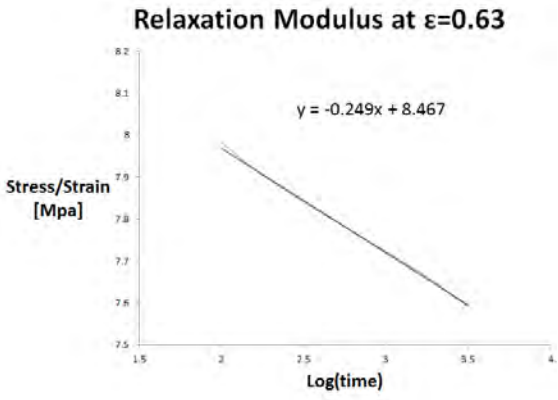

Figure 27. Relaxation modulus of a constrained sample under an initial load of 50 N, maintaining a constant strain of 0.63, with the points in the beginning and end removed to maintain the most linear portion. Has a relaxation modulus of 0.249 MPa.

Next the same sample was tested while maintaining a constant stress and allowing the strain to vary, this provided plots that look similar to those found when maintaining a constant strain however they have a step like appearance. This is most likely due to the fact that as the sample relaxes the force is adjusted in order to maintain a constant stress of 3 MPa. The strain versus time plot is found in Figure 28.

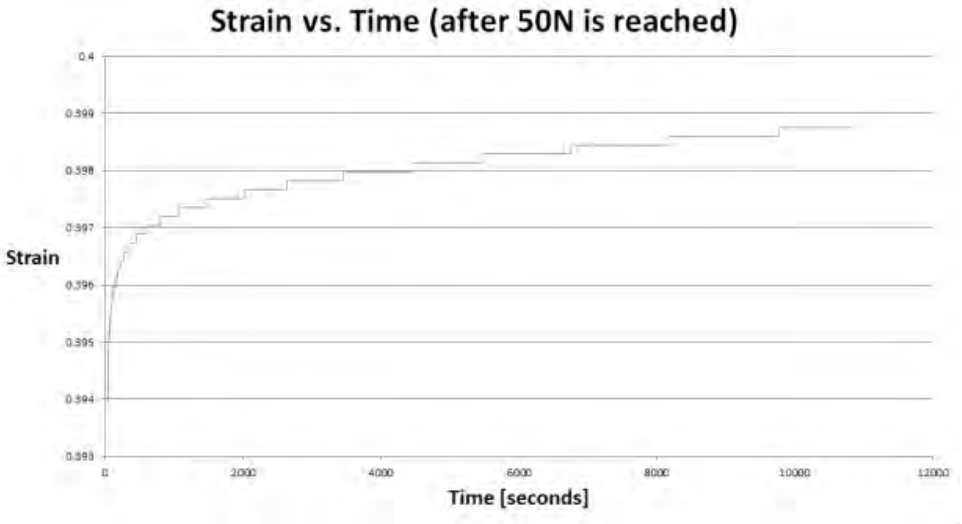

Figure 28. Shows how the strain is changing over time during the two hour constrained constant stress test.

The creep compliance was calculated for the constant stress test and was compared to the plot in Figure 29.

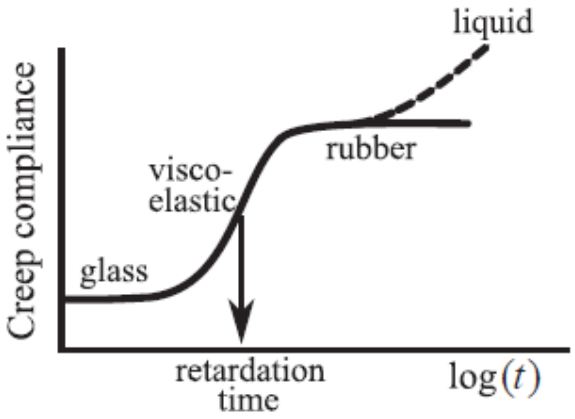

Figure 29. Creep compliance [27].

The creep compliance is the slope of the line during its linear region. Therefore a line has been drawn on the plot in order to determine the relaxation modulus. The creep compliance for the CFF is shown in Figure 30.

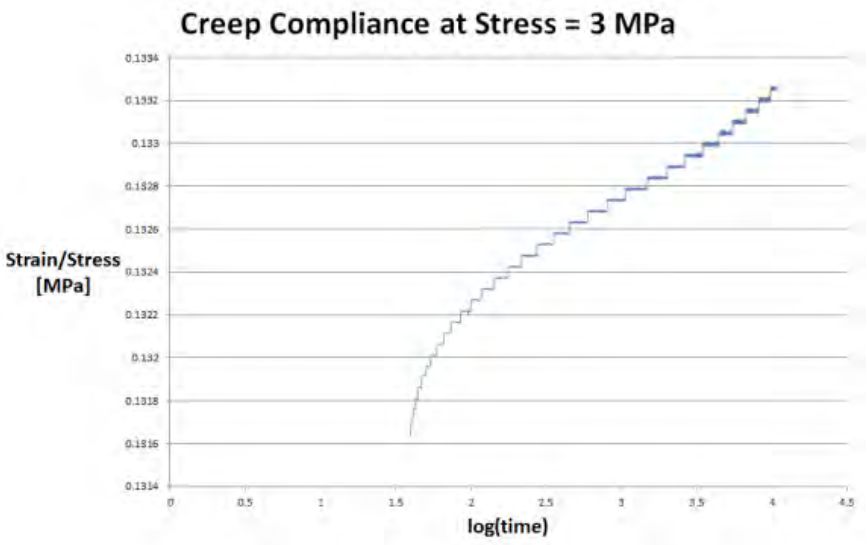

Figure 30. Creep compliance of a constrained sample under a constant load of 50 N, maintaining a constant stress of 3 MPa.

In order to determine this value on the constant strain test the initial values up to log(time)=2 and all information after log(time)=3.5 was removed to find the linear slope shown in Figure 31.

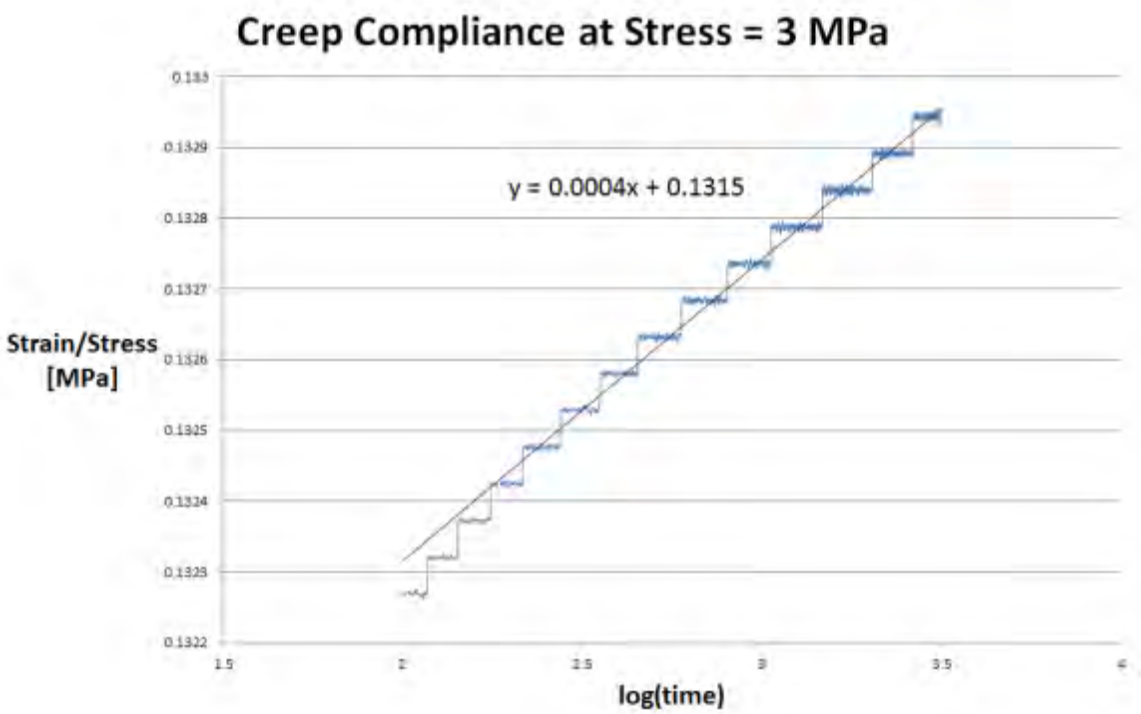

Figure 31. Creep compliance of a constrained sample under a constant load of 50 N, maintaining a constant stress of 3 MPa, with the points in the beginning and end removed to maintain the most linear portion with a value of 0.4 Pa^{-1}.

b. Dynamic

A dynamic cyclic test was performed while compressing the constrained carbon nanofiber foam between 10 and 90 N at an anvil rate of 0.01 mm/second, for 20 cycles. The data was collected and the stress versus strain curve is shown for the entire cycle and the last few cycles in Figure 32.

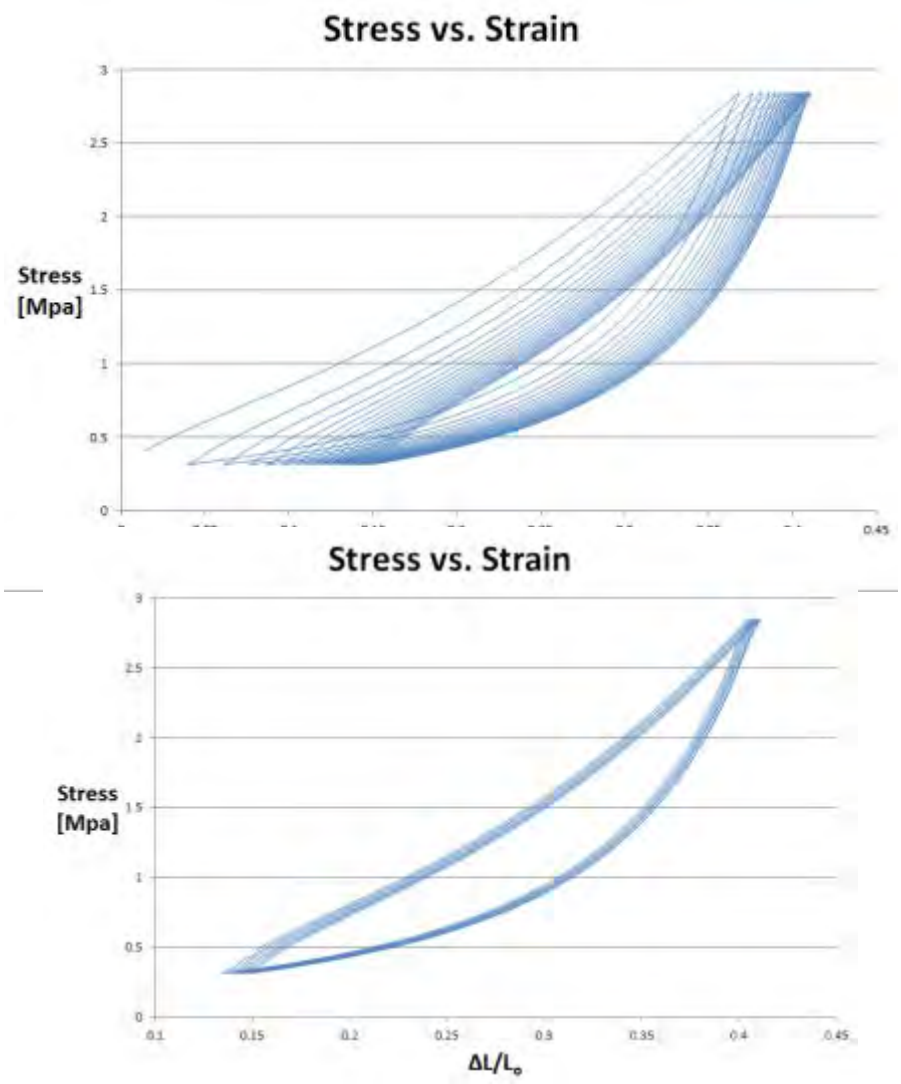

Figure 32. The upper plot shows all 20 of the cycles of the constrained dynamic test cycling between 10 and 90 N. The lower plot shows the last seven cycles of the same test to show that it becomes nearly constant over time.

Now comparing this to what is expected for different types of materials and what the characteristic stress versus strain curves look like as seen in Figure 33. It is easy to see that the graphs shown in Figure 32 of the carbon nanofiber foam match those of the viscoelastic material. Where it returns to the same location that it starts from and the increasing stress cycle is on top, while the reduction in stress cycle is the lower portion.

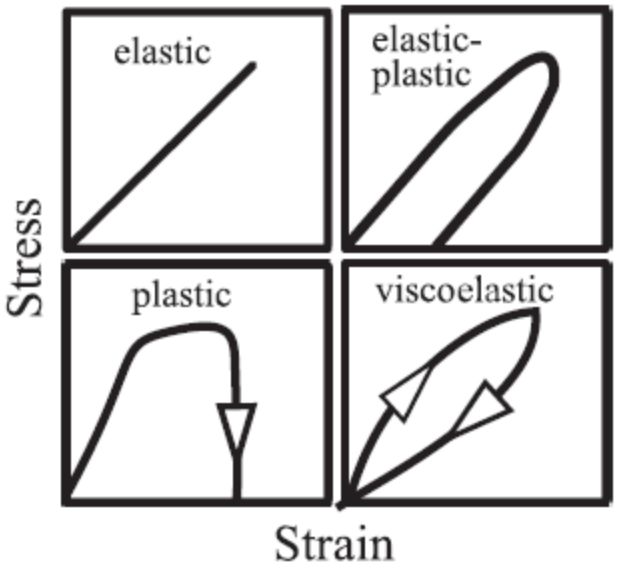

Figure 33. Stress versus strain curve for four different types of material behavior. The viscoelastic material in the bottom right matches the results found while cycling the CFF sample [27].

The hysteresis loop in the sample tested and those shown in Figure 32 are very similar. It also appears that these loops become more and more constant overtime. After the first 17 cycles the last 7 are stable. This demonstrates that the carbon nanofiber foam is a viscoelastic material and gains a stable cycle after less than 20 cycles, which at 0.01 mm/second took just under 35 minutes to complete.

(1) Different Frequency Constrained Test. Two different cyclic frequencies were tested at cycling for 20 cycles between 10 and 90 N. The two frequencies were controlled by controlling the speed at which the INSTRON increased and decreased the pressure. The two speeds chosen for comparison are 0.01 mm/second and 0.05 mm/second. The graph of their stress versus strain can be seen in Figures 34 and 35. Note when calculating the stress the force is applied to the initial measured surface area since the dynamic changing surface area was not measured. The x and y axis are maintained the same in both figures for ease of comparison.

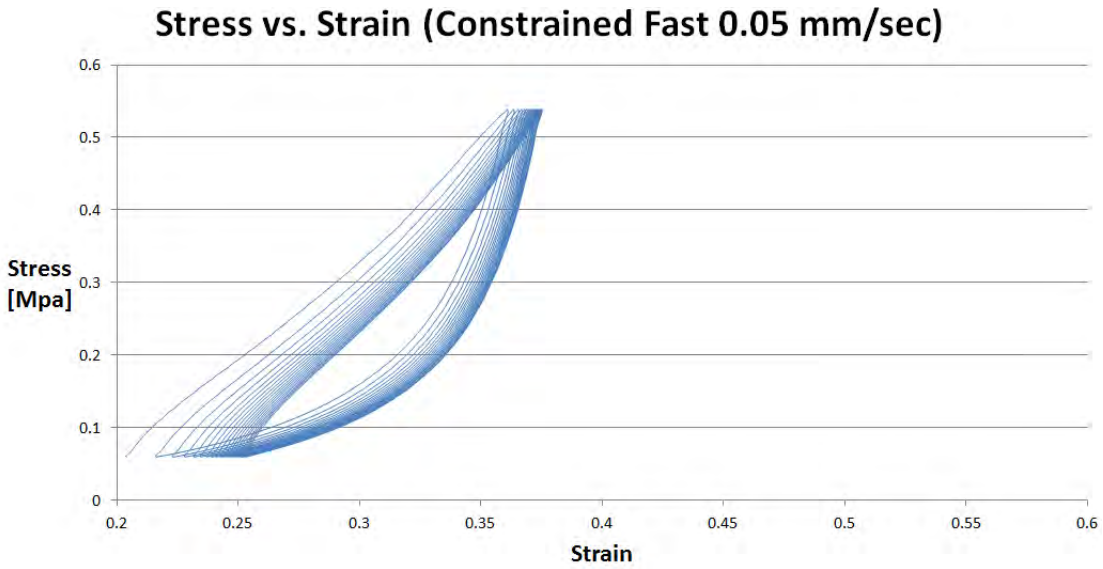

Figure 34. The stress versus strain curve for all 20 cycles for the constrained sample ranging between 10 and 90 N at the faster rate of 0.05 mm/second.

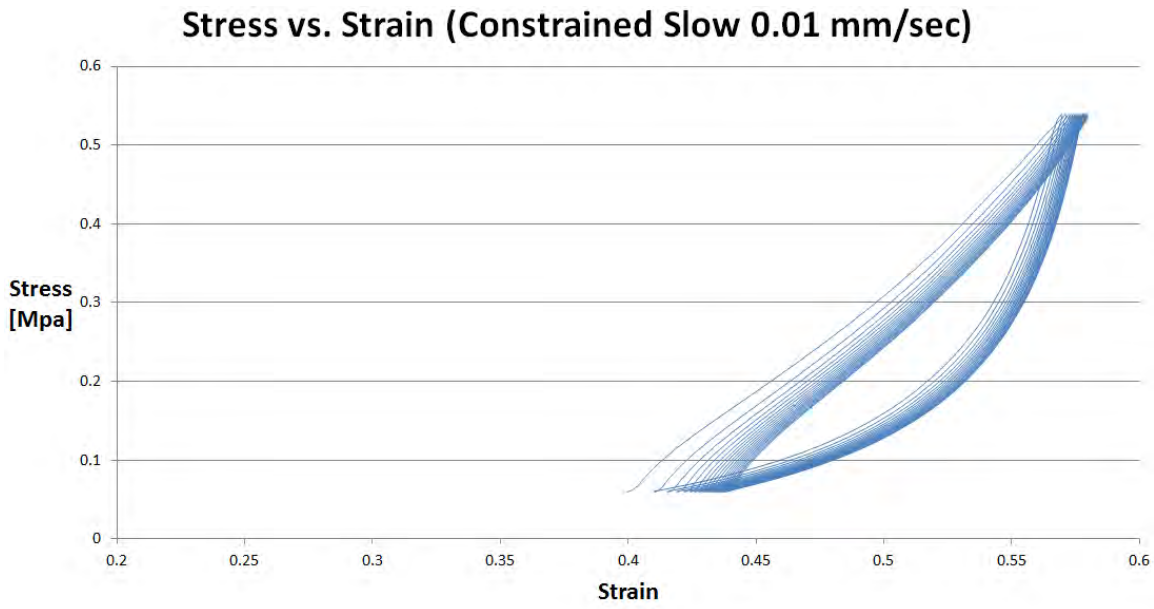

Figure 35. The stress versus strain curve for all 20 cycles for the constrained sample ranging between 10 and 90 N at the slower rate of 0.01 mm/second.

The slower dynamic test does have a slightly steeper slope for both the increasing stress cycle and does seem to vary in strain over the cycle more than that of the faster speed. The slower cycle also is operating in a region with a higher stress than

the faster cycle since it appears to not have the time to relax. As shown in Figure 22 the modulus of the faster cycle is slightly higher than that of the slower cycle. Possibly due to the time the CFF has to relax during the cycle.

C. RESISTANCE TESTING RESULTS

Two resistive behaviors of two types of carbon were studied. First, resistance testing was conducted on the samples produced from the pure palladium particles. Second, the behavior of a second type of 'unwoven fabric' carbon was studied, Grafoil, a commercial material composed of naturally occurring graphite flakes mechanically compressed to form sheet like material. In brief, it was found that only the carbon nanofiber foam gave consistent and reliable results.

Two types of resistance/compression tests were conducted: transient (compress and hold), and dynamic cyclic tests. Also, the impacts of two aspects of the transducer mounting protocol were studied. First, a comparison between in behavior between an unconstrained foam and a foam confined such that lateral extension was not possible was made. Second, a comparison between a foam simple set in the compression device, and one glued to electrical contacts was made. In brief, the best results were obtained for a confined foam.

1. Transient Test

In order to determine the resistance of the carbon fiber foam at different pressures, several different pressures where chosen and held for two hours, in order to allow the resistance to stabilize. These transient test results are summarized in Table 3, and summarized in Figure 36. All these tests were performed on a piece of the carbon fiber foam that was 5.33 x 10.43 x 16.02 mm. This provided a contact surface area of 167 mm^2.

Force [N]	[kPa]	Resistance [Ω]
10	59.85	63.5 ±0.5
20	119.7	48.5 ±0.5
30	179.55	42.5 ±0.5
40	239.4	38 ±0.5
60	359.1	32 ±0.5
70	418.94	30.5 ±0.5
80	478.8	29 ±0.5

Table 3. Resistance measured during the two hour transient test of an unconstrained CFF sample.

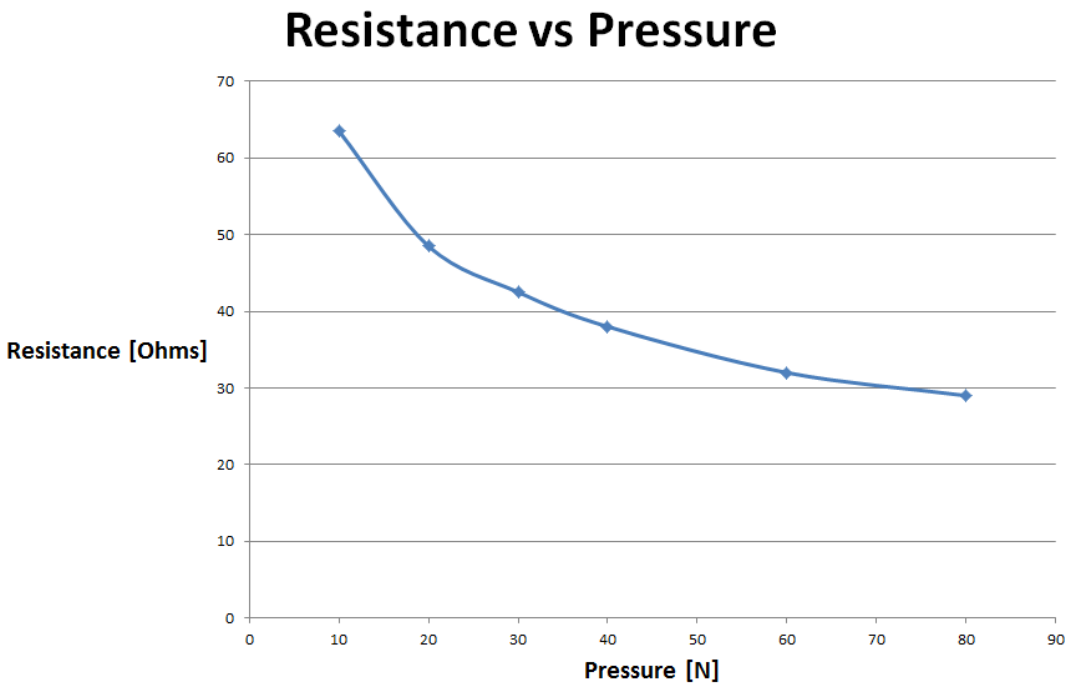

Figure 36. Resistances measured during the two hour transient test on an unconstrained sample.

A complete set of graphs of the data for each of the points can be found in Appendix E. The data shown in Table 3 was the steady state resistance found by holding the sample at a constant pressure using the INSTRON 5942 compression tester for a period of two hours. As one can see in the two plots in Figure 37 the resistance reaches the steady state value after less than 30 seconds, and then maintains that value, within the

±0.5 ohm resistance for the remaining time. Thus the data shown in Figure 37 is an accurate predictor of the expected steady state (>30 seconds) resistance at a given pressure.

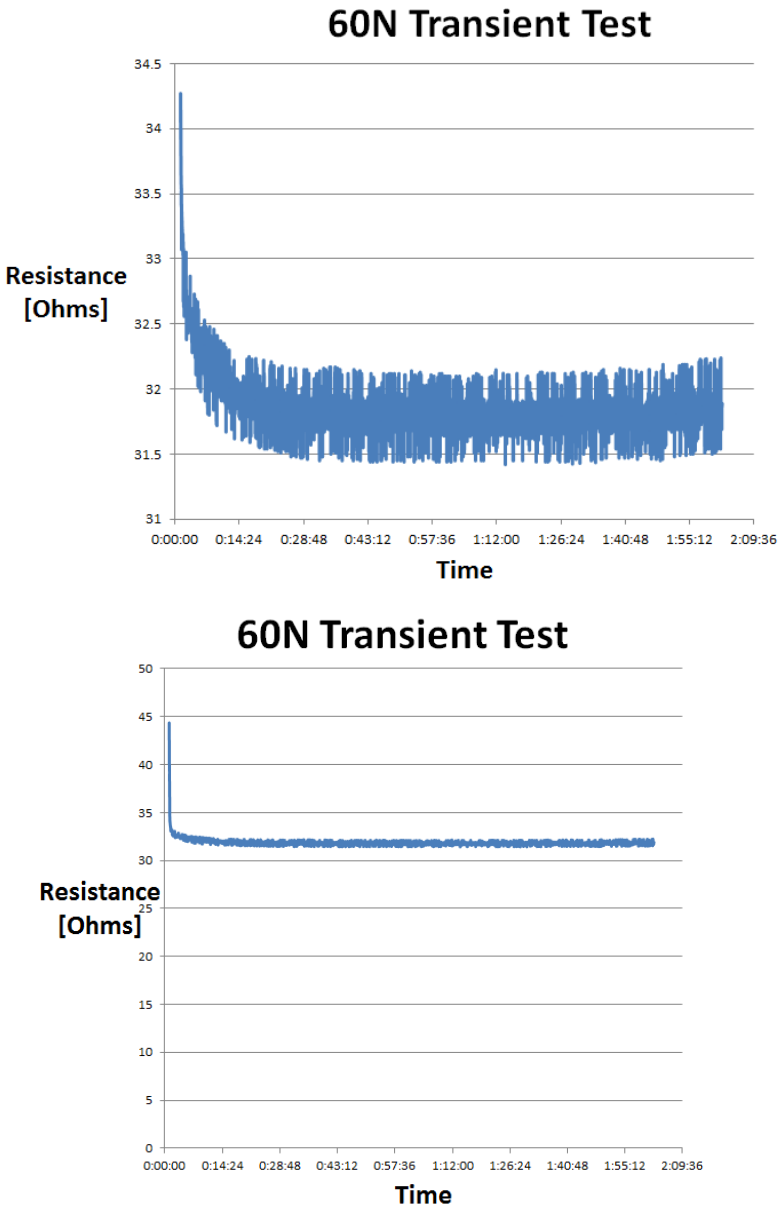

Figure 37. Transient resistance test held at 60 Ns for two hours. Top plot shows a detailed view of the resistance over time, while the lower plot shows the overall resistance changes.

2. Anisotropic Test

The anisotropic test was conducted while maintaining a constant stress. Figure 38 is the resistance results for the resistance tests during the anisotropic testing. Side one was tested first and the measurements of the sample prior to the test were a thickness of 8.25 mm and a contact surface area of 48.42 mm^2. The results initially were high but immediately dropped to the expected value of approximately 21 ± 0.5 ohms.

For the test on side two, the sample was measured as 8.05 mm thick with a contact surface area of 57.9 mm^2. Side two's resistance was approximately 39.5 ± 0.5 Ohms.

For the test on side three the sample was 5.57 mm thick with a contact surface area of 78.5 mm^2. Side three's resistance was approximately 15 ± 0.5 ohms, over the first 20 minutes it fluctuated between 11 and 15 ohms but after 21 minutes it settled around 15 ohms.

The values of the resistance for side one and side three are very similar in nature. The thickness of the sample had an effect on the resistance. Side three was the thinnest side tested. It was thinner due to the fact that the sample did not return to its original shape after being tested twice already. Side three's thickness was approximately 70 percent thinner than side one and side three's resistance stabilized at a value that was approximately 70 percent of the resistance that side one had stabilized. However the resistance values for side two differ from those of side one and side three. This is an indication that the fibers in the foam are not completely random in direction and therefore the direction from which the resistance is measured will potentially vary.

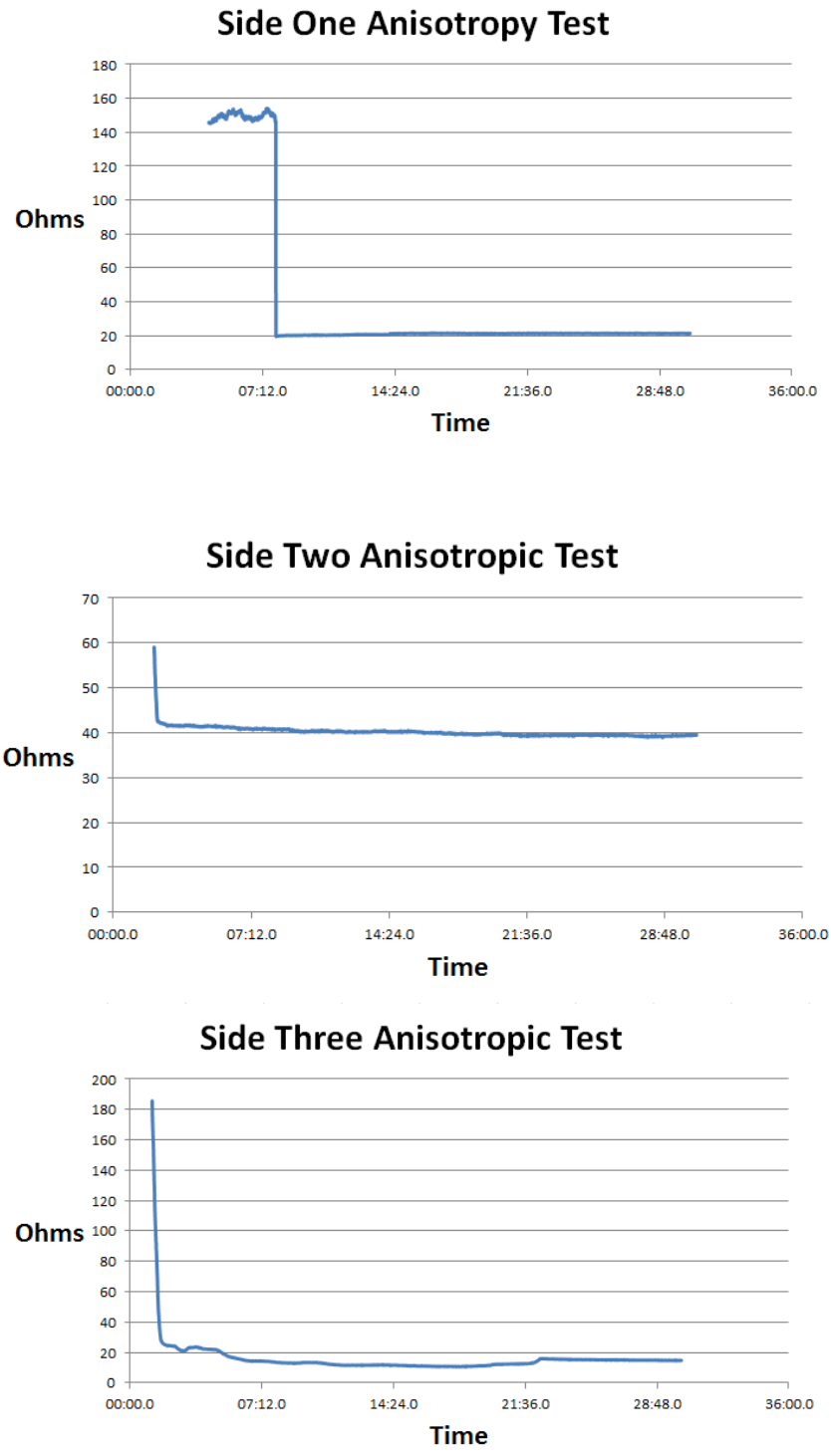

Figure 38. Three sides of a cubical shaped CFF tested for anisotropy.

3. Poisson's Ratio

In order to measure the Poisson's ratio of the CFF an unconstrained cylindrical shaped sample was placed under pressure and the change in diameter was measured using calipers by hand, while the change in height was measured by the INSTRON 5942. The measurements were taken at 80 and 90 N of pressure in order to provide enough of a change that it could be more accurately measured via the handheld calipers. Poisson's ratio is a ratio of the lateral and axial strains as shown in the following equation, where ε_x is the lateral strain and ε_z is the axial strain taken in the direction of the applied stress and are shown in Table 4.

$$\nu = -\frac{\varepsilon_x}{\varepsilon_z}$$

ε_x	ε_z	ν
0.0734	-0.53388	0.1375
0.0755	-0.55207	0.1368

Table 4. Ratio of the lateral and axial strains, and the approximate Poisson ratio of 0.137.

The Poisson ratio is a small value at 0.137 where the average for a metal is around 0.3. The maximum possible value is 0.5 and a purely isotropic material would be 0.25. This low value for the CFF is most likely due to the fact that the material is compressing the internal voids within the material.

4. Dynamic Test

The dynamic testing was performed to determine how the carbon fiber foam would react while under a cyclic compression in which strain was varied linearly as a function of time. That is, although the limits of compression were defined by the starting and final pressures of each cycle, the rate of compression was simply a linear rate of strain.

Testing was performed by cycling between 10 and 90 Newtons. Figure 39 is a graphical representation of the change in resistance over 20 cycles. Note that as time progresses the resistance of the carbon fiber tends to exponentially decrease over each

cycle. The dimensions of the sample tested in Figure 22 were 3.47 x 10.07 x 14.76 mm. The thickness through which the resistance was measured was 3.47 mm and the surface onto which the pressure was placed had an area of 148.63 mm^2.

Looking at Figure 39, it appears that the exponential reduction of the peak resistances is starting to settle. A 50-cycle test was also performed in order to verify if the reduction does settle out, however though all 50 cycles the peak resistance at the low end of the pressure scale still showed signs of exponential decay.

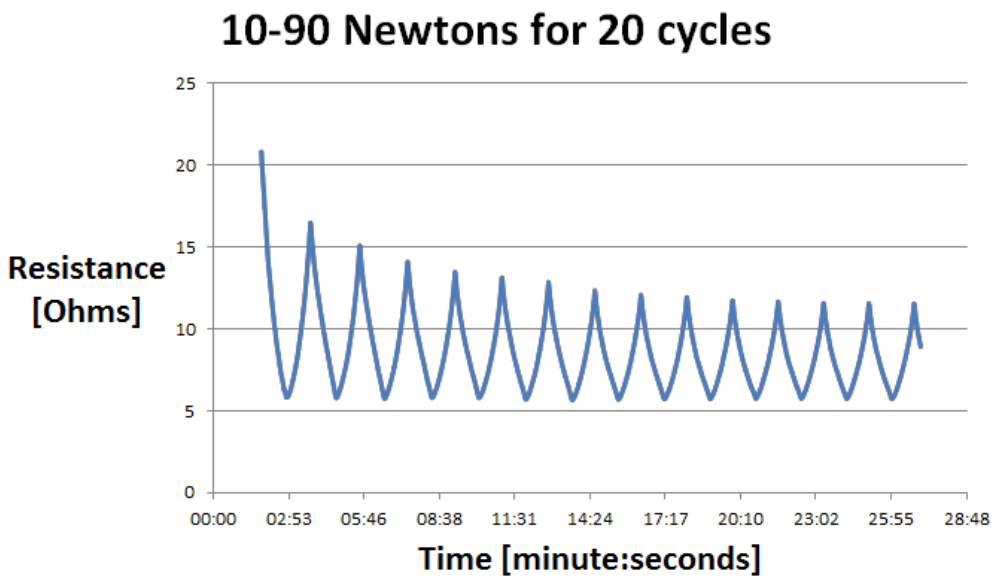

Figure 39. Resistance testing performed between 10 and 90 N over 20 cycles on an unconstrained sample.

In order to determine if the carbon fiber foam reacted differently at lower or higher pressures the pressure cycle was altered to 10 to 40 Newtons and 40 to 90 Newtons separately. Figure 40 shows the results of the 10 to 40 Newton cycle, which was conducted on a sample 4.6 mm thick. This result has the same general shape as the 10 to 90 Newton test. The 40 to 90 Newton test resulted in the same shape graph as well. Therefore, we determined that the reduction of resistance over time during the cycle is not a function of the amount of pressure being applied.

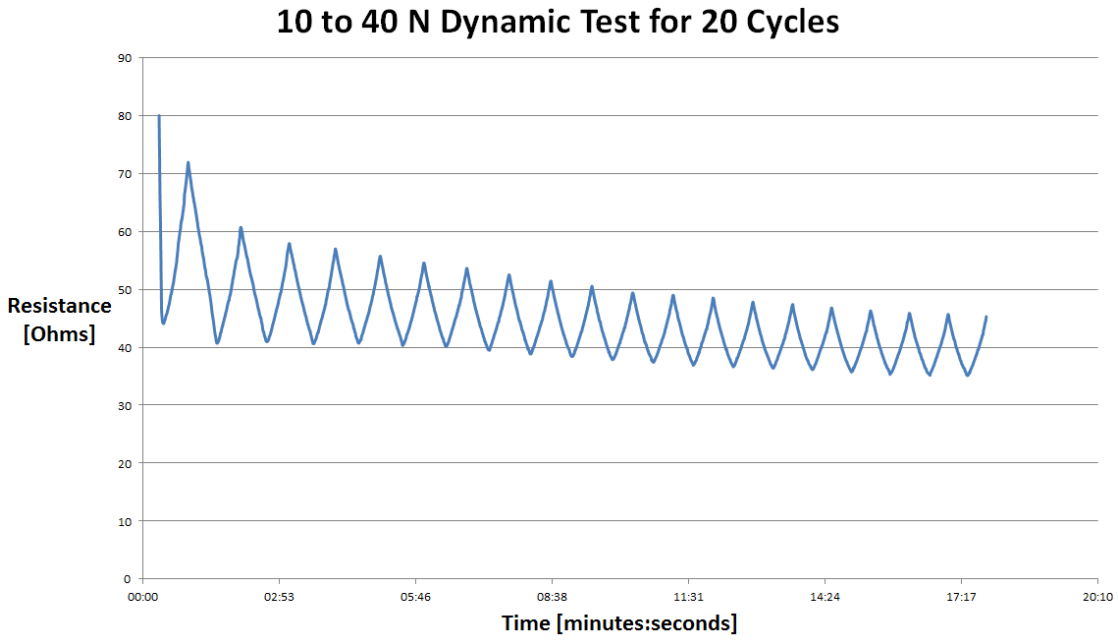

Figure 40. Resistance testing performed between 10 and 40 Newtons for 20 cycles unconstrained.

As can be seen in Figure 40, there was no change in the way the carbon fiber foam reacted at 10 to 40 Newtons compared to the 10 to 90 Newton test.

Originally the experiments were all conducted with unconstrained samples. This allowed the carbon fiber foam to buckle during the testing. In an attempt to alter the exponential decay of the resistance the plexiglass encasement seen in Figure 8 was created by the metal lab at Naval Postgraduate School. The hole was designed in order to allow the anvils to pass freely through the container. The carbon fiber foam was also cut so that it just fit into the plexiglass and then the experiments were run with the buckling of the sample removed. Figure 41 shows the results of a test run on a 5 mm thick piece of carbon fiber foam that was cut ¼ inch in diameter to fit into the plexiglass encasement. As seen in Figure 41, the exponential decay was not removed from the resistance by using the plexiglass encasement.

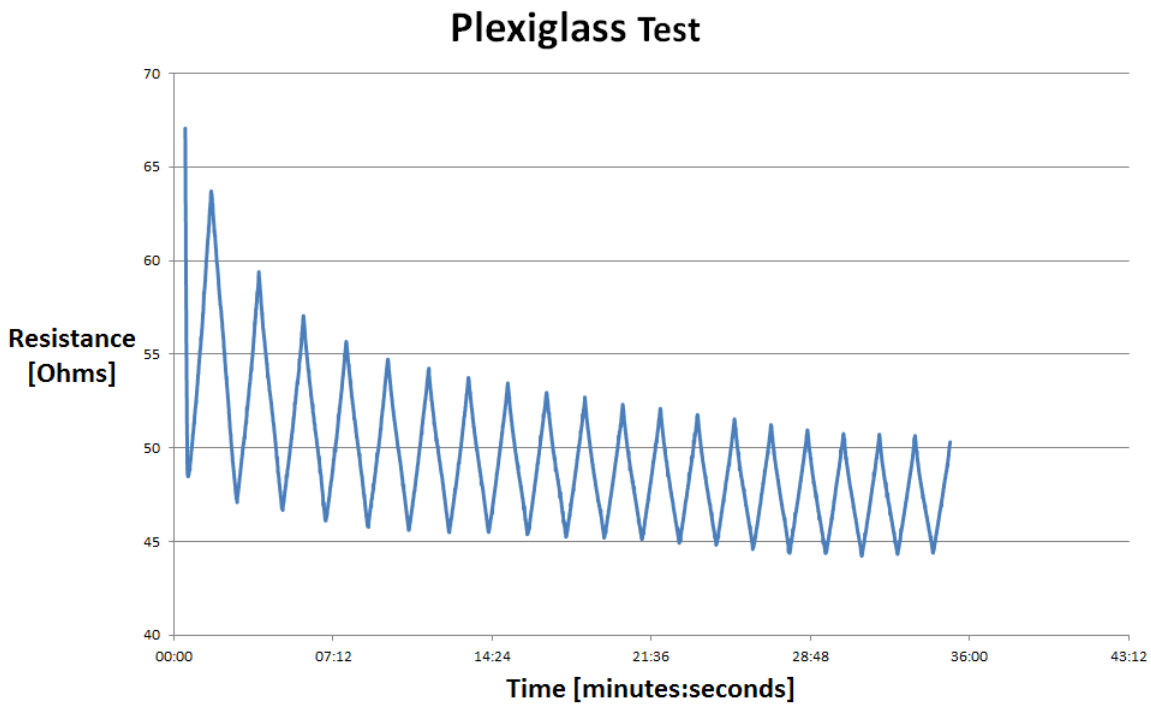

Figure 41. Results contained test while cycling between 10 and 40 N.

This lead to the assumption that the decay might be caused by a changing contact resistance between the carbon fiber foam and the anvil. Therefore a silver paint was applied to the carbon fiber foam and the anvil in order to prevent them from separating. The plot shown in Figure 42 was conducted from 20 to 40 Newtons in order to prevent too little or too much pressure and not cause the paint from breaking off of the carbon fiber foam. The silver paint held the anvils to the carbon fiber foam through several experiments however the results were not consistent with what was found before.

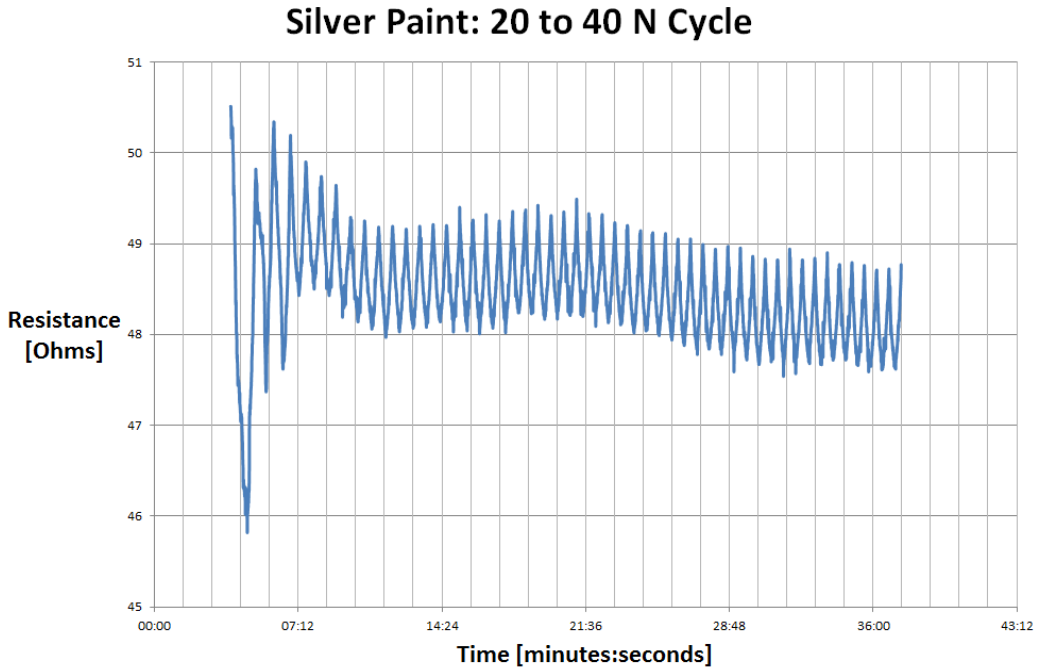

Figure 42. Silver paint attached anvils in order to reduce contact resistance, while using the containment plexiglass.

In order to determine the effect of the speed of the cycling, 0.01 mm/sec and 0.05 mm/sec anvil speeds are tested and are shown in Figures 43 and 44, respectively. The slow test was preformed first and the initial thickness of 5.9 mm and surface area of 176.3 mm^2. The faster test was preformed after the slow test on the same sample. Prior to test the initial thickness was 4.62 mm with a surface area of 188.4 mm^2. The slow test appears to fluctuate between 20 and 25 ohms while the fast test fluctuates between 17 and 22 ohms. The ratio of average resistance to thickness seems to have reduced between the first cycle and the second cycle.

$$\frac{22.5}{5.9} = 3.81$$

$$\frac{19.5}{4.62} = 4.22$$

Therefore, the overall resistance per thickness has increased slightly.

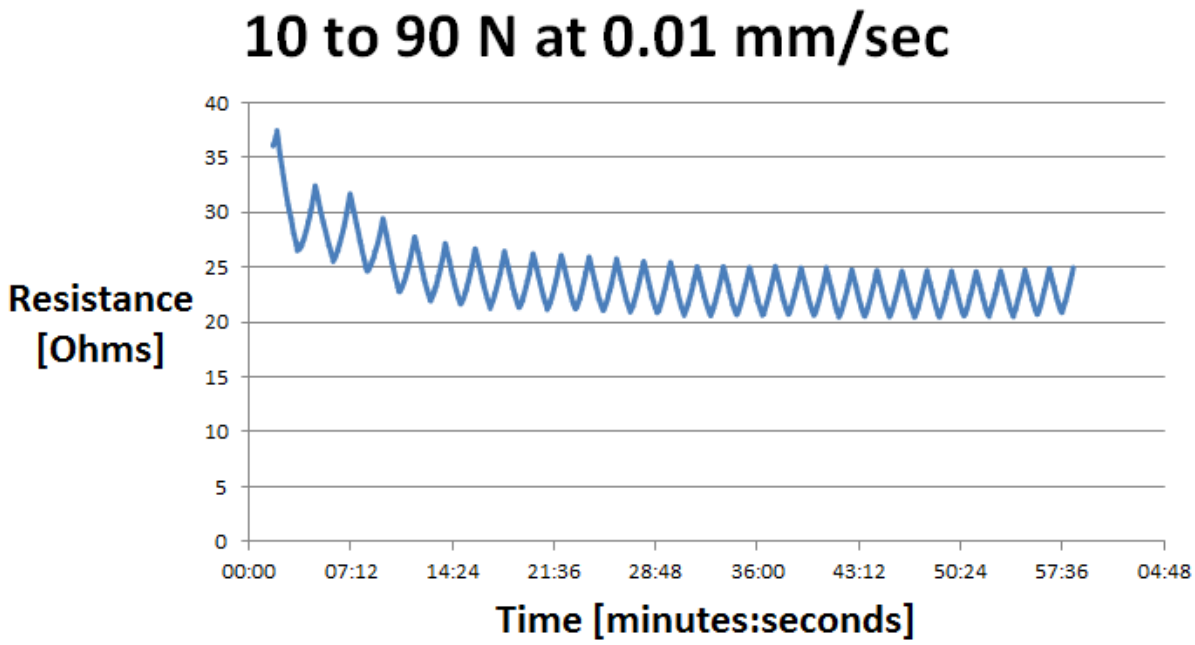

Figure 43. Slow cycle test for 30 cycles on an unconstrained sample.

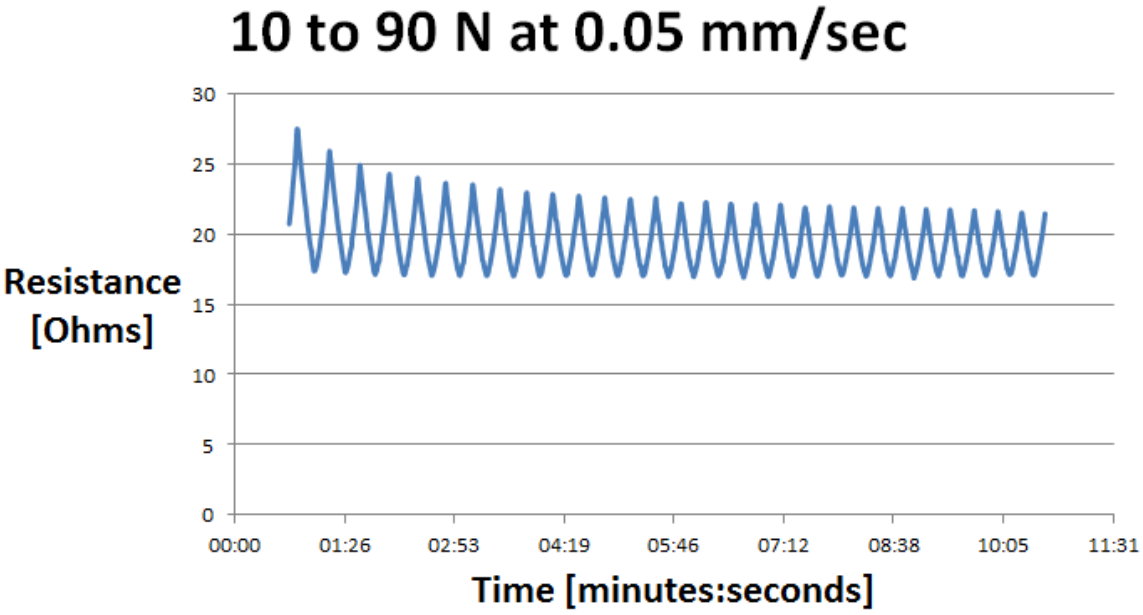

Figure 44. Fast cycle test for 30 cycles on an unconstrained sample.

All of the dynamic tests showed that the CFF electrical properties would stabilize after a few cycles, independent on whether it was constrained or unconstrained. This shows that the material needs a break in period prior to any application that would require its electrical characteristics.

An attempt to plot both the mechanical and electrical data on the same plot can be seen in Figure 45. This is done in order to verify that the maximum resistance point matches the lowest pressure point, which is what would be expected. As the cycles progress as seen in Figure 45 the data does slightly misalign due to the data being taken by two separate programs on two separate computers, where the clock times of the data are slightly misaligned.

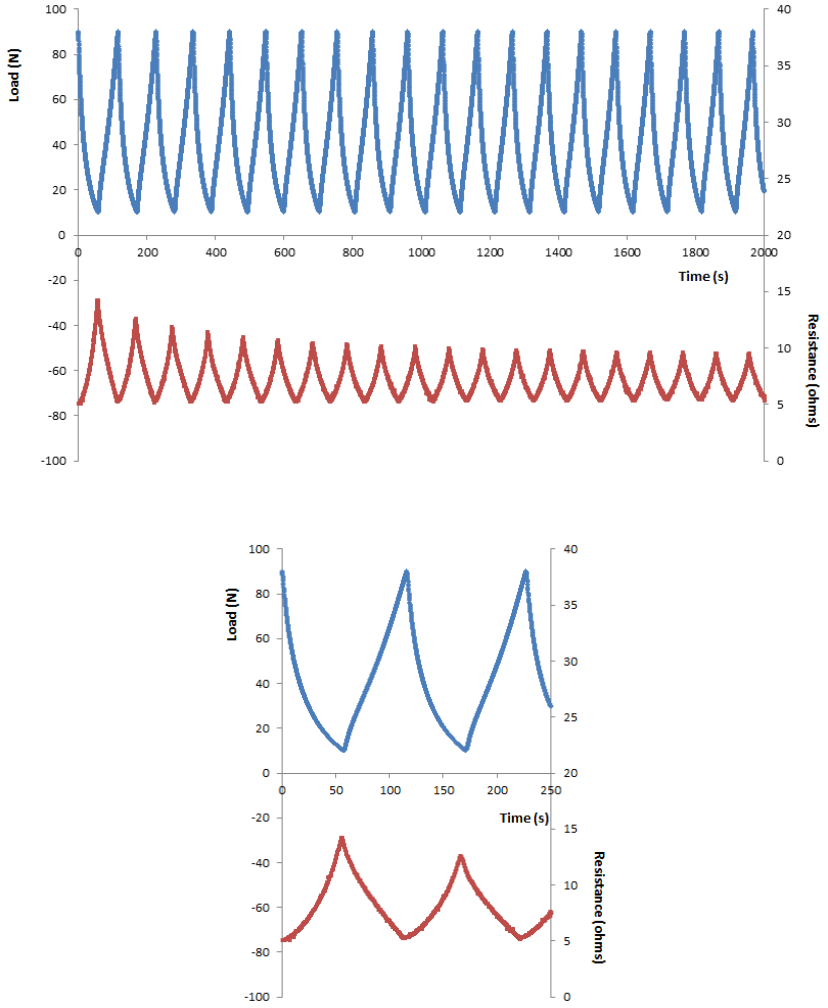

Figure 45. Overlay of the load (blue) and the resistance (red). The lower image is zoomed in for clarification.

5. Dynamic Test of Alternate Carbon Based Material

In order to determine how a different carbon Grafoil was tested to see how its resistivity changed under a cyclic pressure. A maximum pressure of 40 Newtons was chosen due to the thinness of the Grafoil wafers being tested. As shown in Figure 46, the resistance of the Grafoil wafers was not as consistent as that of the carbon fiber foam.

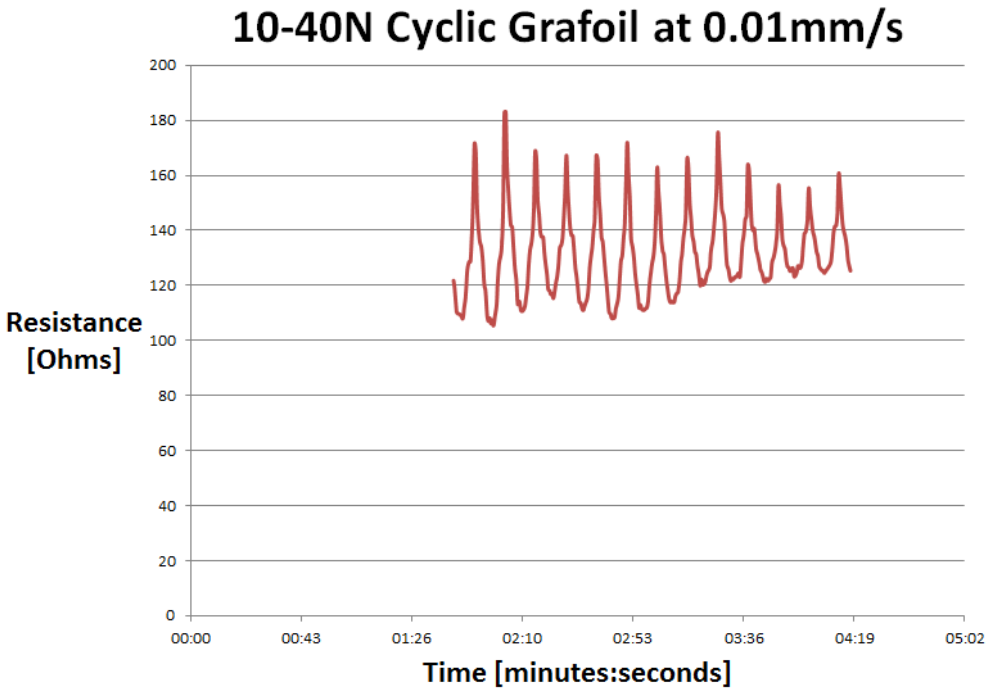

Figure 46. Cyclic tests performed on Grafoil, using the Plexiglas containment.

6. Gauge Factor

Most of the data to this point gives the indication that the sample will work as a strain gauge. In order to determine its sensitivity to strain the gauge factor (GF) is the fractional change in electrical resistance to the fractional change in strain. The following formula is used for its calculation:

$$GF = \frac{\Delta R / R}{\varepsilon} \text{ [33]}$$

A graphical representation of this is in Figure 47.

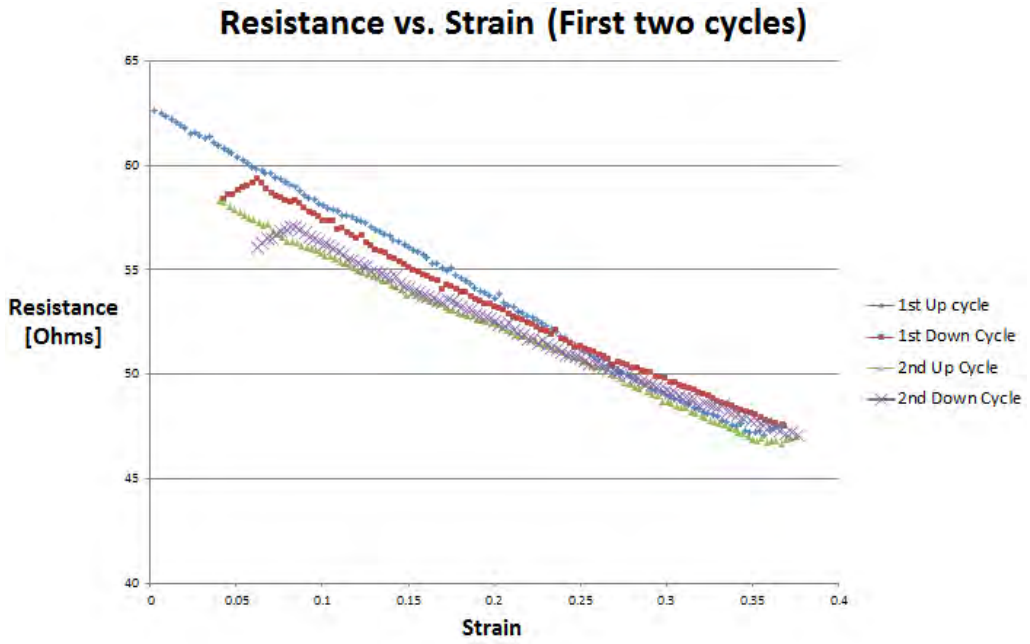

Figure 47. Graphical representation of the first two cycles of the change in resistance versus the change in strain. The slope of this line would represent the gauge factor of the strain gauge.

The first two cycles are the most varying of any of the cycles. Indeed, a theme of this work is that the mechanical properties of the CFF do not stabilize until the material is aged; therefore is not surprising that the behavior is non-linear over the first few cycles. And, as suggested, the material becomes more stable over time, as shown by the linear relationship between strain and the resistance found after ~17 cycles (Figure 47). The last three cycles of the 20 cycle test (Figure 48) are nearly identical and are linear. This suggests that the material can be used as a sensing element in a strain gauge after proper aging protocol.

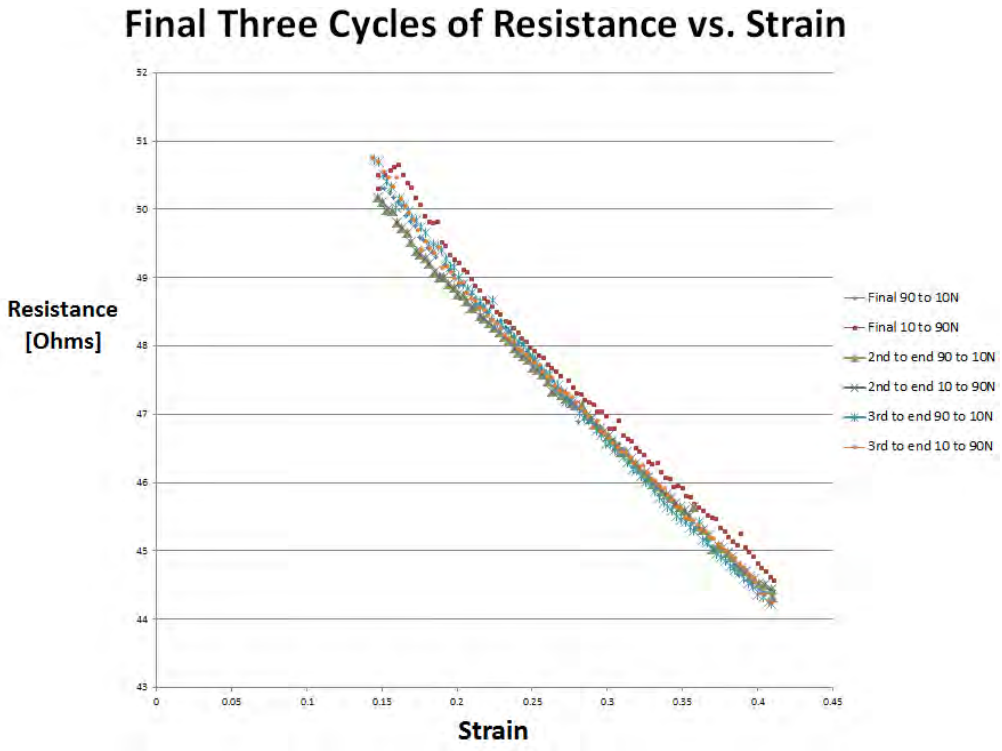

Figure 48. Final three cycles of the resistance versus strain curve. The slope of this line would represent the gauge factor of the strain gauge.

To compare the behavior observed in the foam sample with conventional strain gauges, a brief description of the latter is included below.

7. Strain Gauge

The most common strain gauge measures the change in electrical resistance, which is proportion to the amount of strain being applied. The metallic strain gauge is made with a very fine wire or foil that is arranged in a grid pattern as seen in Figure 49 and is aligned so that the strain is seen in the parallel to the active grid. This is then bonded to the carrier, which is a thin backing and is attached to the specimen being tested. The strain seen by the specimen being tested is then transferred through the carrier to the strain gauge, which the causes a linear change in electric resistance, due to the elongation of the wires or foil. [33]

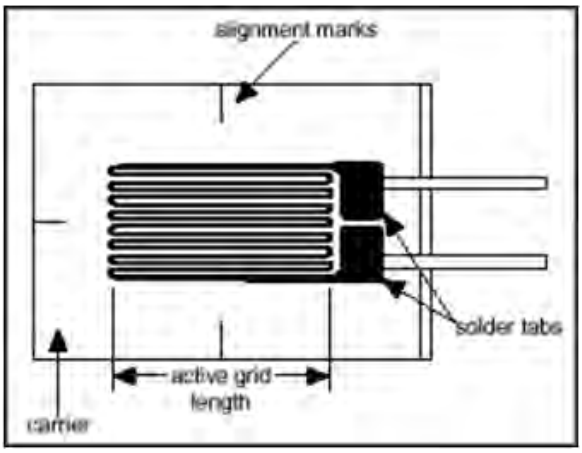

Figure 49. Bonded Metallic Strain Gauge [33].

8. Prototype

A prototype was developed using the carbon fiber foam and a small 22-range pocket digital multimeter purchased from Radio Shack as shown in Figure 50. The leads from the multimeter were cut and soldered to the copper tape attached to the two sides of the carbon fiber foam. The carbon fiber foam and all connections are then wrapped in cellophane to prevent any outside interference from getting into the sample. This was chosen due to its transparent nature that would allow the carbon fiber foam to be seen while in use.

Figure 50. First prototype of device used to demonstrate how the resistance changes with pressure can be monitored.

D. ENVIRONMENTAL TESTING

The environmental testing was performed in order to determine if water, salt water or oil would penetrate the carbon fiber foam. The water test was performed first and the results can be seen in Figure 51. As it can be seen the water bead does not penetrate the sample, and is actually repelled by the carbon fiber foam, consistent with the super hydrophobic nature of carbon nanostructures.. When the test was performed it was very difficult to get the water droplet to remain on the sample. Many attempts were made to get the droplet to remain on the carbon foam. After the test was performed and when the sample was moved the water immediately fell off of the fiber foam. This test verified what was expected that the carbon fiber foam respells water and therefore is not affected by water.

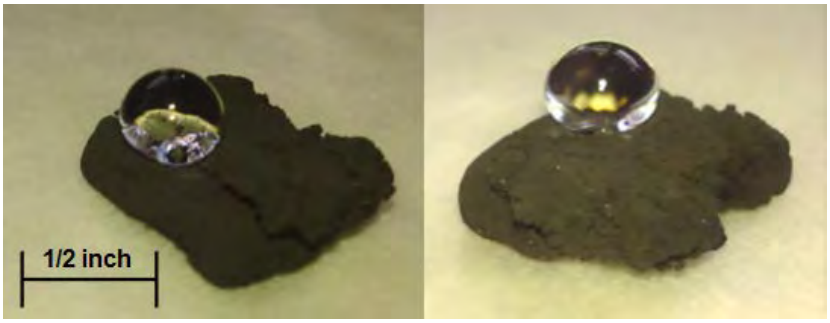

Figure 51. Carbon fiber foam during water environmental testing.

The contact angle in Figure 51 between the surface of the carbon fiber foam and the water droplet can be seen that this angle is an advancing contact angle, which is an indication that the water and the carbon fiber foam reflects the relative strength of the liquid to foam molecular interaction. This interaction is very weak and therefore the carbon fiber foam is a hydrophobic material.

In order to predict the carbon fiber foam interaction with body sweat, saline was used as a substitute. Sweat contains mainly water, as well as some minerals, lactate and urea.

The results for the saline test are in Figure 52. The test was conducted while attempting to place a drop of saline on the sample. The saline did not remain on top of the sample. After repeated attempts the saline was able to balance on top of the foam. The contact angle between the carbon fiber foam and the saline is a receding contact angle, which would indicate that it is more molecular interaction with saline than the water tests showed. However, during the conduction of the test the saline was repelled by the sample as it was in the water test. After the removal of the saline from the carbon fiber foam, the sample was completely dry and showed no evidence of any saline. The picture shows many air pockets between the liquid and the carbon fiber foam indicating as well that it does not want to adhere to the surface.

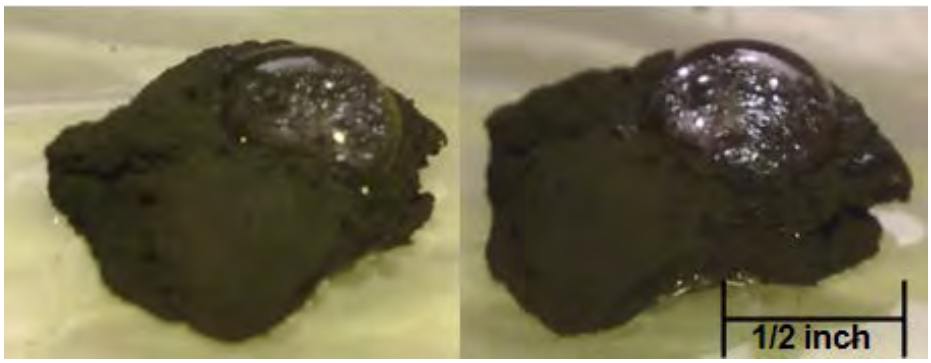

Figure 52. Carbon fiber foam during the saline environmental testing.

The final test was performed to see how the carbon fiber foam would react with the vacuum oil, PFEIFRER D-35614 Asslar Oil P3. The oil was immediately absorbed into the carbon fiber foam, faster than was able to get a photo taken. The photo in Figure 53 shows the carbon fiber foam with the oil already absorbed into the surface. There is no visible difference from what the sample looked prior to the oil being dropped onto the surface and after.

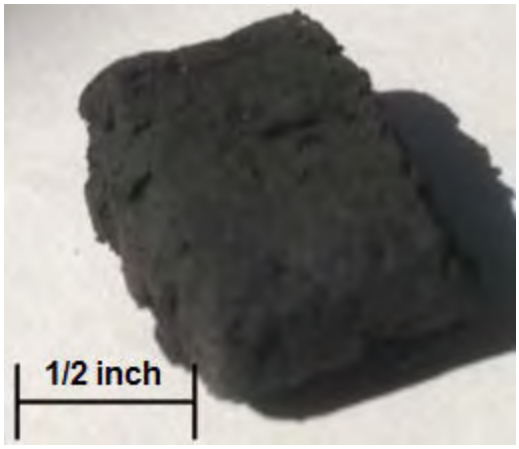

Figure 53. Carbon fiber foam during oil environmental testing.

This indicates that the carbon fiber foam if exposed to oil in the field will absorb the oil into itself. Once the oil had been absorbed the resistance characteristics have changed. Figure 54 shows a difference between a 50 Newton and 90 Newton pressure placed on the sample. The break in the pressure is indicated where the graph breaks

around the two minute point along the timeline. The results vary widely over time ranging between 200 and 450 ohms. The resistance is much higher than expected as well for the results should be well under 100 ohms from previous experiments.

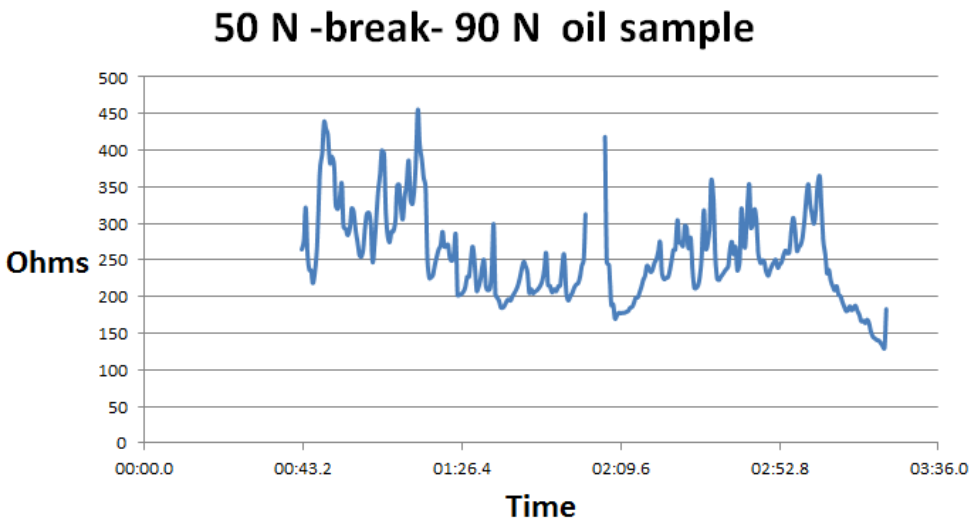

Figure 54. Test of sample exposed to oil, unconstrained. First portion of the graph is a 50 N transient test while the second half of the graph is a 90 N transient test.

Therefore the results demonstrate that the carbon fiber foam is repellent to water based substances, however oils can be absorbed and end up changing the characteristics of the carbon fiber foam.

Regarding the stability of the sample in air, TGA experiments conducted in oxygen containing atmospheres (similar to air environments), are shown in Figure 55. The sample does not burn or suffer weight changes until it reaches 550 ºC. It is worth noting that polymeric counterparts of viscoelastic nature show evidence of decomposition at much lower temperatures shown in Figure 56. Only PTFE and PS could match the stability of the foam studied in this thesis.

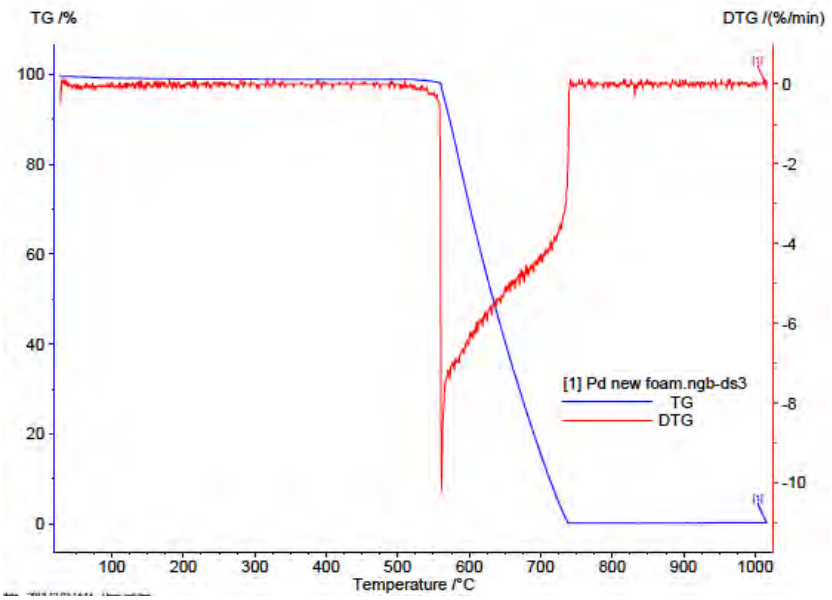

Figure 55. TGA of foam I air. Sample is stable up to more than 550 degrees C.

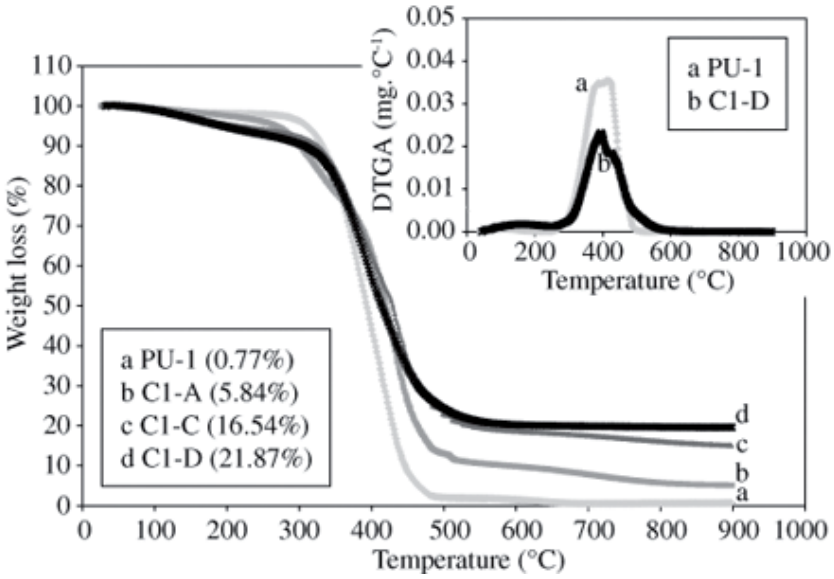

Figure 56. Stability of diverse viscoelastic polyurethane materials in air studied by thermogravimatric analysis [34].

IV. DISCUSSION

The discovery in succession over the last two decades of carbon fullerenes [35], carbon nanotubes [36] and the special properties of graphene [37] dramatically increased the interest in possible unique applications of carbon nanostructures, both on the basis of electrical and mechanical properties. For example, carbon nanotubes are under consideration for use in 'molecular scale' logic circuits. That is, carbon nanotubes are seriously considered as the replacement for silicon in all integrated circuits [38-40]. There is also an enormous effort focused on using nanotubes to strengthen composite materials [41-43]. Presently there is widespread interest in employing graphene in capacitors, as graphene has the highest surface area of any conductor [38, 44-46]. Graphene is also believed to have great potential as a component in corrosion resistant paint, light-strong plastics for cars, sports equipment, aerospace and military applications.

The present work suggests that another novel carbon material, carbon fiber foam (CFF), also has unique electrical and mechanical properties, and these may lead to widespread applications. In particular, the present work provided a variety of data that help define the properties of this material, a first step in evaluation of potential applications. First, we were able to duplicate the generation of the material, previously only generated in a single lab [47], and were also better define the optimal production conditions. Second, we showed for the first time that the material is a true viscoelastic. After a few cycles (ca. 10) its mechanical properties stabilize. Moreover, it is clearly unique among viscoelastic materials in that it has high electrical and thermal conductivity, as well as stability at high temperatures. Third, we were able to show that the material is potentially an excellent material for use as the sensing material in a strain sensor. Each of these advances is discussed below in more detail.

A. PRODUCTION

At present there is only one report of the production of durable carbon fiber foam and it was made under a particular set of circumstances. In the present work we were able to duplicate the production of durable carbon fiber foam, supporting the contention

that the production of carbon fiber foams is simple, and readily duplicated. As described below, the present work also advanced an understanding of two key parameters of the growth process: gas residence time and catalyst identity.

Matching the outcome of the earlier work did take some effort and revealed that gas *residence time* is the key parameter of the process. Indeed, attempts to create CFF failed when precisely the same flow rates and temperatures employed in the earlier work were applied. Following these failed efforts, based on the GSD concept we formulated a new postulate regarding ideal production conditions. To wit: Gas residence time in the heated zone prior to reaching the catalyst chamber must be within a narrow range. Specifically, the physical layout in the earlier report resulted in a far longer "pre-catalyst chamber" residence time for the given flow rates. In order to match 'residence times' in our system with that employed in the earlier work a far lower flow rate was required in our system. Once the residence times were matched, the process was successful.

The significance of residence time found in this work result strongly supports the central chemical hypothesis of GSD. [25] Specifically, according to GSD, carbon structures grow from carbon containing radicals created by homogenous reactions in a fuel rich combustion mixture [25, 47-55]. As in any "flame" the identity and concentration of radicals is a function of residence time. Thus, solid carbon growth from a fuel rich combustion mixture of ethylene and oxygen can and should be a function of position within the flame, hence residence time. Only at certain places within the 'flame' will the proper radicals be present in sufficient concentration to permit rapid solid carbon growth. In several reports on GSD the impact of residence time/radical identity and population has been demonstrated [50, 51]. This work reinforces those findings.

One other issue of significance for broad application of CFF is the cost of the process. Clearly a process that requires a precious group metal, specifically palladium, and that creates a product from which the catalyst cannot be easily recovered, is an expensive process. This suggests the study of the efficacy of alternative, less costly, catalysts. Nickel was chosen as an alternative for study in the present work, because it has been shown that carbon fibers can grow on nickel catalysts [56]. A second alternative catalyst employed was a molecular form of Pd, specifically palladium nitrate.

It was found in the present work that the fibers produced using either Ni or palladium nitrate as a catalysts were of smaller diameter and shorter than those produced using Pd particle catalyst. It was also clear that the solid bodies produced using these catalysts were very frangible, hence of little value. This suggests that the most mechanically robust CFF are composed of fibers of relatively large diameter. In sum, these initial efforts to reduce the catalyst cost associated with CFF fabrication were unsuccessful. Clearly additional effort will be required.

B. VISCOELASTIC BEHAVIOR:

In earlier work the foam like character of the CFF was noted, but the data collected regarding the stress-strain relationship was not sufficient to establish the macroscopic category of the material [51]. In the present case, repeated stress-strain cycling over ~50 cycles allowed the mechanical properties to stabilize, and created a material that shows classic viscoelastic behavior Figures 34 and 35. Thus, this work establishes, with certainty, that CFF represent an entirely new class of viscoelastic materials. The unique aspects of the material include its microstructure, chemical composition, and thermal/electrical properties. Specifically, this is the first viscoelastic material: i) composed entirely of fiber structures, ii) composed only of carbon atoms, and iii) having high electrical and thermal conductivity.

A general sense of the relative mechanical properties of this new fiber foam and existing viscoelastic foams is obtained from measurements of energy loss and moduli. The energy loss was computed and found to be 5834 J/m3 for the fast cycling and 16887 J/m3 for the slower cycle [57]. Moreover; the repeatability of the cycles permitted some key mechanical parameters, such as a modulus between 3 and 4 MPa and a relaxation modulus of approximately 0.249 MPa under a constant strain, to be computed. These values are similar to those found in viscoelastics employed, commercially for cushioning in beds, chairs, helmets, specialty medical applications etc [58-61].

One drawback to the current generation of foams for human application is the difficulty of temperature control. To make the materials suitable for commercial use, relatively complex composite material foams are now employed. Given the far higher

electrical and thermal conductivity of CFF relative to polymer based foams, it should be relatively easy to thermally control these materials. For example, the foams can be heated electrically, or temperature maintained simply by contacting the material over only a fraction of the surface area with a heat sink maintained at a constant temperature. Moreover, the range of temperatures at which carbon foams are stable is likely to be far greater than that observed for polymer based viscoelastics, although more study is required to quantify the temperature range at which CFF remain stable and retain viscoelastic properties.

C. NOVEL FOAM POTENTIAL AS STRAIN GAUGE:

One postulated application of a conductive viscoeleastic material is as a strain gauge. The results of this work indicate that CFF could be used in this application. The key feature of a stain gauge is the availability of a single value electrical signal as a function of strain, a value that reports strain as a 'state property', and is not a function of the history of stress/strain of the material. As shown in Figure 50, the relationship between strain and measured resistance of CFF in a simple single axis compression remains linear over many cycles. Resistance is shown to have a single value, within ~2 percent, as a function of strain. Thus, resistance can serve as the single value electrical signal required to determine strain.

A second requirement of a strain gauge is that there is a high gauge factor. That is, the change in 'signal' must be high relative to the change in strain. In this case the proper measure of this factor is:

$$\frac{\Delta R/Ro}{\Delta L/Lo}$$

The gauge factor based on Figures 47 and 48, which is very large compared to those of comparable strain gauges [14, 62]. Our gauge factor ranged between 22.5 and 33.7 over the entire 20 cycles. Evaluation of the potential use of CFF in multi-axis strain gauges would be appropriate for future studies.

It is perhaps surprising that there is a hysteresis clearly observed in the stress-strain curve, but not in the relationship between strain and resistance. The former

indicates that energy of mechanical deformation observed during the compression leg of a cycle 'relaxes' during the decompression leg and is released as heat. What does the lack of hysteresis in the latter parameter suggest regarding the mechanism of resistance change as a function of strain?

In earlier work it was postulated that resistance changed as a function of strain because the number of 'contacts' between fibers increased with increasing strain, and this would lead to more electrical paths, hence lower resistance. The present work suggests this may not be correct. Indeed, it is generally understood that mechanical relaxation is associated with physical re-arrangement. In the case of a fiber foam, that implies that the individual fibers change shape to reduce their mechanical potential energy during relaxation. Certainly this relaxation of many fibers would change the number of fiber-fiber junctions, thus changing resistance. Hence, a change in resistance that matched the magnitude of the change in stress might be expected during transient experiments. This is not observed. Their resistance change, relatively, is much smaller than the stress relaxation. An alternative suggests itself: The conductivity of the individual fibers is changed by strain. That is, there is a relationship between fiber strain and fiber resistance. Specifically, the resistance of each individual fiber decreases as the fiber is shortened. Integrated over a large ensemble of fibers, of many orientations, geometries and sizes, such as that found in a CFF, this leads, on a macroscopic level, to a linear relationship between strain and resistance.

The above suggestion of a relationship between strain and the resistance of individual fibers is in fact consistent with the theory of conductor type strain gauges. Indeed, it is generally understood that single 'wires' change resistance because of shape changes, during strain. Broader and shorter wires have lower resistance. In fact, this is the basic physical fact exploited in the design of most strain gauges. Hence, it is a reasonable extension of current understanding of the impact of strain on metal resistance, to apply the same logic to carbon fiber resistance. Moreover, all findings in this work are consistent with this postulate. Finally, there are studies that show the resistances of individual carbon fibers are a function of strain [14]. It is noted this is a reasonable topic for future study.

THIS PAGE INTENTIONALLY LEFT BLANK

V. CONCLUSION

The goals of this thesis in developing a viable protocol for growing carbon nanofibers into a foam, analyze its microstructure, mechanical and electrical characteristics were completed successfully while conduction transient and dynamic loadings with loads ranging from 10 to 90 N. We were able to analyze the CFF's microstructure using the electron microscope and were able to determine its stability over a range of temperatures. In doing so a greater understanding of several aspects of carbon fiber foams resulted from this work specifically, i) the impact, both on the micro scale and the macro scale of catalyst identity, ii) the finding that CFF are true viscoelatic materials, and represent a new category of materials of this class, iii) the fact that electrical resistance is nearly a linear function of strain, hence thesefoams may make excellent sensing elements for strain gauges and iv) that mechanical and electrical properties require a few stress/strain cycles to stabilize.

Regarding the first point: Only palladium particles were capable of creating coherent macro scale CFF that were robust under repeated stress-strain cycles. This was traced to the micro structure. It was ascertained that long, 'thick' fibers were required to produce viable foam. Indeed, palladium particles produced long, and thicker, order of half a micron, fibers, the other catalysts only produced short, clearly only 100s of nm, and/or very thin, orders of 10s of nm, fibers.

Regarding the second point: Both transient and dynamic test results of the robust CFF created using palladium particles were consistent with the macroscopic behavior of visco-elastic material. Moreover, some key parameters such as the shape memory, and mechanical characteristics were similar to those of commercially employed viscoelastic materials.

It is also clear that CFF represent a new 'category' of visco-elastics as the microstructure is not open foam, closed foam, or any other form of the currently known visco-elastics. It is entirely fibers. Another unique aspect of this material is its high electrical, and concomitantly, thermal conductivity. All other visco-elastics are known to

be electrically and thermally insulating. This suggests that CFF could have superior properties for many applications.

Regarding the third point: The electrical resistance of the CFF was shown to be a strong, but linear, function of the strain. It was clearly shown that there is a unique resistance at each strain value, and that the gauge factor is very large. These two factors suggest that the material would make an excellent sensor of strain, hence strain gauge. A prototype, Figure 49, was created in order to demonstrate how the resistance changes on the device as a stress is applied to the carbon fiber foam. The prototype works over a repeated usage and is a very good demonstration of the viscoelastic capabilities of the carbon fiber foam.

Regarding the fourth point: The materials made for this study were shown to 'stabilize' both mechanically and electrically after of order 10 cycles of stress and strain. This is important for any material that will be deployed for real applications.

Overall we have improved the synthesis protocol of a newly discovered material made entirely of carbon fibers, and demonstrated that it belongs on the macroscopic level to the category of viscoelastic material. Yet, on the microscopic level its 'fiber only' structure makes it a unique viscoelastic. This unique microstructure leads to unique electrical and thermal properties, relative to all known visco-elastics. These properties suggest CFF can have many applications, including use as the sensing element in a strain gauge.

VI. RECOMMENDATIONS FOR FUTURE RESEARCH

Future work should be conducted to test the effects of temperature on the resistance versus strain, and to see at what range of temperature the viscoelastic results are valid.

The process of growing the carbon fiber foam on nickel and palladium salt were not successful however cheaper than growing on pure palladium. Future growth should be tested using powder cobalt as a catalyst.

Attempts to strengthen the carbon fiber foam could be tested by researching a composite foam where growing the carbon fibers with the boat filled with different fibers. In theory the carbon fibers would grow between and around the other fibers thereby increasing their strength. The tests described in this thesis should then be repeated and compared.

THIS PAGE INTENTIONALLY LEFT BLANK

APPENDIX A. NICKEL PROCEDURE

Flush

- Place 20 mg of palladium powder on the edges and center of the metal rectangular mold. Placing most of the powder near the outlet of the metal boat.
- Flush with nitrogen (N_2) at 300 SCCM for 20 min
- Turn on Furnace and set to 550°C
- Turn off nitrogen
- Run argon/hydrogen (Ar/H_2) at 20 SCCM for 30 minutes

Growth

- Turn off argon/hydrogen
- Run nitrogen (N_2) at 30 SCCM
- Run ethylene (C_2H_4) at 42 SCCM
- Run oxygen (O_2) at 3 SCCM
- After 5 min set oxygen to 10 SCCM
- After 5 min set oxygen to 15 SCCM
- Run for 1 hour at 550°C
- Turn off ethylene and oxygen

Cool Down

- Turn off furnace
- Turn on side fans
- Cool to room temperature with 30 SCCM of (N_2)
- Turn off (N_2) when the sample has reached room temperature
- Turn off side fans
- Remove sample

THIS PAGE INTENTIONALLY LEFT BLANK

APPENDIX B. PALLADIUM SALT (PD (NO_3)*H_2O) PROCEDURE

Flush

- Place 20 mg "equivalent" of palladium salt on the edges and center of the metal rectangular mold, placing most of the powder near the outlet of the metal boat.
- Flush withnitrogen (N_2) at 100 SCCM @ 250°C for 4 hours
- Turn on furnace and set to 550°C
- Flush 1 hour Ar/H_2 at 20 SCCM

Growth

- Once it is at 550°C, turn on ethylene at 15 SCCM and oxygen at 5 SCCM for 5 min then 10 SCCM for 5 min then 15 SCCM
- Run for 2 to 3 hours
- Turn off ethylene (C_2H_4) and oxygen (O_2)

Cool Down

- Turn off furnace
- Turn on side fans
- Cool to room temperature with 30 SCCM of nitrogen (N_2)
- Turn off nitrogen (N_2) when the sample has reached room temperature
- Turn off side fans
- Remove sample

THIS PAGE INTENTIONALLY LEFT BLANK

APPENDIX C. PALLADIUM (PD POWDER 99.9%) PROCEDURE

Flush

- Place 20 mg of palladium powder on the edges and center of the metal rectangular mold.
- Flush with nitrogen (N_2) at 100 SCCM
- Turn on furnace and set to 550°C

Growth

- Once it is at 550°C, turn on ethylene at 15 SCCM and oxygen at 5 SCCM for 5 min then 10 SCCM for 5 min then 20 SCCM
- Run for 2 to 3 hours
- Turn off ethylene (C_2H_4) and oxygen (O_2)

Cool Down

- Turn off furnace
- Turn on side fans
- Cool to room temperature with 30 SCCM of nitrogen (N_2)
- Turn off nitrogen (N_2) when the sample has reached room temperature
- Turn off side fans
- Remove sample

THIS PAGE INTENTIONALLY LEFT BLANK

APPENDIX D. MKS 647A OPERATION

Turning on

- On switch is in the top left of the back side of the MKS 647a
- If screen has timed out press any button to return to main screen

Main Menu

- Main menu looks as follows:

- In order to get to the main menu press 'ESC' this will return you one screen

Operation

- Choose "Extended Display" either by pressing 2 or with the up and down arrows. Once it is highlighted press "enter." Single quotes are reserved for quotes within quotes. Otherwise, use "regular" quote marks.
- In the Extended Display screen there are two options you can control, your set-point or on and off.
- Use the forward and back arrows to select the set-point you want and enter the digits for your SCCM/SLM you desire for your flow. Continue to scroll through and turn the status to 'on' by pushing the up and down arrows once your status is selected. Turn all regulators status to 'off' that you are not using. (Note: 1.000 SLM = 1000 SCCM).

- Turn on gas by pressing ‘On’ then press ‘ALL’. Note: Flow on or Flow off will be displayed in the bottom center.
- To Turn off press ‘Off’ then press ‘All’. Then verify that flow is now off in the center bottom of the screen.

Errors

- If there is an error it will be displayed in the bottom left corner of the extended display screen. It will display a number next to the error to show the number of errors that have occurred.
- Go to Main Menu.
- Select ‘4’ or ‘Diagnostics.’
- Select ‘1’ or ‘Error listing.’
- Here you can read what trip has occurred on the left and what channels have tripped on the right.

Reset Gasses and Trip Points

- The following is the setting you should see: (Make sure “Unit”, “Range FS.” and “Gas” match).

- If not then:
- Go to Main Menu.
- Select ‘5’ or ‘Instrument Setup.’
- Select’1’ or ‘Range Select.’
- Enter the appropriate value in the ‘Range FS’. Appropriate value is on each instrument labeled. The value is entered by pressing the up/down arrows. Channels are selected by pressing the right/left arrows.
- Next under ‘Instrument Setup’ select ‘2’ or ‘gas…’

- Now select the gas for the channel. Pushing the up/down arrow scrolls through the different gasses. For channel 4: C2H4 is not a selection, therefore for this gas you will leave the gas on ‘USER’ and enter ‘0.600’ for the Factor.
- Next reset the regulators to zero, under ‘Instrument Setup’ select ‘4’ or ‘Zero Adj.’
- Push the right arrow until EXC is highlighted. Then push the down arrow, it should now say ‘DONE’ for a few seconds and the flow should now be zeroed for that channel. Repeat for all channels.

THIS PAGE INTENTIONALLY LEFT BLANK

APPENDIX E. PLOTS OF THE DATA FOR HOLD TEST

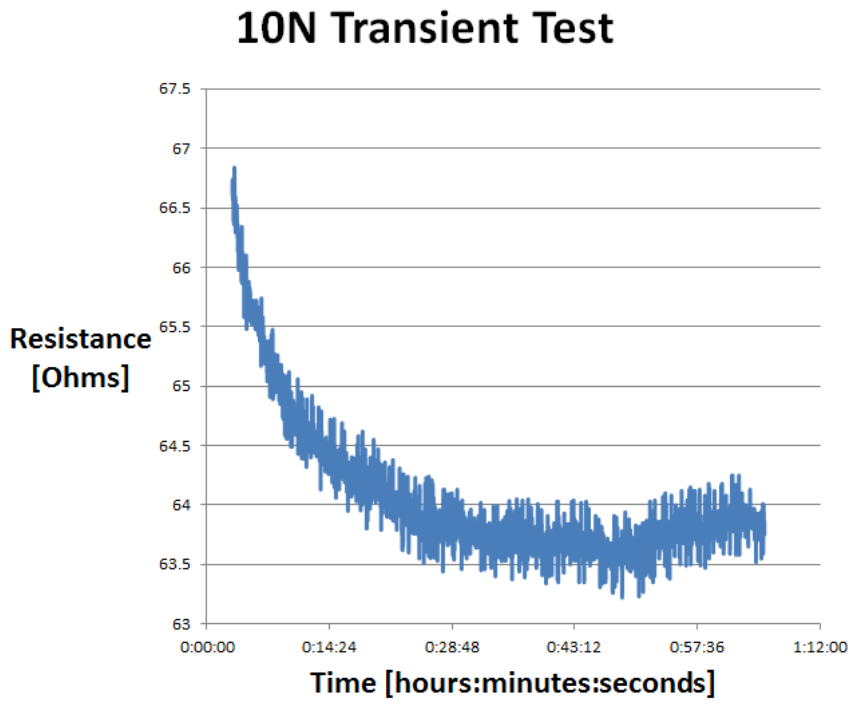

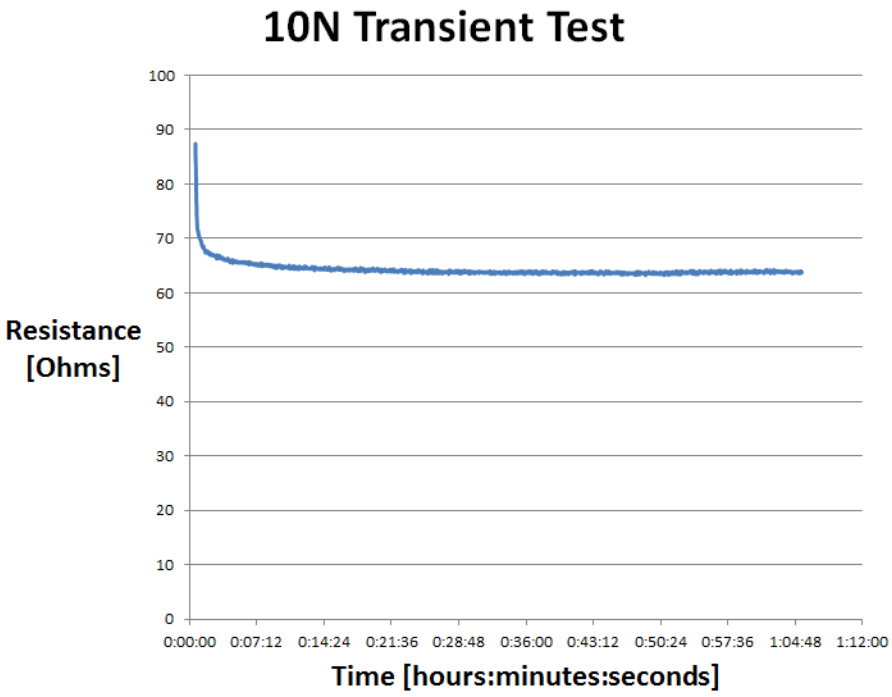

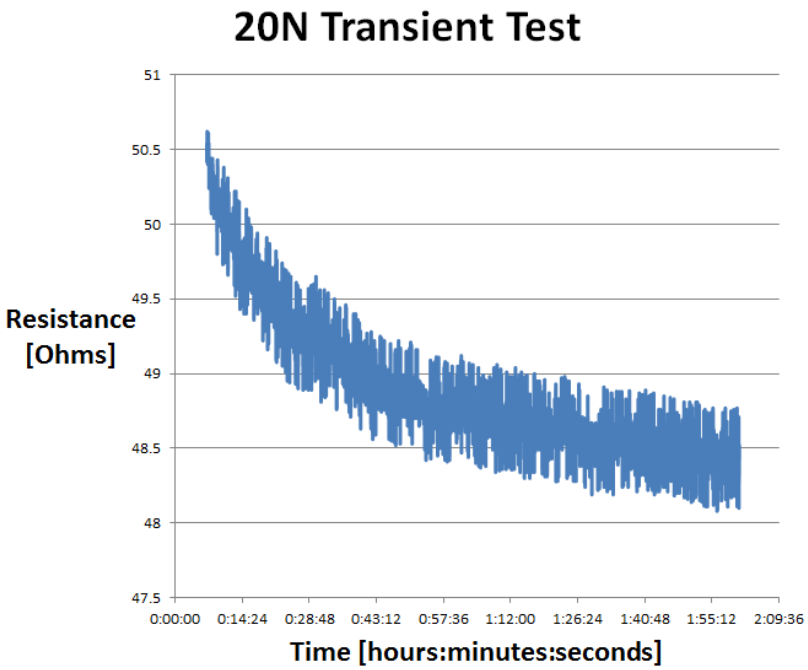
20N Transient Test
Resistance [Ohms]
51
50.5
50
49.5
49
48.5
48
47.5
0:00:00
0:14:24
0:28:48
0:43:12
0:57:36
1:12:00
1:26:24
1:40:48
1:55:12
2:09:36
Time [hours:minutes:seconds]

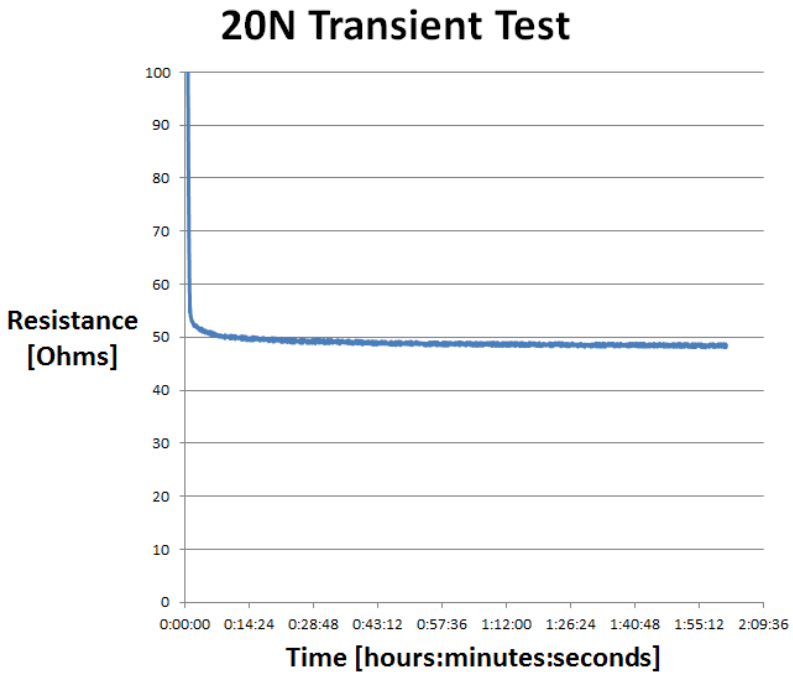
20N Transient Test
Resistance [Ohms]
100
90
80
70
60
50
40
30
20
10
0
0:00:00
0:14:24
0:28:48
0:43:12
0:57:36
1:12:00
1:26:24
1:40:48
1:55:12
2:09:36
Time [hours:minutes:seconds]

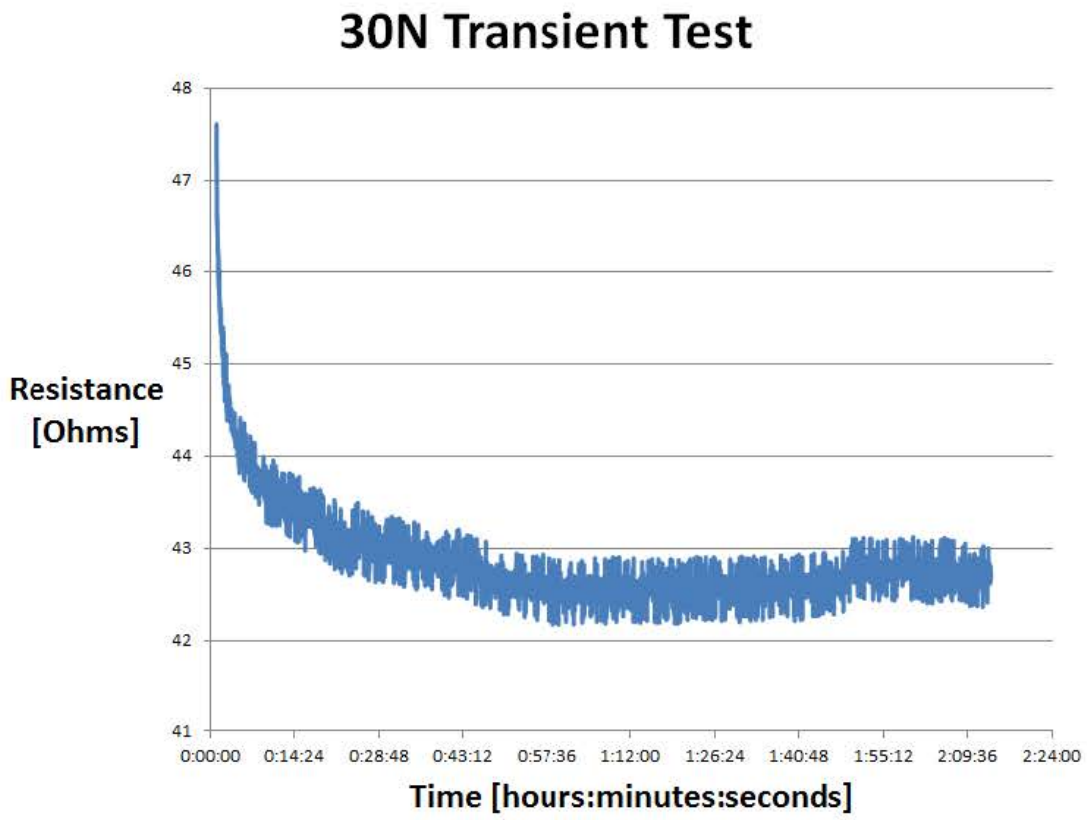
30N Transient Test
Resistance [Ohms]
48
47
46
45
44
43
42
41
0:00:00
0:14:24
0:28:48
0:43:12
0:57:36
1:12:00
1:26:24
1:40:48
1:55:12
2:09:36
2:24:00
Time [hours:minutes:seconds]

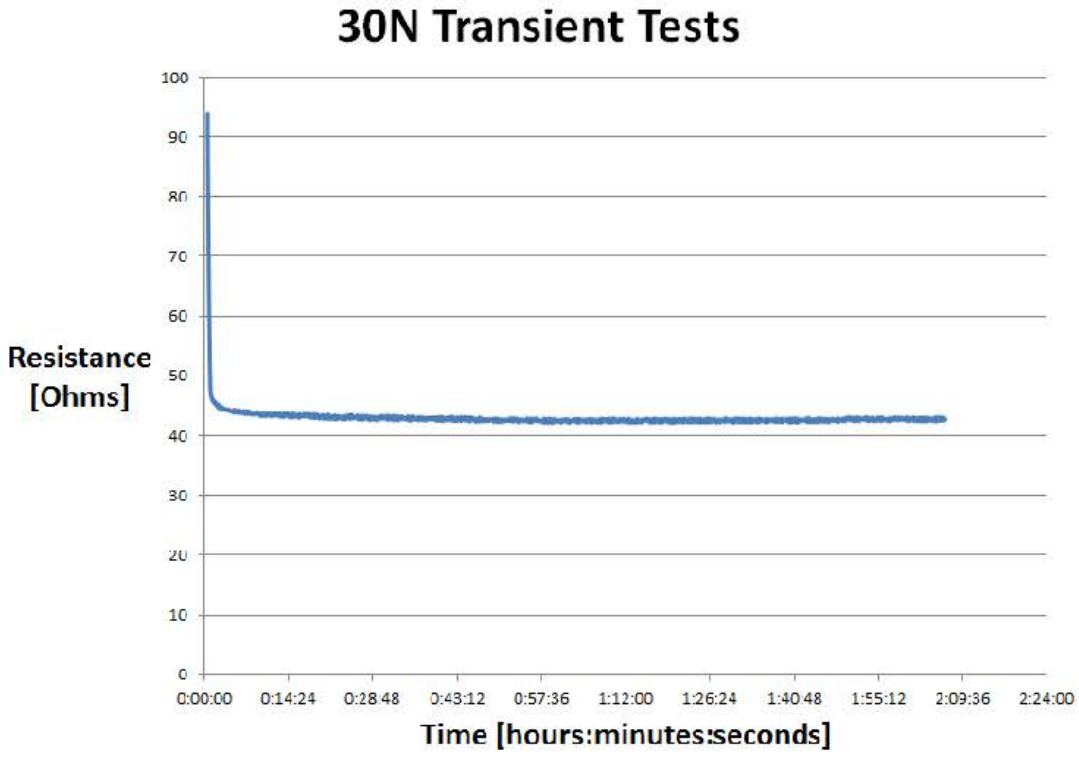
30N Transient Tests
Resistance [Ohms]
100
90
80
70
60
50
40
30
20
10
0
0:00:00
0:14:24
0:28:48
0:43:12
0:57:36
1:12:00
1:26:24
1:40:48
1:55:12
2:09:36
2:24:00
Time [hours:minutes:seconds]

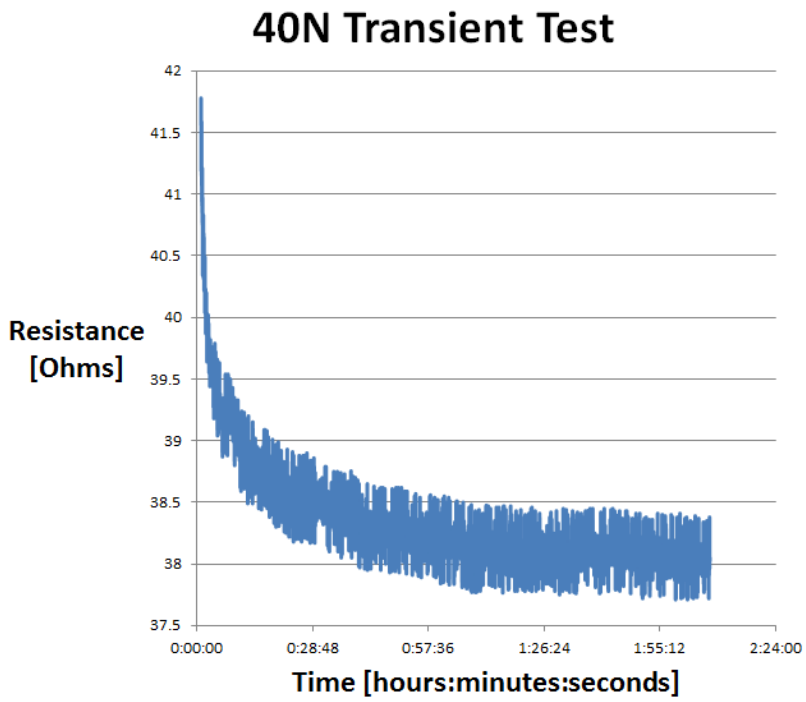
40N Transient Test
Resistance [Ohms]
42
41.5
41
40.5
40
39.5
39
38.5
38
37.5
0:00:00
0:28:48
0:57:36
1:26:24
1:55:12
2:24:00
Time [hours:minutes:seconds]

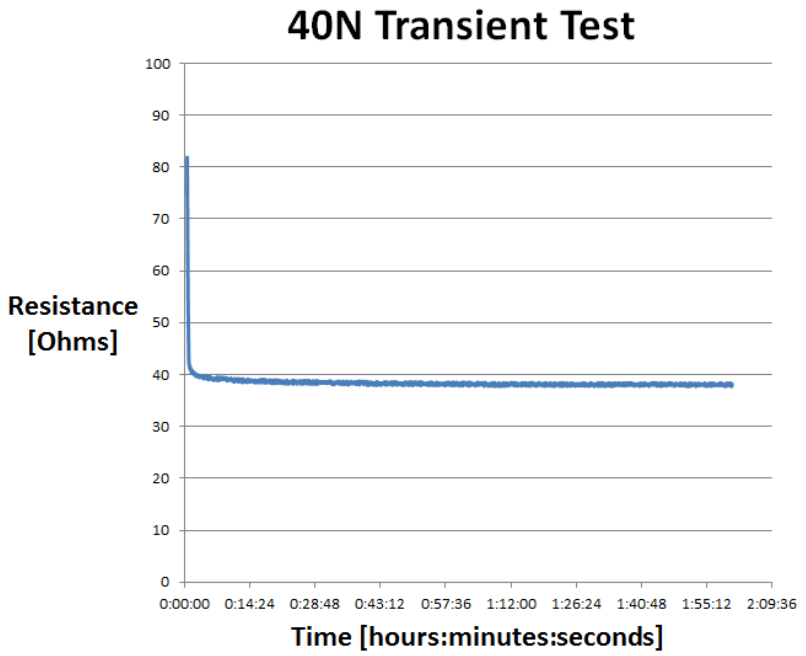
40N Transient Test
Resistance [Ohms]
100
90
80
70
60
50
40
30
20
10
0
0:00:00
0:14:24
0:28:48
0:43:12
0:57:36
1:12:00
1:26:24
1:40:48
1:55:12
2:09:36
Time [hours:minutes:seconds]

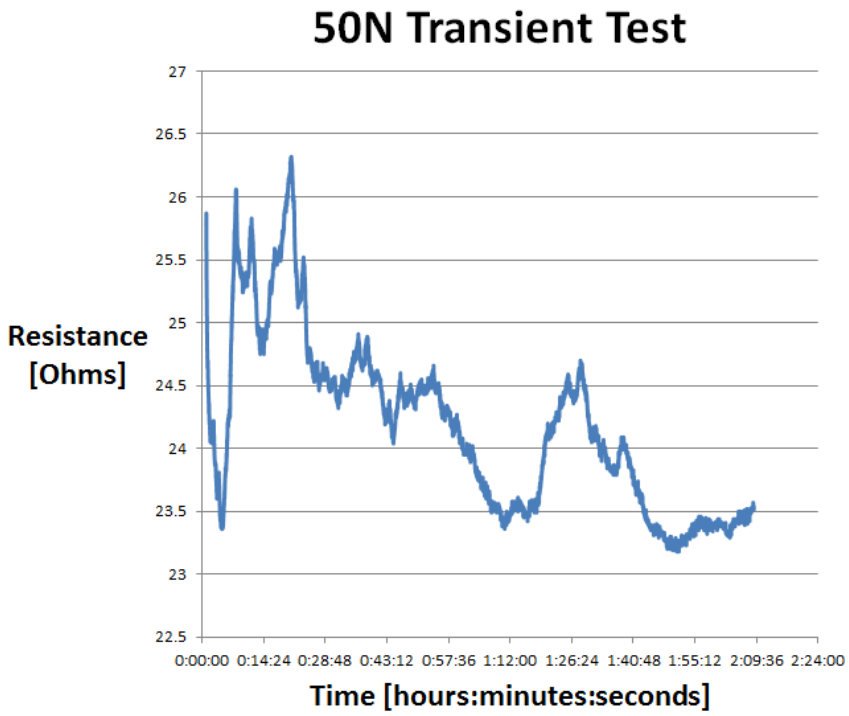
50N Transient Test
Resistance [Ohms]
27
26.5
26
25.5
25
24.5
24
23.5
23
22.5
0:00:00 0:14:24 0:28:48 0:43:12 0:57:36 1:12:00 1:26:24 1:40:48 1:55:12 2:09:36 2:24:00
Time [hours:minutes:seconds]

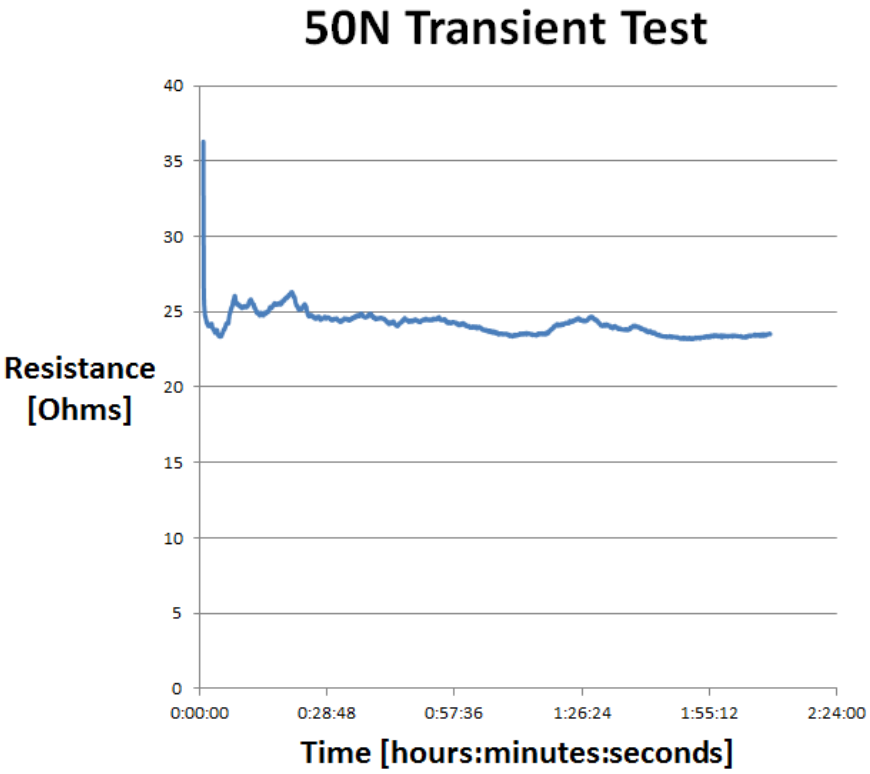
50N Transient Test
Resistance [Ohms]
40
35
30
25
20
15
10
5
0
0:00:00 0:28:48 0:57:36 1:26:24 1:55:12 2:24:00
Time [hours:minutes:seconds]

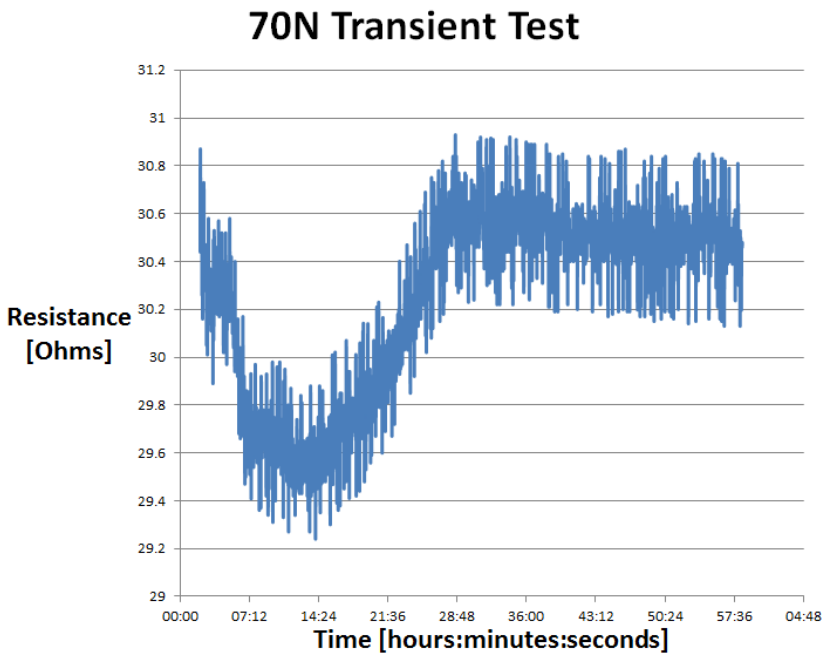
70N Transient Test
Resistance [Ohms]
31.2
31
30.8
30.6
30.4
30.2
30
29.8
29.6
29.4
29.2
29
00:00
07:12
14:24
21:36
28:48
36:00
43:12
50:24
57:36
04:48
Time [hours:minutes:seconds]

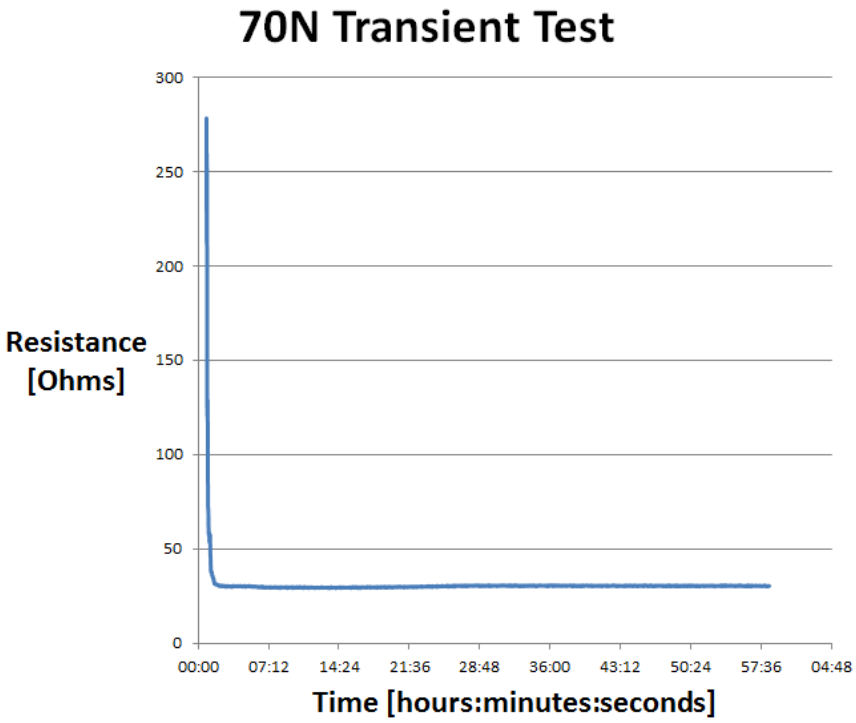
70N Transient Test
Resistance [Ohms]
300
250
200
150
100
50
0
00:00
07:12
14:24
21:36
28:48
36:00
43:12
50:24
57:36
04:48
Time [hours:minutes:seconds]

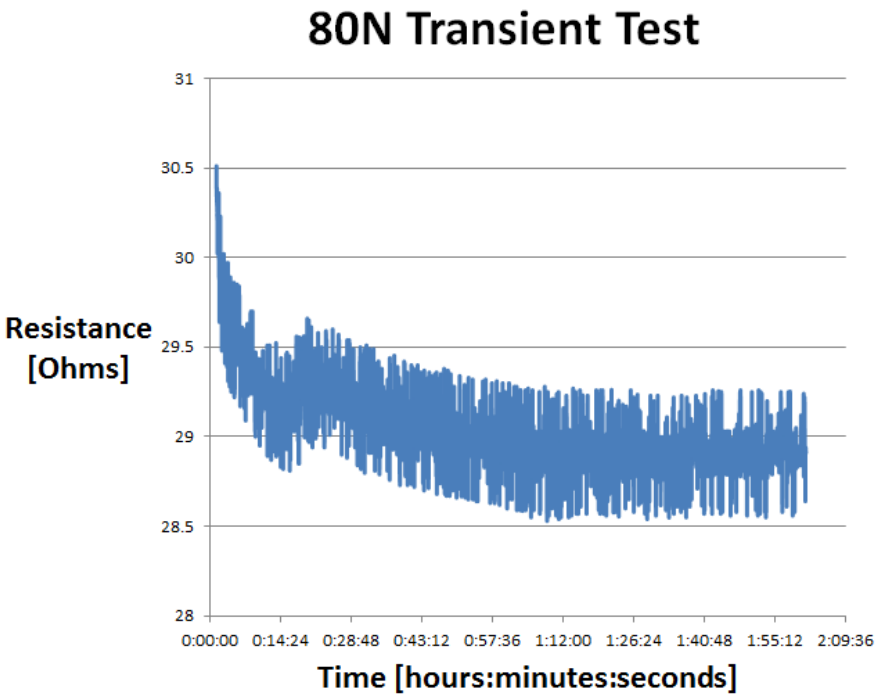
80N Transient Test
Resistance [Ohms]
31
30.5
30
29.5
29
28.5
28
0:00:00 0:14:24 0:28:48 0:43:12 0:57:36 1:12:00 1:26:24 1:40:48 1:55:12 2:09:36
Time [hours:minutes:seconds]

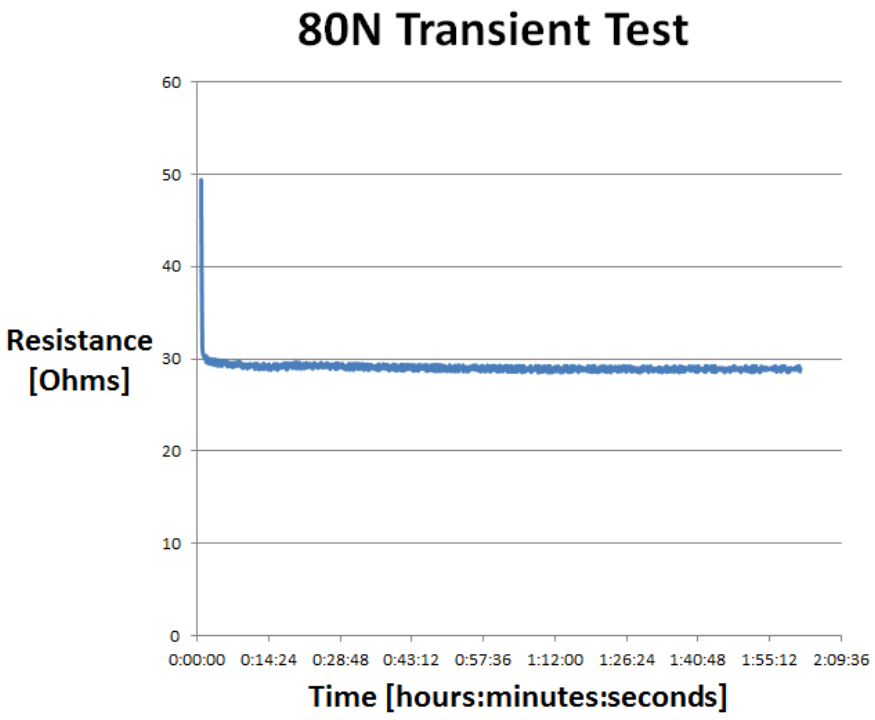
80N Transient Test
Resistance [Ohms]
60
50
40
30
20
10
0
0:00:00 0:14:24 0:28:48 0:43:12 0:57:36 1:12:00 1:26:24 1:40:48 1:55:12 2:09:36
Time [hours:minutes:seconds]

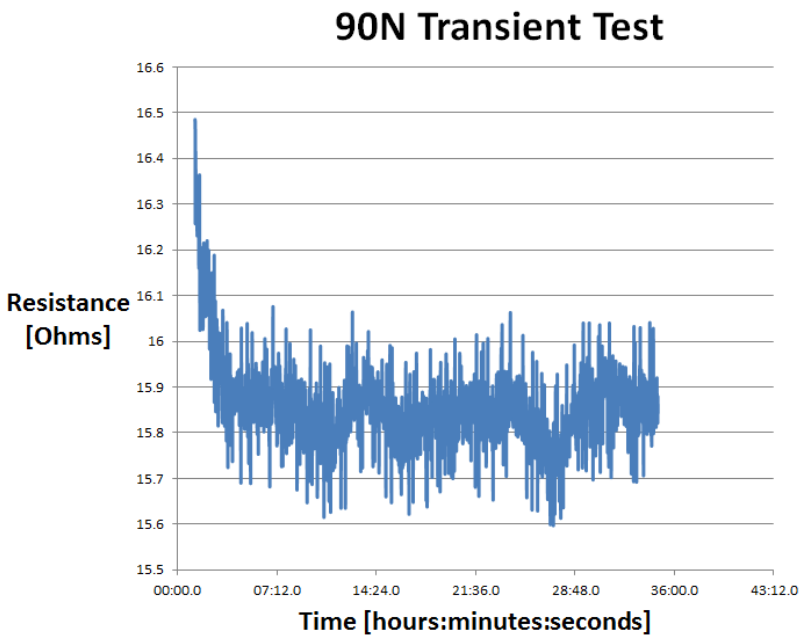
90N Transient Test
Resistance [Ohms]
16.6
16.5
16.4
16.3
16.2
16.1
16
15.9
15.8
15.7
15.6
15.5
00:00.0
07:12.0
14:24.0
21:36.0
28:48.0
36:00.0
43:12.0
Time [hours:minutes:seconds]

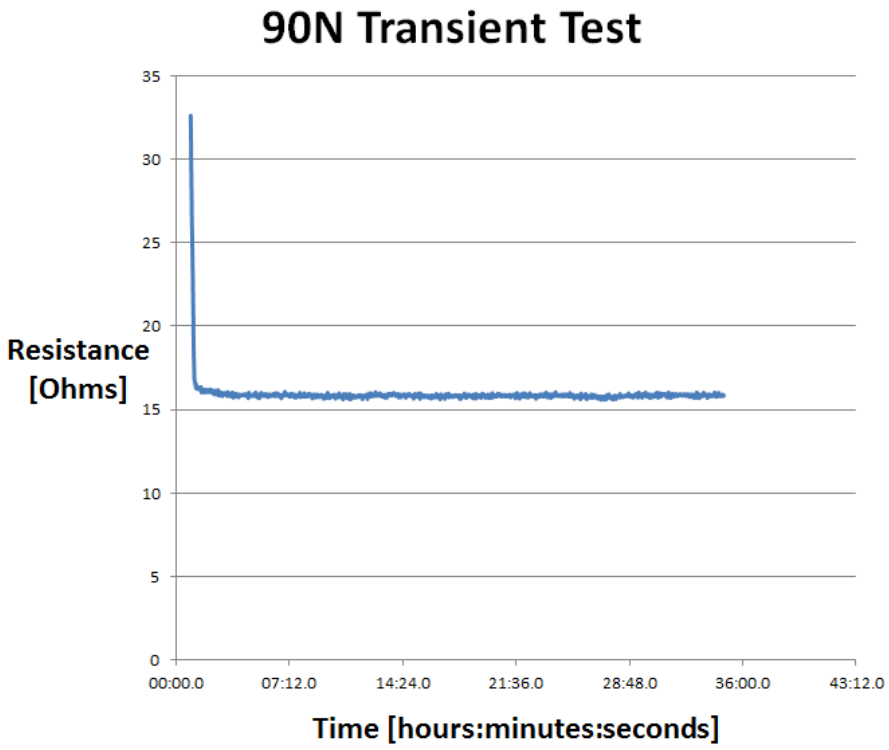
90N Transient Test
Resistance [Ohms]
35
30
25
20
15
10
5
0
00:00.0
07:12.0
14:24.0
21:36.0
28:48.0
36:00.0
43:12.0
Time [hours:minutes:seconds]

LIST OF REFERENCES

[1] L. Yang et al., "Band-gap change of carbon nanotubes: Effect of small uniaxial and torsional strain," *Phys. Rev. B,* vol. 60, pp. 13874–13878, Nov 1999.

[2] L. Yang and J. Han, "Electronic structure of deformed carbon nanotubes," *Phys. Rev. Lett.*, vol. 85, pp. 154–157, Jul 2000.

[3] E. Minot et al., "Tuning carbon nanotube band gaps with strain," *Phys. Rev. Lett.*, vol. 90, pp. 156–401, Apr 2003.

[4] J. Cao, Q. Wang and H. Dai, "Electromechanical properties of metallic, quasimetallic, and semiconducting carbon nanotubes under stretching," *Phys. Rev. Lett.,* vol. 90, pp. 157–601, Apr 2003.

[5] R. Grow et al., "Piezoresistance of carbon nanotubes on deformable thin-film membranes," *Appl. Phys. Lett.,* vol. 86, pp. 093–104, Feb 2005.

[6] J. Hwang et al., "Poly(3-hexylthiophene) wrapped carbon nanotube/poly(dimethylsiloxane) composites for use in finger-sensing piezoresistive pressure sensors," *Carbon,* vol. 49, pp. 106–110, Jan 2011.

[7] E. Choi et al., *Flexible and Transparent Touch Sensor using Single-Wall Carbon Nanotube Thin-Films.* New York: IEEE, 2010.

[8] J. Zhang et al., "Single MWNT-glass fiber as strain sensor and switch," *Adv Mater*, vol. 23, pp. 3392–+, Aug 2011.

[9] V. T. Dau et al., "Integrated CNTs thin film for MEMS mechanical sensors," *Microelectron. J.*, vol. 41, pp. 860–864, Dec 2010.

[10] N. Hu et al., "Investigation on sensitivity of a polymer/carbon nanotube composite strain sensor," *Carbon*, vol. 48, pp. 680–687, Mar 2010.

[11] M. Knite et al., "Polyisoprene-carbon black nanocomposites as tensile strain and pressure sensor materials," *Sens. Actuator A-Phys*., vol. 110, pp. 142–149, Feb 2004.

[12] K. S. Karimov et al., "A carbon nanotube-based pressure sensor," *Phys. Scripta*, vol. 83, pp. 065–703, Jun 2011.

[13] C. Su et al., "Fabrication of high sensitivity carbon microcoil pressure sensors," *Sensors*, vol. 12, pp. 10034–10041, Aug 2012.

[14] S. Luo and T. Liu, “Structure-property-processing relationships of single-wall carbon nanotube thin film piezoresistive sensors,” *Carbon,* vol. 59, pp. 315–324, Aug 2013.

[15] C. Rao et al., “Large aligned-nanotube bundles from ferrocene pyrolysis,” *Chem. Commun*., pp. 1525–1526, Aug 1998.

[16] L. Dai et al., “Aligned nanotubes,” *ChemPhysChem,* vol. 4, pp. 1150–1169, Nov 2003.

[17] N. Franklin and H. Dai, “An enhanced CVD approach to extensive nanotube networks with directionality,” *Adv Mater*, vol. 12, pp. 890–894, Jun 2000.

[18] N. Chakrapani et al., “Capillarity-driven assembly of two-dimensional cellular carbon nanotube foams,” *Proc. Natl. Acad. Sci. U. S. A.*, vol. 101, pp. 4009–4012, Mar 2004.

[19] D. N. Futaba et al., “Shape-engineerable and highly densely packed single-walled carbon nanotubes and their application as super-capacitor electrodes,” *Nat. Mater*., vol. 5, pp. 987–994, Dec 2006.

[20] A. Kumar et al., “Contact transfer of aligned carbon nanotube arrays onto conducting substrates,” *Appl. Phys. Lett.,* vol. 89, pp. 120–163, Oct 2006.

[21] S. Kaur et al., “Design and characterization of three-dimensional carbon nanotube foams,” *J Phys Chem B*, vol. 110, pp. 21377–21380, Oct 2006.

[22] W. Khalid et al., “High-aspect-ratio, free-form patterning of carbon nanotube forests using micro-electro-discharge machining,” *Diam. Relat. Mat.,* vol. 19, pp. 1405–1410, Nov 2010.

[23] G. Lalwani et al., “Fabrication and characterization of three-dimensional macroscopic all-carbon scaffolds,” *Carbon*, vol. 53, pp. 90–100, Mar 2013.

[24] W. H. Hung et al., “Rapid prototyping of three-dimensional microstructures from multiwalled carbon nanotubes,” *Appl. Phys. Lett*., vol. 91, pp. 093–121, Aug 2007.

[25] J. Phillips et al., “Graphitic structures by design,” *Langmuir*, vol. 22, pp. 9694–9703, Nov 2006.

[26] M. A. Atwater et al., “The production of carbon nanofibers and thin films on palladium catalysts from ethylene-oxygen mixtures,” *Carbon*, vol. 47, pp. 2269–2280, Aug 2009.

[27] J. Vincent, “Chapter one: Basic elasticity and viscoelasticity,” in *Structural Biomaterials*, 3rd ed. Princeton: Princeton University Press., 2012, p. 1.

[28] ASM International, *ASM Handbooks*, vol. 1 & 2. Materials Park, OH: ASM International, 2005.

[29] ASM International, "Engineered materials handbooks," vol. 1 and 4. Materials Park, OH: ASM International, 2005.

[30] American Society for Metals, *Metal Handbook: Properties and Selection: Nonferrous Alloys and Pure Metals*, 9th ed. Material Park, OH: ASM international.

[31] Callister et al., *Material Science and Engineering: An Introduction*. Hoboken, NJ: John Wiley & Sons, Inc., 2010.

[32] R. F. Floral and S. T. Peters, "Composite structures and technologies, tutorial notes," 1989, in Callister et al., eds., *Material Science and Engineering: An Introduction*. Hoboken, NJ: John Wiley & Sons, Inc., 2010.

[33] National Instruments Austin Texas, "2. The strain gage," 2013. Available: http://www.ni.com/white-paper/3642/en/

[34] (May 31, 2007). *Attachment of inorganic moieties onto aliphatic polyurethanes*. Available:http://www.scielo.br/scielo.php?pid=S151614392007000200005&script=sci_arttext. DOI: Aug 18, 2006.

[35] M. Poikelispaa et al., "The effect of partial replacement of carbon black by carbon nanotubes on the properties of natural rubber/butadiene rubber compound," *J Appl Polym Sci,* vol. 130, pp. 3153–3160, Dec 5, 2013.

[36] Y. Yu et al., "Direct electron transfer of glucose oxidase and biosensing for glucose based on PDDA-capped gold nanoparticle modified graphene/multi-walled carbon nanotubes electrode." *Biosens. Bioelectron*., vol. 52, pp. 147–152, 2014.

[37] T. Pustelny et al., "The sensitivity of sensor structures with oxide graphene exposed to selected gaseous atmospheres," *Bull. Pol. Acad. Sci. -Tech. Sci*., vol. 61, pp. 705–710, Sep 2013.

[38] M. Ozmaian and R. Naghdabadi, "Semi-conducting carbon nanotube as variable capacitor," *Physica E*, vol. 54, pp. 9–14, Dec 2013.

[39] S. Ren and G. Y. Lee, "A robust low power carbon nanotube sensor interface circuit in 180 nm CMOS technology," *IEEE Sens. J*., vol. 13, pp. 4786–4795, Dec 2013.

[40] J. Cheon et al., "Fabrication of [GRAPHICS]-type CNT field-effect transistor using energy band engineering layer between CNT and electrode," *IEEE Electron Device Lett.*, vol. 34, pp. 1436–1438, Nov 2013.

[41] K. Song et al., “Structural polymer-based carbon nanotube composite fibers: Understanding the processing-structure-performance relationship,” *Materials*, vol. 6, pp. 2543–2577, Jun 2013.

[42] A. Kroustalli et al., “Carbon nanotubes reinforced chitosan films: mechanical properties and cell response of a novel biomaterial for cardiovascular tissue engineering.” *Journal of Materials Science.Materials in Medicine*, vol. 24, pp. 2889–2896, Dec 2013.

[43] H. Kwon and M. Leparoux, “Hot extruded carbon nanotube reinforced aluminum matrix composite materials,” *Nanotechnology*, vol. 23, pp. 415–701, Oct 2012.

[44] X. Chen et al., “One-pot hydrothermal synthesis of reduced graphene oxide/carbon nanotube/alpha-Ni(OH)(2) composites for high performance electrochemical supercapacitor,” *J. Power Sources,* vol. 243, pp. 555–561, Dec 2013.

[45] Z. Li et al., “Rapid synthesis of graphene/cobalt hydroxide composite with enhanced electrochemical performance for supercapacitors,” *J. Power Sources,* vol. 245, pp. 224–231, Jan 1, 2014.

[46] Q. Wang et al., “Fe3O4 nanoparticles grown on graphene as advanced electrode materials for supercapacitors,” *J. Power Sources,* vol. 245, pp. 101–106, Jan 1, 2014.

[47] M. A. Atwater et al., “Direct synthesis and characterization of a nonwoven structure comprised of carbon nanofibers,” *Carbon,* vol. 57, pp. 363–370, Jun 2013.

[48] N. Wu and J. Phillips, “Catalytic etching of platinum during ethylene oxidation,” *J. Phys. Chem.,* vol. 89, pp. 591–600, 1985.

[49] N. Wu and J. Phillips, “Carbon deposition on platinum during ethylene oxidation,” *J. Catal.,* vol. 113, pp. 383–397, Oct 1988.

[50] M. A. Atwater et al., “Formation of carbon nanofibers and thin films catalyzed by palladium in ethylene-hydrogen mixtures,” *J. Phys. Chem. C,* vol. 114, pp. 5804–5810, Apr 2010.

[51] M. A. Atwater et al., “Accelerated growth of carbon nanofibers using physical mixtures and alloys of Pd and Co in an ethylene-hydrogen environment,” *Carbon*, vol. 49, pp. 1058–1066, Apr 2011.

[52] M. A. Atwater et al., “The effect of powder sintering on the palladium-catalyzed formation of carbon nanofibers from ethylene-oxygen mixtures,” *Carbon*, vol. 48, pp. 1932–1938, Jun 2010.

[53] C. C. Luhrs et al., “Generation of carbon nanofilaments on carbon fibers at 550 degrees C,” *Carbon*, vol. 47, pp. 3071–3078, Nov 2009.

[54] M. Al-Haik et al., “Novel growth of multiscale carbon nanofilaments on carbon and glass fibers,” *Nanosci. Nanotechnol. Lett*., vol. 1, pp. 122–127, Jun, 2009.

[55] A. Phillips et al., “Preparation of Graphitic Articles,” U.S. Patent 7713577, 2004.

[56] Y. Fernandez et al., “Graphitic encapsulation of micron- and nano-sized Ni particles using ethylene as precursor,” *Appl. Surf. Sci*., vol. 256, pp. 194–201, Oct 2009.

[57] J. Cook, “Microstructural analysis of the failure mechanisms of carbon nanofibers and inorganic fullerenes WS2.” M.S., thesis. Naval Postgraduate School, Monterey CA, 2013.

[58] D. Lebuisson and F. Earith, “Intraocular use of viscoelastics - Application to Anterior Segment Surgery Survey,” *J. Fr. Ophthamol*., vol. 15, pp. 133–153, 1992.

[59] P. Singhal et al., “Low density biodegradable shape memory polyurethane foams for embolic biomedical applications.” *Acta Biomaterialia*, vol. 10, pp. 67–76, Jan 2014.

[60] K. S. S. Kumar et al., “Progress in shape memory epoxy resins,” *React Funct Polym*, vol. 73, pp. 421–430, Feb 2013.

[61] H. Liu, Z et al., “Surperhydrophobic polyurethane foam modified by graphene oxide,” *J Appl Polym Sci*, vol. 130, pp. 3530–3536, Dec 2013.

[62] M. Tsai and S. Huang, “Analysis of the strain of the great saphenous vein in motion,” *Biomed. Mater. Eng*., vol. 24, pp. 1093–1099, 2014.

THIS PAGE INTENTIONALLY LEFT BLANK

INITIAL DISTRIBUTION LIST

1. Defense Technical Information Center
   Ft. Belvoir, Virginia

2. Dudley Knox Library
   Naval Postgraduate School
   Monterey, California